

Evaluation of process concepts for liquid-liquid systems exemplified for the indirect hydration of cyclohexene to cyclohexanol

Dissertation

zur Erlangung des akademischen Grades

**Doktoringenieur
(Dr.-Ing.)**

von **M.Tech. Rayees Ahamed Imam**

geb. am 14.10.1981 in Guduvancheri, India

genehmigt durch die Fakultät für Verfahrens- und Systemtechnik
der Otto-von-Guericke-Universität Magdeburg

Gutachter:

Prof. Dr.-Ing. Kai Sundmacher

Prof. Dr.-Ing. Hannsjörg Freund

Prof. Dr.-Ing. Zhiwen Qi

Promotionskolloquium am: 25.07.2014

Acknowledgements

I thank my supervisor Prof. Dr.-Ing. Kai Sundmacher for all the hope he has put on me. He has enlightened me through his wide knowledge of process systems engineering which is indispensable for this thesis. I thank my advisor Prof. Dr. -Ing. Hannsjoerg Freund for his immense support, motivation and for the wonderful discussions which have been the essential driving force that kept the clock ticking. I would like to express my gratitude to DSM Netherlands for the project funding. I would like to especially thank Dr. Ruud Guit, Dr. Celine Fellay and Dr. Rob Meyer for the intelligent discussions that have been the catalyst which speeded up the work. I would like to express my gratitude to all my group members for their kind cooperation. I thank Mr. Markus Ikert and Mr. Patrick Siegmund for their support in experimental set up, measurements and analytical support. In addition, I thank the Max-Planck Institute for Dynamics of Complex Technical Systems, for the financial funds I received. I thank the Otto-von-Guericke-Universität, Magdeburg for giving me the space under its umbrella to submit this thesis. I am very grateful to all my friends who made life in the institute and Magdeburg in general a pleasurable experience. Most importantly, I thank my family for giving me the much needed love and moral support. I thank the almighty, Alhamdulillah !

To my family

Contents

List of Figures	vii
List of Tables	ix
List of Appendices	xi
Notation	xii
German Abstract	xvi
Abstract	xviii
Chapter	
1. Introduction	1
1.1 Oxidation of cyclohexane	2
1.2 Hydrogenation of phenol	4
1.3 Hydration of cyclohexene	5
1.4 Limitations of the conventional process routes	7
1.5 Indirect hydration of cyclohexene to cyclohexanol	8
1.5.1 Coupled reactive distillation column process concept	9
1.6 Motivation and outline of the thesis	11
2. Complexities of liquid-liquid processes	13
2.1 Introduction	13
2.2 Literature overview of multiple steady states	13
2.3 Model formulation (LTIP)	16
2.3.1 Binary system	16
2.3.2 A generalized non-equilibrium model for liquid-liquid systems	17
2.3.3 Separation factor	21

2.4	Simulation	22
2.5	Bifurcation analysis	23
2.5.1	One parameter continuation	23
2.5.2	Two parameter continuation	26
2.5.3	Visualization of multiple steady states	29
2.5.4	Physical explanation for multiple steady states	32
2.6	Summary of Chapter 2	32
3.	Process concepts for the indirect hydration of cyclohexene to cyclohexanol	34
3.1	Introduction	34
3.1.1	Formic acid vs Acetic acid	35
3.2	Thermodynamic analysis	36
3.2.1	Activity model	36
3.2.2	Thermodynamic limitation of direct hydration	36
3.3	Thermo-morphic solvents	39
3.4	Reaction kinetics	45
3.5	Kinetic experiments	46
3.5.1	Materials	47
3.5.2	Choice of catalyst	48
3.5.3	Measurement and analysis	48
3.5.4	Experimental setup	48
3.5.5	Batch kinetic reaction measurement	50
3.5.6	Parameter estimation	51
3.5.7	Experimental data	51
3.6	Process concepts: overview and description	60
3.6.1	Asahi benchmark	60
3.6.2	RS process concepts	62
3.6.3	R1S1+R2S2 process concepts	62
3.7	Modeling and simulation fundamentals	63
3.7.1	General modeling strategy	63
3.7.2	Phase equilibrium calculations	65
3.7.3	Simulation environment	66
3.7.4	Chemical equilibrium constant	66
3.7.5	Dimensionless formulation of PFTR model	67
3.7.6	Reactive extraction model	69
3.8	Process Simulations	72
3.8.1	Ideal RS process concept	73
3.8.2	Real RS process concept	74
3.8.3	RS countercurrent cascade process concept	78
3.8.4	R1S1 + R2S2 cascade process concept	83
3.9	Summary of Chapter 3	93
4.	Conclusion and outlook	97

4.1	Conclusion	97
4.2	Outlook	100
Appendices	102
A.1	NRTL parameters	102
A.2	Antoine parameters	102
B.1	Esterification experiments	104
B.2	Comparison of Amberlyst 15 and Zeolite ZSM-5	108
	B.2.1 Esterification	108
	B.2.2 Hydrolysis	110
B.3	Reverse hydrolysis experiments	113
B.4	Thermo-morphic LLE data	117
	B.4.1 DMSO-cyclohexene	117
	B.4.2 NMF-cyclohexene	117
	B.4.3 Ternary DMSO - Ene - Water	118
	B.4.4 Batch kinetic experiment: direct hydration in DMSO	119
Bibliography	120

List of Figures

Figure

1.1	Overview of production routes of cyclohexanol	1
1.2	Process route for oxidation of cyclohexane	2
1.3	Boric acid modification of oxidation of cyclohexane	2
1.4	Process flow diagram for the oxidation of cyclohexane	3
1.5	Process flow diagram for the hydrogenation of phenol	4
1.6	Partial hydrogenation of benzene and hydration of cyclohexene	5
1.7	Process flow diagram for the Asahi process	6
1.8	Reactions: (a) direct hydration, (b) esterification, (c) hydrolysis	9
1.9	Coupled reactive distillation column process concept	10
2.1	Schematic diagram of a Liquid-Liquid CSTR	16
2.2	Bifurcation diagram: phase fraction	24
2.3	Bifurcation diagram: composition	25
2.4	Bifurcation diagram: separation factor	25
2.5	2p continuation A and St	27
2.6	2p continuation St and Kr	28
2.7	Geometrical representation of steady state, $St = 0.3$, $A = 2.2$, $Kr = 1.0$ (Region I)	30
2.8	Geometrical projections at the points selected in different regions of Figure 2.5	31
3.1	Direct hydration chemical equilibrium at 393 K	37
3.2	Effect of temperature on direct hydration chemical equilibrium	38
3.3	Binary LLE diagram, NMF-cyclohexene	41
3.4	Binary LLE diagram, DMSO-cyclohexene	42
3.5	Ternary LLE diagram DMSO-cyclohexene-water	43
3.6	Batch kinetic experiment, direct hydration with DMSO as solvent	44
3.7	Schematic representation of experimental setup.	49
3.8	Sensitivity of esterification chemical equilibrium to the heat of formation of cyclohexylformate	53
3.9	Esterification experiments and simulations with fitted parameters.	55
3.10	Reverse hydrolysis experiments and simulations with fitted parameters	57
3.11	Esterification experiments. Zeolite ZSM5 vs. Amberlyst 15	58

3.12	Hydrolysis experiments. Zeolite ZSM5 vs. Amberlyst 15	59
3.13	Process concepts overview	61
3.14	Modeling Strategy	64
3.15	PFTR model	67
3.16	Countercurrent reactive extraction model	70
3.17	RS process concept	73
3.18	Performance of the ideal RS case	74
3.19	Effect of catalyst loading for real RS process concept	76
3.20	Effect of Ene:Water ratio for real RS process concept	77
3.21	Effect of Acid:Ene ratio for real RS process concept	78
3.22	Effect of temperature for real RS process concept	79
3.23	RS countercurrent cascade process concept	80
3.24	Comparison of RS and RS countercurrent cascade. 343K, Catalyst(Amberlyst) loading 30%, Ene:Water = 0.1, Acid:Ene = 0.1	81
3.25	Profiles of RS, RSCa, RSCb	82
3.26	Effect of water on esterification	84
3.27	Energy requirement R1S1	85
3.28	R1S1+R2S2C case A process concept	86
3.29	Effect of Ester:Water ratio R2S2Ca	87
3.30	Effect of extraction R2S2Ca	88
3.31	Separation design R2S2Ca	88
3.32	R1S1+R2S2C case B process concept	90
3.33	Effect of cyclohexanol split fraction R2S2Cb	92
3.34	Effect of Acid:Water ratio on R2S2Cb	93
3.35	Comparison of Acid:Ene and Acid:Water ratio, R2S2Cb	94

List of Tables

Table

2.1	Stoichiometric coefficients ν_{ij} of the transition process	18
2.2	Definition of dimensionless terms	18
2.3	Transition rates	19
2.4	Parameters	22
3.1	Thermodynamic data and Langmuir-Hinshelwood adsorption parameters of Steyer et al. [1]	45
3.2	Reaction kinetic parameters of Steyer et al. [1]	46
3.3	Heat of formation of cyclohexylformate	52
3.4	Updated kinetic parameters	60
3.5	Stoichiometric coefficient ν_{ij}	67
3.6	Asahi benchmark	72
3.7	Energy requirement R2S2Ca	89
4.1	Overview of effects of parameters/intensification concepts	98
4.2	Process concepts summary	99
A.1	NRTL parameters	103
A.2	Antoine parameters	103
B.1	Esterification: mol ratio 1:1	104
B.2	Esterification: mol ratio 1:2	106
B.3	Esterification: mol ratio 1:3	107
B.4	Esterification: mol ratio 1:1, without catalyst	107
B.5	Zeolite, 333 K, Esterification	108
B.6	Zeolite, 343 K, Esterification	108
B.7	Amberlyst, 343 K, Esterification	109
B.8	Amberlyst, 333 K, Esterification	110
B.9	Zeolite, 343 K, Hydrolysis	110
B.10	Amberlyst, 343 K, Hydrolysis	111
B.11	Zeolite, 333 K, Hydrolysis	112
B.12	Amberlyst, 333 K, Hydrolysis	112
B.13	Reverse hydrolysis, without catalyst	113
B.14	Reverse hydrolysis, 333 K, 1:1	113
B.15	Reverse hydrolysis, 333 K, 2:1	114

B.16	Reverse hydrolysis, 333 K, 1:2	115
B.17	Reverse hydrolysis, 313 K, 1:2	115
B.18	Reverse hydrolysis, 313 K, 1:1	116
B.19	Binary LLE: DMSO-cyclohexene	117
B.20	Binary LLE:NMF-cyclohexene	117
B.21	Ternary LLE: DMSO - Ene - Water	118
B.22	Solvent DMSO: Direct hydration	119

List of Appendices

Appendix

A.	Physico-chemical parameters	102
B.	Experimental data	104

Notation

Abbreviations

Acid	formic acid
Anol	cyclohexanol
CMB	component material balance
CMO	constant molar overflow approximation
CO	carbon monoxide
CSTR	continuous stirred tank reactor
Da	Damköhler number
DAE	differential-algebraic-equations
DMSO	dimethylsulfoxide
Dx	decanter
Ene	cyclohexene
Ester	cyclohexylformate
Ex	extraction column
FID	flame ionization detector
GC	gas chromatography
GC-MS	gas chromatography coupled to mass spectrometer
HOF	heat of formation
LH	Langmuir-Hinshelwood
LLE	liquid-liquid equilibrium
LTIP	linear thermodynamics of irreversible processes
MESH	mass-equilibrium-summation-enthalpy equations
MSS	multiple steady states
NMF	n-methylformamide
PFTR	plug flow tubular reactor
R1RD1	reactor 1 reactive-distillation 1
R1S1+R2S2	reactor 1 separator 1 + reactor 2 separator 2 process concept
R2S2C	reactor 2 separator 2 with counter-current reactor decanter cascade
RD	reactive distillation
RS	reactor separator process concept
RSC	reactor separator with counter-current reactor decanter cascade
S	separation section (set of distillation column and decanters)
TCD	thermal conductivity detector
TMB	total material balance
UCST	upper critical solution temperature
VLE	vapor-liquid equilibrium
VLLE	vapor-liquid-liquid equilibrium

Nomenclature

A	parameter of margules activity model	
Ak	affinity	
A_i	species i	
a	activity of component	
$C_{p,j}$	specific heat capacity of component i	$\text{J mol}^{-1} \text{K}^{-1}$
Da	Damköhler number	
Da_j^{het}	dimensionless Damköhler number of heterogeneous reaction j	
Da_j^{hom}	dimensionless Damköhler number of homogeneous reaction j	
$E_{A,i}^{het}$	activation energy of heterogeneous reaction	J mol^{-1}
$E_{A,i}^{hom}$	activation energy of homogeneous reaction	J mol^{-1}
E_k	extract flow rate	mol s^{-1}
f	dimensionless flow rate	
F	feed flow rate	mol s^{-1}
F_{in}	molar flow rate of feed	mol s^{-1}
F_{out}	molar flow rate of product	mol s^{-1}
g_{ij}	NRTL binary interaction energy parameters	J mol^{-1}
G	molar Gibbs free energy	J mol^{-1}
ΔG_{rxn}^j	Gibbs energy of reaction j	J mol^{-1}
H_i^0	standard heat of formation of component i	J mol^{-1}
ΔH_{rxn}^j	heat of reaction j	J mol^{-1}
k	intrinsic transition rate constant	s^{-1}
Kr	ratio of the rate constants of transition processes	
K_{ads}	adsorption equilibrium constant	
K_{eq}	chemical equilibrium constant	
K_{eq}^j	chemical equilibrium constant of reaction j	
$k_{f,0,i}^{het}$	heterogeneous forward reaction rate constant	$\text{J mol}^{-1} \text{kg}^{-1}_{cat}$
$k_{f,0,i}^{hom}$	homogeneous forward reaction rate constant	$\text{J mol}^{-1} \text{mol}_{FA}^{-1}$
L	length of PFTR	m
M	total number of transitions between species	
m_{cat}	mass of catalyst	kg
n	total number of species	
N	mole number	mol
NC	total number of components	
N_T	total molar hold up	mol
n_{FA}	total moles of formic acid	mol
NR	total number of reactions	
NS	total number of stages	
r	reaction rate	mol s^{-1}
r_j	intrinsic reaction rate or transition rate of a transition process j	s^{-1}
r'_j	dimensionless rate of reaction j	
R_{gas}	universal gas constant	$\text{J mol}^{-1} \text{K}^{-1}$
R_k	raffinate flow rate	mol s^{-1}
s	source (phase transfer or chemical reaction)	s^{-1}
S_i^0	standard entropy of pure component i	J mol^{-1}

Nomenclature continued . . .

ΔS_{rxn}^j	entropy of reaction j	J mol^{-1}
St	Stanton number	
t	time	s
T	temperature	K
T_{ref}	reference temperature (298 K)	K
V	total volume of reactor	m^3
x	overall mole fraction in liquid phase	
y	pseudo mole fraction	
α_{ij}	NRTL non-randomness parameter	
η	separation factor	
γ	activity coefficient	
μ	chemical potential	J mol^{-1}
ν	stoichiometric coefficient	
ν_i^T	total stoichiometric molar change of reaction	
Φ	phase fraction	
ρ	dimensionless transition rate	
ρ_i	molar density of component i	mol m^{-3}
ρ_{avg}	average molar density	mol m^{-3}
ε	void fraction of reactor	
ζ	dimensionless distance (length) of PFTR	
τ	dimensionless time (time divided by residence time)	

Subscripts and superscripts

avg	average
aq	aqueous
cat	catalyst
e	equilibrium
F	feed
FA	formic acid
i	component index
in	inlet to reactor
j	reaction or transition process index
k	stage index
out	outlet from reactor
org	organic
r	transition
ss	steady state
t	total
T	total
θ	reference conditions
0	standard reference conditions (298 K)

German Abstract

Cyclohexanol wird kommerziell über unterschiedliche Prozessrouten hergestellt. Die jüngste ist die partielle Hydrierung von Benzol zu Cyclohexen mit anschließender Hydratisierung von Cyclohexen zu Cyclohexanol, wie sie im ASAHI Prozess realisiert wird. Die technische Umsetzung des Hydratisierungsprozesses wird erschwert durch mehrere systembedingte Limitationen, wie langsame Reaktionsgeschwindigkeiten aufgrund geringer gegenseitiger Eduktlöslichkeiten, und einem niedrigen Gleichgewichtsumsatz. Daraus resultiert ein sehr hoher Energieverbrauch im nachgeschalteten Prozess. In der Arbeit von Steyer et al. [2] wird eine indirekte Reaktionsroute, basierend auf Ameisensäure als reaktiven Entrainer vorgestellt [1–3]. Durch diesen Ansatz können einige Einschränkungen des herkömmlichen Asahi Prozesses umgangen werden [1, 4–6]. Die technische Machbarkeit dieser Prozessroute wurde anhand eines gekoppelten Reaktivdestillationskolonnen-Konzeptes durch Simulationen von Katariya et al. [7, 8] demonstriert und durch Pilotanlagenexperimente von Kumar et al. [9–11] validiert. Das Konzept ermöglicht eine fast vollständige Umsetzung von Cyclohexen zu Cyclohexanol. Der Energieverbrauch ist jedoch sehr hoch. Zusätzlich wird der Prozess durch das Auftreten mehrerer stationärer Zustände (MSS), welche nur ein schmales Betriebsfenster zulassen, begrenzt.

Um ein robustes und kostengünstiges Verfahren zu verwirklichen muss das zugrundeliegende Flüssig-Flüssig-Reaktionssystem in seiner Komplexität verstanden werden. Die Nichtlinearitäten dieses Systems entstehen durch verschiedene Faktoren, wie zum Beispiel der Reaktionskinetik. Der wichtigste Faktor, der solch stark nichtidealen Phasenzersfalls-Systemen innewohnt, sind jedoch die Nichtlinearitäten des Aktivitäts-Modells. Diesem Gedanken folgend wird eine generelle Nicht-Gleichgewichts-Modellierung auf der Basis linearer Thermodynamik irreversibler Prozesse (LTIP) vorgestellt und die Dynamik eines Flüssig-Flüssig-Systems wird systematisch untersucht. Es wird gezeigt, dass selbst die Nichtlinearitäten des einfachsten nicht-idealen Aktivitäts-Modells eine Ursache für MSS darstellen. Parameter, welche die Löslichkeit

beeinflussen, wie z.B. Temperatur, können eine wichtige Rolle für die Existenz von MSS im System spielen.

Es gibt noch weitere Herausforderungen, die mit der indirekten Hydratisierung von Cyclohexen verbunden sind. Insbesondere sollte das Zusammenspiel von Reaktion, Phasengleichgewicht, Trennung und Feedback (Rückführströme) verstanden werden. Daher werden systematische Untersuchungen verschiedener Prozesskonzepte durchgeführt. Ausgehend von den Grundlagen werden verschiedene Verfahrenskonzepte mit unterschiedlicher Komplexität entwickelt. Diese Konzepte lassen sich in zwei Kategorien einteilen, RS und R1S1 + R2S2. In den RS Prozesskonzepten erfolgen alle drei Reaktionen simultan in der Reaktionsstufe (R), welcher ein Trennschritt (S) folgt. In der R1S1 + R2S2 Reihe von Verfahrenskonzepten erfolgen Veresterung und Hydrolyse in verschiedenen Prozessabschnitten. In R1 erfolgt die Veresterungsreaktion, gefolgt von der Esterreinigung S1. In R2 erfolgt die Hydrolysereaktion, gefolgt von der Produktreinigung S2.

Um die Gültigkeit des kinetischen Modells in weiten Bereichen der Prozessbedingungen zu gewährleisten wurden Experimente zielgerichtet durchgeführt. Die Bildungsenthalpie von Cyclohexylformat konnte in Langzeit-Batch-Experimenten mit hoher Präzision bestimmt werden. Die entwickelten Verfahrenskonzepte wurden verglichen und in Bezug auf das Asahi Verfahren ausgewertet [4–6]. Als wichtiger Indikator für die Wirtschaftlichkeit des Prozesses wird der Energieverbrauch analysiert.

Die Arbeit zeigt die Komplexität der indirekten Hydratisierung von Cyclohexen auf und gibt Leitlinien für weiterhin erforderliche Forschung, um diese neue Prozessroute in der industriellen Anwendung zu realisieren.

Abstract

Cyclohexanol is commercially produced via several process routes. The most recent is the Asahi process which involves partial hydrogenation of benzene to cyclohexene and subsequent hydration of cyclohexene to cyclohexanol. The hydration step has several limitations, namely, very slow reaction rates due to the extremely limited mutual solubility of the reactants and low equilibrium conversion. As a consequence, in the downstream process the energy consumption is high. An indirect hydration process route was proposed by Steyer et al. [2], in which formic acid is used as a reactive entrainer [1–3]. This route overcomes several limitations of the conventional Asahi process [1, 4–6]. To realize this new process route a coupled column reactive distillation process concept was demonstrated by the simulations of Katariya et al. [7, 8], and supported by the pilot plant experiments of Kumar et al. [9–11]. The process concept is feasible with nearly complete conversion of cyclohexene to cyclohexanol. However, the energy consumption is very high. Moreover, the coupled column process is limited by multiple steady states (MSS) with a narrow operating window.

To realize a robust and economical process concept the underlying complexities of the liquid-liquid reacting system have to be understood. The nonlinearities in these systems can arise from various factors such as, e.g., kinetics. But the most important factor which is inherent in such highly non-ideal phase splitting systems is the nonlinearity in the activity model. In this direction, a generalized non-equilibrium modeling approach based on Linear Thermodynamics of Irreversible Processes (LTIP) is presented, and the dynamics of a liquid-liquid system is studied systematically. It is shown that the nonlinearity present in even the simplest non-ideal activity model acts as a source for MSS. The parameters that affect the solubility, e.g. temperature, can play a critical role on the existence of MSS in the system.

There are further challenges associated with the indirect hydration of cyclohexene. Particularly, the interplay of reactions, phase equilibrium, separation and feed back

(recycle streams) should be understood. Therefore, a systematic study of process concepts is carried out. Starting from the fundamentals, different process concepts with varying degrees of complexity are developed. These concepts can be grouped into two categories, namely RS and R1S1+R2S2. In the RS set of process concepts, all the three reactions occur together in the reaction step (R) followed by a separation step (S). In the R1S1+R2S2 set of process concepts, esterification and hydrolysis are carried out in different stages. R1 performs the esterification reaction followed by ester purification in S1. R2 performs the hydrolysis reaction followed by product purification in S2.

Dedicated experiments were carried out in order to ensure the validity of the kinetic model at wide ranges of process conditions. Longtime batch experiments provided an accurate estimation of the heat of formation of cyclohexylformate. The developed process concepts are compared and evaluated with respect to the benchmark Asahi process [4–6]. As an important indicator of the economic viability, the energy consumption is analyzed.

The thesis outlines the various complexities involved in the indirect hydration of cyclohexene and gives guidelines for further required research in order to realize this new process route in industrial application.

Chapter 1

Introduction

Cyclohexanol is a bulk chemical with an annual production capacity of more than 3.5 million metric tonnes [12, 13]. The major use of cyclohexanol is in the production of caprolactam and adipic acid, which are the intermediates in the manufacture of nylon 6 and nylon 66. The conventional processes for the production of cyclohexanol are based on the oxidation of cyclohexane [14, 15], the hydrogenation of phenol [16, 17] and the direct hydration of cyclohexene [18–23]. Figure 1.1 provides an overview of these process routes.

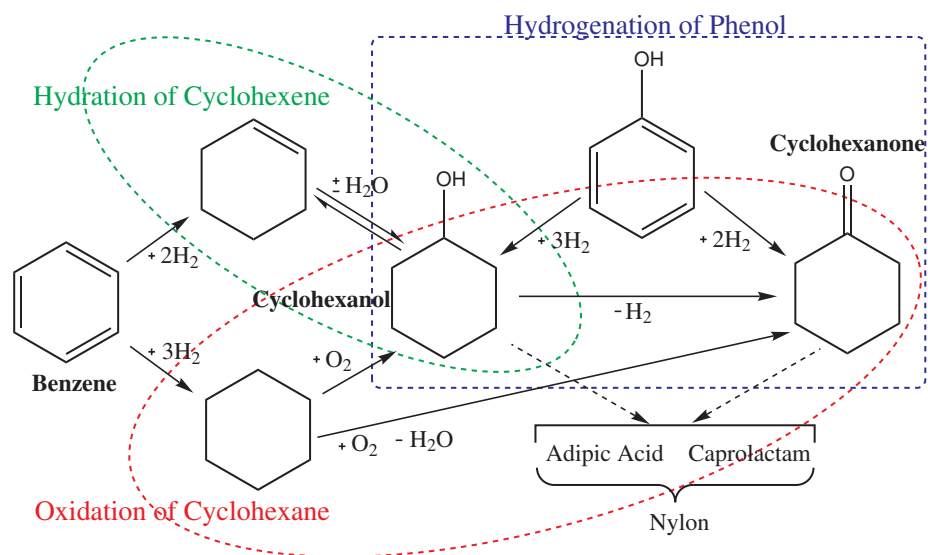


Figure 1.1: Overview of production routes of cyclohexanol

A brief description of these commercial processes is provided in the following paragraphs.

1.1 Oxidation of cyclohexane

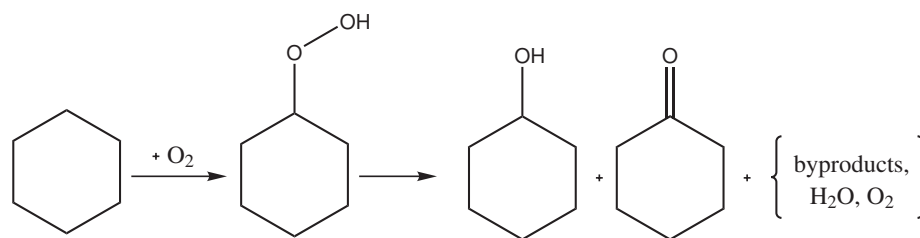


Figure 1.2: Process route for oxidation of cyclohexane

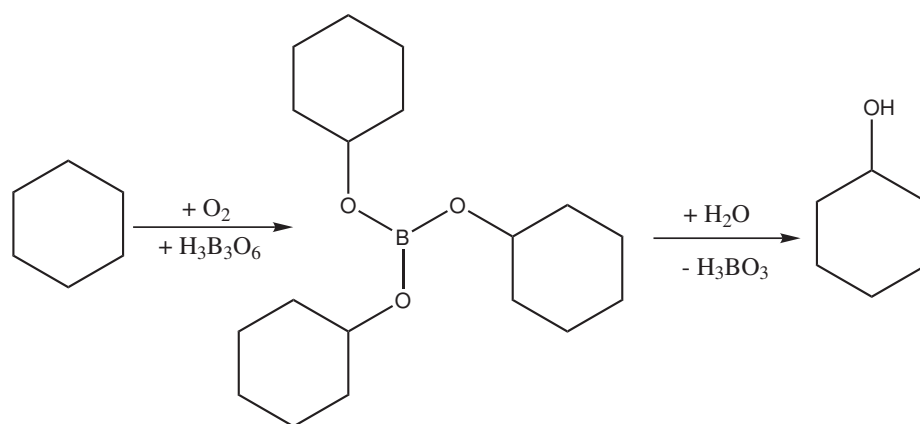


Figure 1.3: Boric acid modification of oxidation of cyclohexane

Cyclohexanol is widely produced by the liquid-phase air oxidation of cyclohexane to cyclohexanol and cyclohexanone. The reaction can be carried out with or without catalyst. Usually a soluble cobalt catalyst is employed. The process route is given in Figure 1.2. The reaction is carried out in a series of stirred tank reactors (Figure 1.4). The cyclohexanol to cyclohexanone ratio in the product stream can be influenced by the choice of catalyst used in the air oxidizers. The intermediate cyclohexyl hydroperoxide and the products, cyclohexanol and cyclohexanone, are more readily oxidized than cyclohexane. Therefore, to maximize the yield, the conversion of cyclohexane in the air oxidizers must be kept low (under 6%). Depending on the conversion, the total yield of alcohol, ketone, and hydroperoxide varies from 70 to 90%. Byproducts of the oxidation include a wide range of mono and dicarboxylic acids, esters, aldehydes, and other oxygenated materials. The cyclohexane oxidation process route is further developed by using anhydrous metaboric acid (Figure 1.3). Metaboric acid is added as a slurry to the first of several staged air oxidation vessels, followed by recovery of boric acid. Refer to [13] for further details.

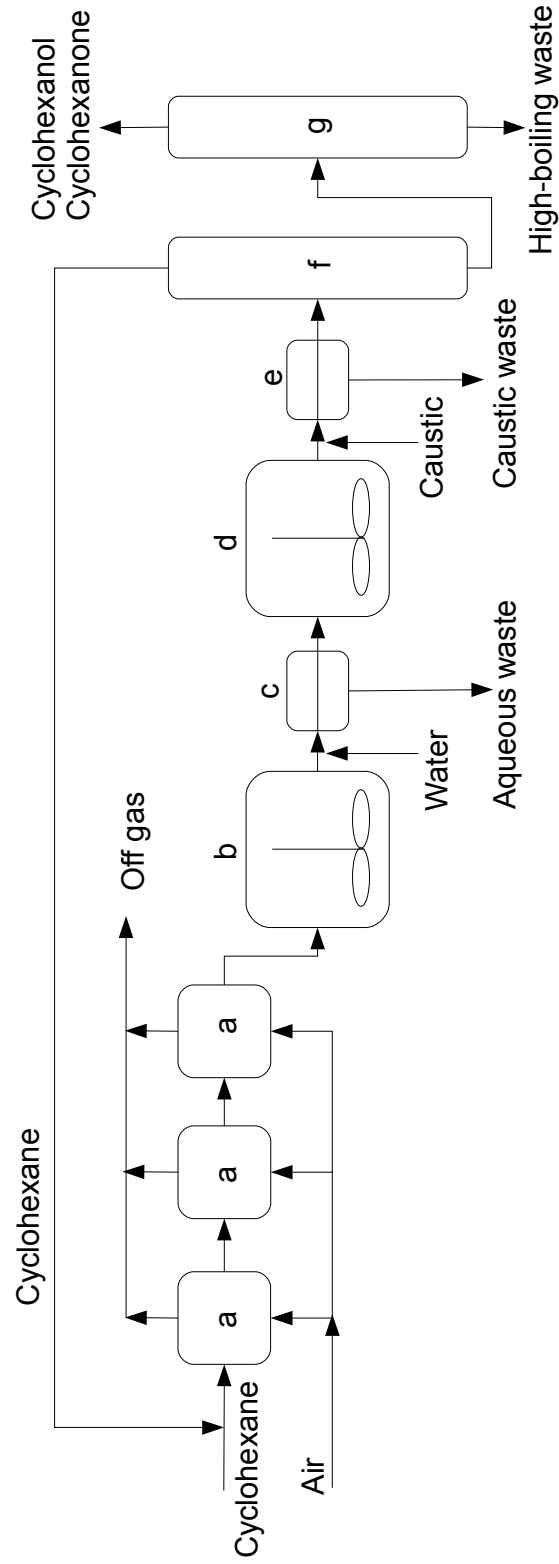


Figure 1.4: Oxidation of cyclohexane; (a) Air oxidizers, (b) Water wash decanter, (c) Decantation, (d) Caustic decomposition reactor, (e) Caustic decomposition, (f) Cyclohexane recovery column, (g) Cyclohexanol/cyclohexanone recovery column

1.2 Hydrogenation of phenol

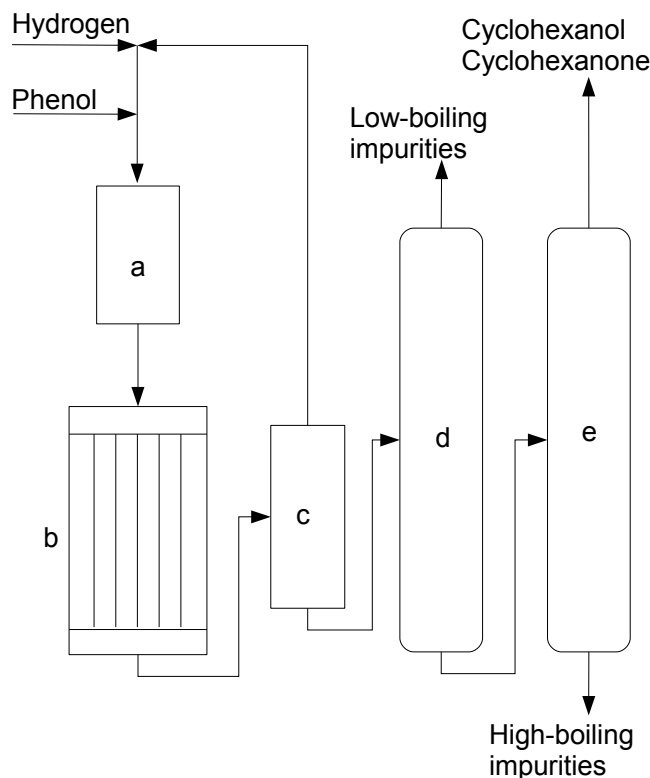


Figure 1.5: Hydrogenation of phenol; (a) Phenol evaporator, (b) Hydrogenation reactor, (c) Condenser, (d) Low-boiler removal column, (e) Cyclohexanol/cyclohexanone recovery column

Cyclohexanol can be produced by vapor or liquid-phase hydrogenation of phenol using metal catalysts [16, 17, 24, 25]. The reaction yields a mixture of cyclohexanol and cyclohexanone and the mixture ratio is determined by the metal catalyst. The commonly employed catalyst is nickel or a nickel alloy with copper, cobalt, or manganese. The catalyst is supported usually by alumina or silicic acid. The hydrogenation reaction can also be catalyzed by a large variety of noble metal catalysts such as palladium, platinum, iridium, ruthenium and osmium. The operating conditions are usually about 413 - 443 K and atmospheric pressure. The reaction gives very high yield 95%-99% at nearly 100% conversion. Very high selectivity for cyclohexanol can be achieved for instance, a Raney nickel catalyst can give a 99.9% selectivity for cyclohexanol [13]. A process flow diagram of the vapor phase hydrogenation of phenol is

provided in Figure 1.5. Phenol is evaporated and hydrogenated in a packed bed catalytic reactor. The product stream is then partially condensed and the vapor stream consisting of unconverted hydrogen is recycled. Cyclohexanol is recovered from the liquid stream using a series of distillation columns.

1.3 Hydration of cyclohexene

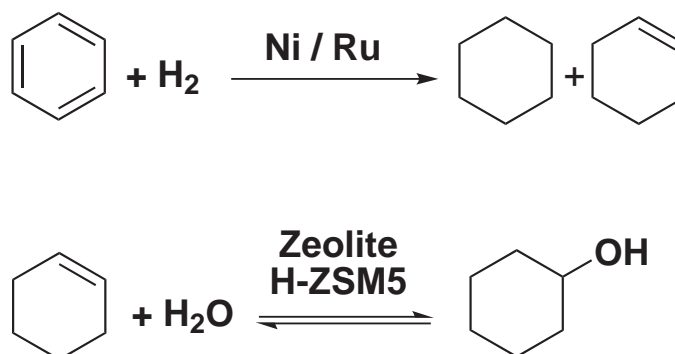


Figure 1.6: Partial hydrogenation of benzene and hydration of cyclohexene

The most recent commercial process route for the production of cyclohexanol is the Asahi process (commercialized in the 1990s) [4–6]. As presented in Figure 1.7, the Asahi process can be subdivided into three steps: the partial hydrogenation of benzene to cyclohexene (since the selectivity is not 100% there is always also cyclohexane produced); the separation of the cyclohexene from cyclohexane and the unconverted benzene; and the hydration of the cyclohexene to cyclohexanol. The reactions are given in Figure 1.6. The first-step, i.e. the partial hydrogenation of benzene, produces a mixture of cyclohexene and cyclohexane [26–30]. The reaction is carried out using a nickel catalyst. The conversion per pass is about 50%, at which point the product consists of about 35% cyclohexene, 15% cyclohexane, and 50% unconverted benzene. The selectivity of this reaction is very sensitive to impurities such as sulfur and iron. Therefore, the benzene must be purified and the hydrogenation vessel is lined with an inert material. The selectivity towards cyclohexene can be improved by the use of Ruthenium-Zinc catalyst [31–35]. The research is highly active on the development of catalysts for the partial hydrogenation of benzene and several research papers have been published since the past two decades [36–40].

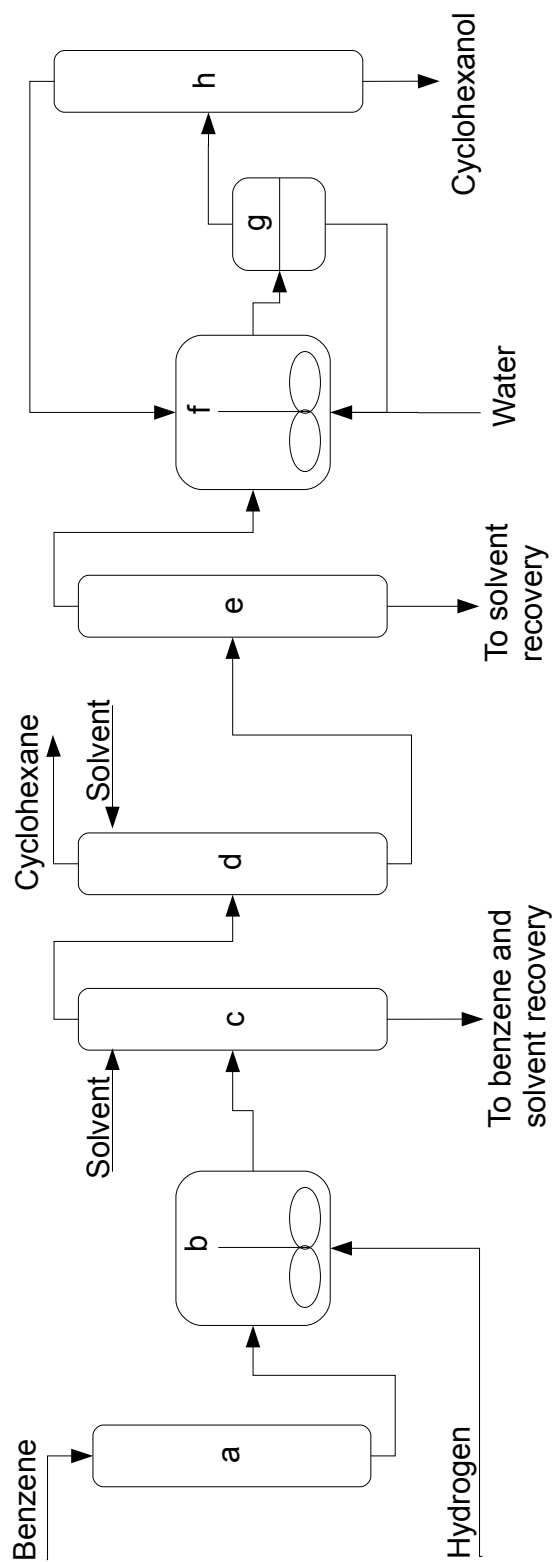


Figure 1.7: Partial hydrogenation of benzene and hydration of cyclohexene to cyclohexanol; (a) Benzene purification, (b) Partial hydrogenation, (c) Separation of uncverted benzene from cyclohexene and cyclohexane, (d) Separation of cyclohexene from cyclohexane, (e) Separation of cyclohexene from extractive solvent, (f) Hydration of cyclohexene, (g) decantation, (h) Recovery of cyclohexanol

The mixture of cyclohexane, cyclohexene, and benzene can not be distilled easily due to close boiling points and the existence of azeotropic mixtures. Therefore, they are separated using two successive extractive distillation columns [13] (Figure 1.7). The cyclohexene purified in this way is then hydrated in a series of slurry reactors.

The hydration reaction is catalyzed by a Zeolite ZSM5-type [5]. Zhang et al. [41] studied various solid acid catalysts such as Amberlyst, Zeolite ZSM5 and mordenite. A Zeolite ZSM5 catalyst with Silica/Alumina ratio of 30-50 gave the best performance with up to 99% selectivity.

The size of the catalyst particle and the Si:Al ratio of the catalyst are designed so that the catalyst remains in the aqueous phase. Water is used several times in excess to the stoichiometric amount (an order of magnitude). The heterogeneous product stream is decanted. The aqueous phase containing the catalyst is recycled back to the reactors. The product cyclohexanol is recovered from the organic phase using distillation and the unconverted cyclohexene-water mixture is recycled back to the slurry reactors. The yield of this process from benzene to cyclohexanol is extremely high, greater than 95%. But the extent of hydration is limited by the equilibrium constant, which would restrict the conversion to about 14% (the details of this limitation will be discussed in Chapter 3).

1.4 Limitations of the conventional process routes

The oxidation process suffers from safety risks due to the build up of explosive mixtures in the air oxidizers. Several accidents have been reported and the most significant one is that of 1974 when an explosion occurred at a Nipro plant in Flixborough, England [42]. The whole plant was destroyed and a total of 28 lives were lost. In addition to the safety risk, the process suffers from high hydrogen consumption. This is because three molecules of hydrogen are required to convert benzene into cyclohexane. Therefore, the energy demand is high as the hydrogen production is energy intensive. If cyclohexanol can be produced from cyclohexene (instead of cyclohexane) the hydrogen consumption can be brought down by one third. The process route is also characterized by low selectivity due to byproducts which is why the conversion is kept very low (less than 6% per pass) so as to maximize the yield. As cyclohexanol is produced in millions of tons per year, the amount of these byproducts is enormous.

Phenol hydrogenation usually suffers from high phenol prices when compared to that of benzene and cyclohexane. The process route has lost its dominating position in the last few decades. Today, there are only a few phenol based processes that operate

economically, especially in the regions where the phenol prices are attractive (e.g., in the United States). Similar to the oxidation process, three hydrogen molecules are required which leads to high hydrogen consumption.

The Asahi process overcomes several of the aforementioned disadvantages. It is safe and requires less hydrogen. In addition to that, the overall yield from benzene to cyclohexanol is extremely high. But the third step of this process route, i.e. hydration of cyclohexene is limited by very low conversion per pass and very low effective reaction rates as a consequence of the strongly limited mutual solubility of the reactants. As a result of this, a large fraction of the organic stream comprising mainly unconverted cyclohexene has to be distilled and recycled back. Therefore, the energy consumption is high.

In recent years considerable efforts have been carried out to improve the direct hydration process route. Steyer et al. studied a reactive distillation process to carry out the hydration of cyclohexene [43, 44]. Even though theoretically it was feasible, very slow reaction rates required extremely large hold ups. Furthermore, the fine size of Zeolite catalyst complicated the practical implementation of the concept. Peschel et al. studied simultaneous hydrogenation of benzene and hydration of cyclohexene in a reactive distillation column [45]. But the selectivity towards cyclohexanol was very low. Solvent based hydration of cyclohexene was studied by several groups [46–52], but these process routes are affected by the need for solvent recovery in the downstream as large amount of solvent has to be used to bridge the miscibility gap. The effect of solvents on the reaction rate could also be an added constraint as for e.g. the protonation of cyclohexene, which has been reported to be affected by some solvents [49–52].

1.5 Indirect hydration of cyclohexene to cyclohexanol

A promising alternative process route was developed by Steyer et al. [1–3] which is the indirect hydration of cyclohexene using formic acid as a reactive entrainer. Esterification of olefins by carboxylic acids have been long known [53–55]. Of all carboxylic acids, formic acid reacts fastest with cyclohexene. Saha et al. [56] reported on experimental feasibility studies of the reaction with formic acid.

Steyer et al. [2] investigated the reaction in more detail, and proposed an alternative process route to produce cyclohexanol. It is a two step process route as illustrated in Figure 1.8. In the first step formic acid and cyclohexene react to produce the ester, i.e. cyclohexylformate. In the second step the ester is hydrolyzed to produce

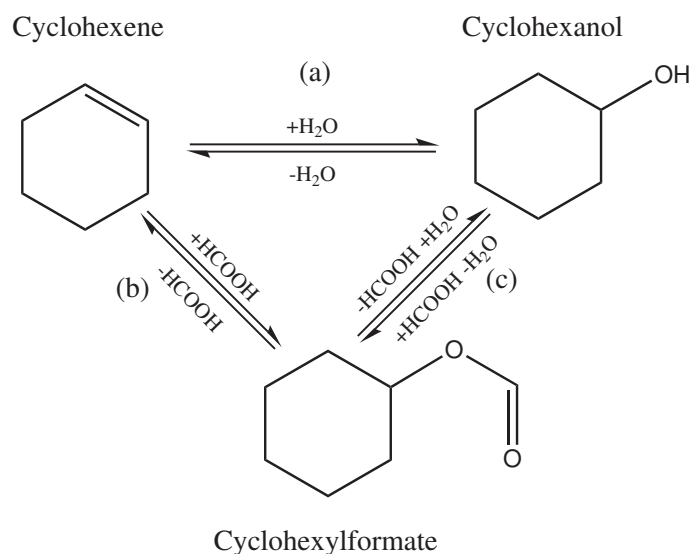


Figure 1.8: Reactions: (a) direct hydration, (b) esterification, (c) hydrolysis

cyclohexanol. The reaction is catalyzed by a strong acid, e.g. the ion exchange resin Amberlyst 15. The reactions are faster compared to the direct hydration and can be conducted at a lower temperature [1]. Substantial amount of work has been done by Steyer et al. [1–3, 57, 58] on the data generation for this new system.

1.5.1 Coupled reactive distillation column process concept

Using residue curve map analysis, Steyer et al. proposed a coupled column reactive distillation as potential process concept [2] for the indirect hydration of cyclohexene. Following the developments of Steyer, Katariya et al. [7, 8, 11] performed model based analysis and simulations that demonstrated the feasibility of the proposed coupled column reactive distillation process concept. The study used the kinetic and thermodynamic data generated by Steyer during the analysis. Kumar et al. [9–11] performed extensive pilot plant experiments and verified the feasibility of the process concept.

The process concept is schematically given in Figure 1.9. The first preliminary design of the columns was derived from reactive residue curve map analysis [2, 3]. The first reactive distillation column performs the esterification reaction and produces nearly pure ester. The reactive stages are placed in the rectifying section where formic acid is fed from the top of the reactive section while the cyclohexene is fed from the bottom of the reactive section. A small stripping section is provided to get nearly pure ester as bottom product. When no inert such as cyclohexane is present in the

feed, the overhead liquid as in Figure 1.9 is totally recycled to the top of the reactive section. In case cyclohexane is present in the feed, the overhead must be decanted and the polar phase rich in formic acid will be recycled totally to the top of the reactive section. The organic phase rich in cyclohexane is withdrawn as distillate. In this case, a partial recycle of the organic phase will enable effective removal of cyclohexane. In the publications [2, 3] a nearly complete conversion of cyclohexene to cyclohexylformate is reported.

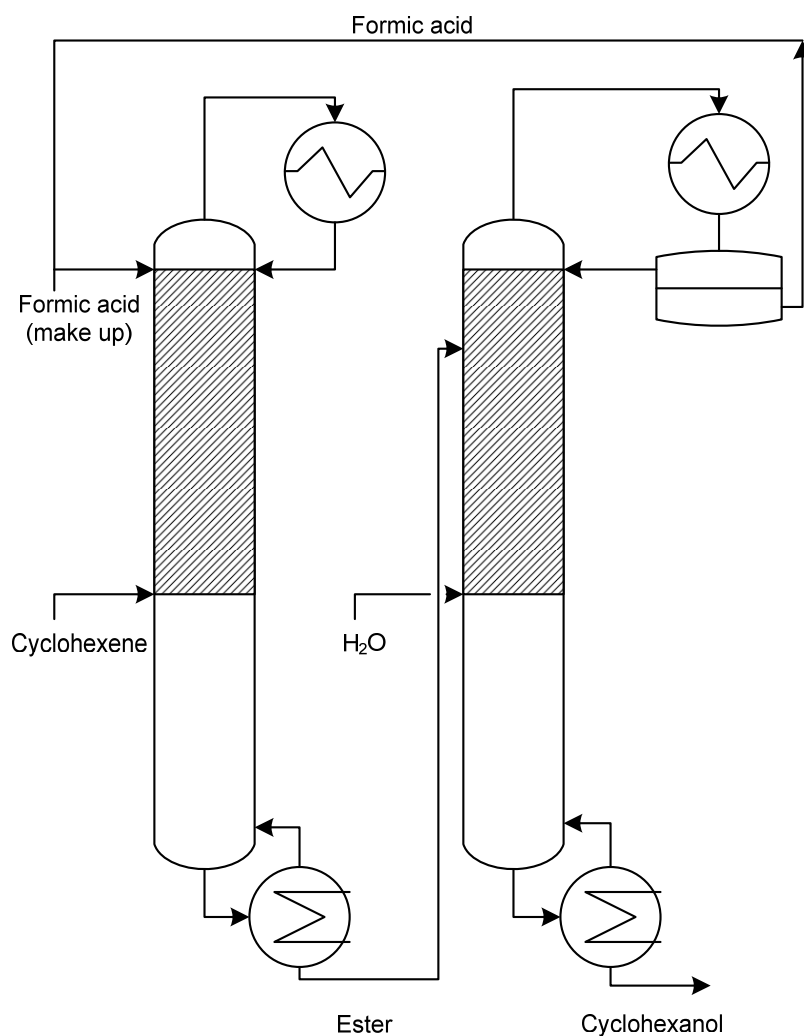


Figure 1.9: Coupled reactive distillation column process concept

The second reactive distillation column performs the hydrolysis of ester. The purified ester from the bottom of the first reactive distillation column is then fed to the top of the second reactive distillation column where the ester hydrolysis to cyclohexanol and formic acid is realized. Water is fed at the bottom of the reactive section. In this column, along with the ester hydrolysis reaction, the reverse of the esterification

reaction, i.e., the back-splitting of the ester to cyclohexene and formic acid also takes place. The hydrolysis reactive distillation column is complicated by competing reactions, distillative separation and liquid-liquid phase splitting. Even though nearly complete conversion is possible, the operation of the column is restricted by multiple steady states to a narrow operating window where a yield of 99% can be realized. Furthermore, the reboiler duty (energy requirement) for this narrow operating window is very high. This could be because of the mismatch between the reaction conditions and separation conditions. The column was operated at vacuum conditions, because lower pressure helps effective separation of cyclohexanol from ester. It also keeps the reaction temperature low so that the decomposition of formic acid is not appreciable. But a low pressure would require very high reflux rates in order to keep appreciable concentration of water in the reactive section. A very high reboiler ratio is also required to purify cyclohexanol in the stripping section while pushing all the ester back into the reactive stages. Due to these reasons, the energy requirement for this process concept was very high.

1.6 Motivation and outline of the thesis

The coupled RD process concept provided nearly complete conversion of cyclohexene to cyclohexanol. However, due to the very high complexity of the process system the operating window was limited by multiple steady states. The hydrolysis step in particular was very complex due to multiple reactions, phase splitting, and mismatch between the reaction conditions and separation conditions.

In order to overcome these limitations, the underlying complexities of indirect hydration need to be understood. A systematic development of process concepts is required to search for other promising alternatives to the coupled reactive distillation process concept. To help a smooth narration of the whole work the thesis is subdivided into the following chapters.

Chapter 2

There could be several sources of multiple steady states exhibited by the present system. Not only with the current system, but in general many liquid-liquid phase splitting systems are known to exhibit these phenomena. Therefore, a generalized nonlinear dynamic study of these liquid-liquid systems is important from a theoretical point of view. The multiple steady states are caused by nonlinearities and feedback present in the system. Kinetic nonlinearities and positive feed back such as

thermal coupling have been extensively studied in the literature as sources of multiple steady states. But an important nonlinearity in such highly non-ideal phase splitting systems, is that of the activity models. Little attention has been given in this regard in the literature so far. This chapter addresses this need using a dynamic model based on Linear Thermodynamics of Irreversible Processes.

Chapter 3

This chapter describes the development of several process concepts from the fundamentals. The developed process concepts cover wider ranges of concentration and temperature. Therefore, extensive experiments have been carried out and described. It includes extensive experimental data generation, parameter estimation, development of process concepts, modeling, simulation and evaluation of process concepts. The challenges, the limitations, and the way forward for the indirect hydration of cyclohexene are addressed.

Chapter 4

This chapter summarizes the work and describes the outcome of the thesis. The outlook part shows interesting directions to realize the indirect hydration process route.

Chapter 2

Complexities of liquid-liquid processes

2.1 Introduction

As discussed in the previous chapter, the coupled column reactive distillation process concept proposed by Steyer et al. [2, 8] was limited by a narrow operating window due to multiple steady states (MSS) in the hydrolysis section. By nature the system is highly non-ideal, and there are several sources of nonlinearities present that could cause multiple steady states. Liquid-liquid phase splitting adds more complexity to the system. The complexities of liquid-liquid reacting systems makes them interesting to study from a theoretical point of view. It is also important that before any further process development, the sources of multiple steady states in these liquid-liquid processes are understood. In this regard, the current chapter presents an overview of different sources of multiple steady states with respect to liquid-liquid systems.

2.2 Literature overview of multiple steady states

MSS are caused by nonlinearities and feedback effects present in the system. Non-linearity in chemical kinetics have been extensively studied in the literature as a source of MSS [59]. Feedback effects such as thermal coupling (coupling of heat transfer rate with arrhenius temperature dependency of reaction rate), chemical reaction coupling (e.g. autocatalytic reactions, biochemical reactions, Belousov Zhabotinsky reaction)[60], and recycle (reactor-separator coupling) have been widely reported in the literature as sources of complex dynamic behavior such as MSS, oscillations and chaos [59]. But an important nonlinearity in highly non-ideal phase splitting systems is the nonlinearity present in the activity model. Little attention has been given in the

literature in this regard. The current chapter addresses the effect of this nonlinearity using Linear Thermodynamics of Irreversible Processes (LTIP) [61].

Many industrially relevant chemical reactions such as e.g. hydroformylation, esterification, alkylation, nitration and hydration often involve two liquid phases (polar and non polar). Therefore, related chemical operations such as extraction, azeotropic distillation, integrated processes such as reactive distillation and reactive extraction, many times deal with two liquid phases. The behavior of such liquid-liquid processes is different from that of the homogeneous ones [62]. The interaction of mass transfer, chemical reaction, heat transfer, surface phenomena such as the Marangoni effect make the modeling and analysis of these systems quite challenging.

These processes have been usually modeled by equilibrium approaches and more recently by non-equilibrium approaches as well. The assumption of phase equilibrium makes the problem/system relatively simple to solve and analyze. In reality, however, processes take place at a finite rate, and thus the use of more realistic non-equilibrium models has increased in the last two decades. Krishna et al. [63] have shown that equilibrium models do not just fail quantitatively but they may also fail qualitatively with regard to stability and attainable regions, e.g. distillation boundary crossing phenomena. With the increasing use of non-equilibrium models, research was started on the effect of mass transfer rate on the behavior of these processes. To mention a few examples, Svandova et al. [64] and Sundmacher and Qi [65] have reported the impact of mass transfer on the qualitative behavior of reactive distillation systems.

The study of the dynamics of these multi-stage multi-phase units is very important for their efficient design and control. It has been reported that many of these processes such as for instance continuous reactive distillation, exhibit complex dynamic behavior [66–68]. For the case of a coupled reactor-separator system, Zeyer et al. [69] illustrated several potential sources of instability.

For non-reacting systems, a number of studies have been performed as well. Morud and Skogestad [70] investigated the effect of mass and energy recycle on the dynamics of the integrated plants. They reported that the behavior of an integrated plant can be very different from an individual unit and that recycle acts as a feedback which also causes complex dynamic behavior of these systems. Gani and Jorgensen [71] reported that the multiplicities are sensitive to design variables, e.g. number of stages in a distillation column. From the above works it can be concluded that several factors can induce complex dynamic behavior in the systems. These earlier works rely on the use of an equilibrium approach. However, when using non-equilibrium models the system can behave qualitatively different. The stable steady states predicted by

equilibrium models can become unstable with even an infinitesimal departure from equilibrium [62]. In the present study a non-equilibrium model is employed, in order to understand the effect of mass transfer nonlinearity (i.e. the activity model, the driving force for mass transfer) on the MSS of the system.

Furthermore, in order to allow for a clear understanding of the dynamics of a multi-stage heterogeneous process, the first step is to understand in detail a single-stage heterogeneous process. Then, the problem can be extended to multiple stages where the effect of recycle and design variables can be analyzed distinctively. A fundamental analysis of a single stage non-equilibrium liquid-liquid system is carried out in this chapter.

The nonlinear dynamics of homogeneous systems have been extensively studied in the past. A recent review on this subject was given by Elnashaie [59]. But when it comes to liquid-liquid systems the studies in the literature are scarce even though works were started as early as 1963 by Schmitz and Amundson [62, 72–74] who made a comprehensive study of a two phase CSTR (with thermal-coupling) and showed the effect of different parameters on the MSS. It was concluded in their works that MSS and sustained oscillations are more likely to exist in a multiphase CSTR than in a single phase CSTR. Schmitz and Amundson were also the first to investigate the two-phase reactors by means of a non-equilibrium model. These investigations covered several issues; particularly they concluded that mass and heat transfer resistances between the phases, whatever small they may be, can play a critical role on the MSS behavior of the reactor. Recently Abashar [75] studied an equilibrium model based on the work by Schmitz and Amundson with a more detailed analysis and showed new dynamic features (e.g. isola, mushroom patterns and study of non-autonomous system) of two-phase systems assumed to be in phase equilibrium. After the pioneering works of Schmitz and Amundson, while a good number of studies have been done on gas-liquid reactors, only a few studies can be traced on the dynamics of liquid-liquid systems that use a non-equilibrium model in their analysis [76, 77]. Most of the models studied in the literature were either non-isothermal models (thermal coupling is well known to be a source of multiplicity) or models with nonlinear reaction rate expressions, focusing on specific applications. To carry out a more general study of liquid-liquid systems, in this chapter a simplified non-equilibrium model based on Linear Thermodynamics of Irreversible Processes (LTIP) [61] is presented and a systematic study of the origin of MSS in non-equilibrium liquid-liquid systems is carried out.

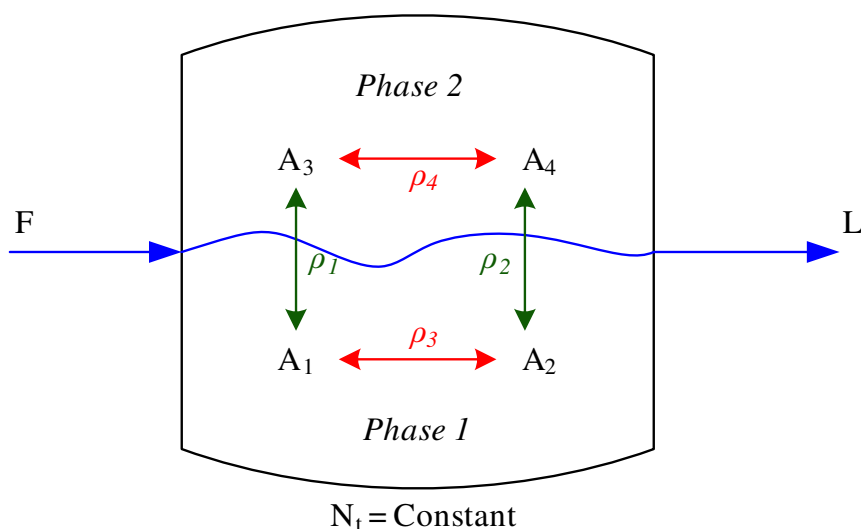


Figure 2.1: Schematic diagram of a Liquid-Liquid CSTR

2.3 Model formulation (LTIP)

2.3.1 Binary system

As a starting point for the fundamental investigations carried out in this study, a hypothetical binary system is considered where the following assumptions are made:

- The system is isothermal
- The total number of moles in the stirred tank remains constant
- There is no change in volume or density of the hold up.

Even though real systems might in some cases deviate significantly from the above assumptions, they are assumed here for a better analysis. Particularly, the first assumption excludes the effects of thermal feed back (thermal coupling) which has been already identified in the literature to be responsible for MSS behavior of a homogeneous CSTR. This makes the present study particularly different from the previous ones which were carried out along with other sources of nonlinearities. The idea here is to separate the sources of multiplicities, understand them individually and then extend the understanding to interactions between different sources of nonlinearities.

Figure 2.1 shows a schematic representation of the stirred tank with two phases, an input stream and an outlet stream. The two components in the first phase are denoted as A_1 and A_2 , and the same in the other phase are denoted as A_3 and A_4 , respectively. Even though they are the same components, they are denoted as entirely

different species which enables us to maintain an analogy between mass transfer and chemical reaction with a common driving force of chemical potential differences based on LTIP [61]. In this approach it is assumed that the second phase always exists, be it infinitesimal in homogeneous conditions. This modeling approach has two main advantages: there is no need for explicit phase equilibrium calculation and it can be readily extended to multi-stage processes without the problem of featuring any discontinuity (caused by phase splitting zones) in the model. The promising features of this approach were discussed in an earlier study by Steyer et al. [78]. This approach is also utilized later in Chapter 3; Section 3.7.2 for phase equilibrium calculation.

2.3.2 A generalized non-equilibrium model for liquid-liquid systems

$$\frac{dN_i}{dt} = F_i - L_i + N_t s_i \quad i = 1, 2, \dots, 4 \quad (2.1)$$

The component material balance for the liquid-liquid system of Figure 2.1 is given in Eq. 2.1. The subscript index 'i' refers to components and the s refers to the source term such as mass transfer or chemical reaction, N_i is the number of moles of component A_i in the tank, F_i is the molar flow rate of A_i in the feed, L_i is the molar flow rate of A_i in the outlet, N_t is the total number of moles in the tank. In this study, N_t is assumed to be constant. Overall there are four molar amounts that can change dynamically. However, only three are independent because of the constant total molar constraint (Eq. 2.2).

$$N_4 = N_t - N_1 - N_2 - N_3 \quad (2.2)$$

The source term in Eq. 2.1 is defined as

$$s_i = \sum_{j=1}^M \nu_{ij} r_j \quad (2.3)$$

$$r_j = k_j \frac{(-\Delta_R G_j)}{RT} = k_j \sum_{i=1}^n -\nu_{ij} \frac{\mu_i}{RT} \quad (2.4)$$

In Eq. 2.3, M is the total number of transitions between species (i.e. phase transfer steps or chemical reactions), r_j is the intrinsic transition rate of process j which is given in Eq. 2.4 and ν_{ij} is the stoichiometric coefficient (Table 2.1).

According to LTIP, the transition rate expressions are formulated with linear dependencies on the species chemical potentials. This formulation is valid for systems

Species A_i	Transition process j			
	1	2	3	4
A_1	-1	0	-1	0
A_2	0	-1	1	0
A_3	1	0	0	-1
A_4	0	1	0	1

Table 2.1: Stoichiometric coefficients ν_{ij} of the transition process

Dimensionless term	Definition
Vector of pseudo mole fractions	$Y = (y_1, y_2, y_3, y_4)$ with $y_i = \frac{N_i}{N_t}$
Real mole fractions in the two phases	phase 1: $x_1 = \frac{y_1}{(y_1 + y_2)}$; $x_2 = \frac{y_2}{(y_1 + y_2)}$ phase 2: $x_3 = \frac{y_3}{(y_3 + y_4)}$; $x_4 = \frac{y_4}{(y_3 + y_4)}$
Dimensionless residence time	$\tau = \frac{t}{(N_t/F)}$
Dimensionless transition rates	$\rho_j = \frac{N_t}{F} r_j$
Stanton number	$St_j = \frac{N_t}{F} k_j$

Table 2.2: Definition of dimensionless terms

with $Ak \ll RT$ [61], where Ak are the affinities of transition. "Affinity" in non-equilibrium thermodynamics refers to the driving force for any transitional process such as, e.g., the temperature gradient for heat transfer. This assumption is usually true for the transfer of heat and mass, while most of the chemical reactions are beyond this linear regime.

In order to formulate the model equations in dimensionless form, a few dimensionless terms are defined in Table 2.2. The Stanton number is a dimensionless mass transfer coefficient, i.e. the ratio of the mass transfer coefficient to the bulk mean fluid velocity; in case of a chemical reaction rate constant this definition would correspond to the Damköhler number.

j	Process	Transition rate r_j
1	$A_1 \Leftrightarrow A_3$	$r_1 = k_1 \frac{(\mu_1 - \mu_3)}{RT}$
2	$A_2 \Leftrightarrow A_4$	$r_2 = k_2 \frac{(\mu_2 - \mu_4)}{RT}$
3	$A_1 \Leftrightarrow A_2$	$r_3 = k_3 \frac{(\mu_1 - \mu_2)}{RT}$
4	$A_3 \Leftrightarrow A_4$	$r_4 = k_4 \frac{(\mu_3 - \mu_4)}{RT}$

Table 2.3: Transition rates

In terms of pseudo mole fractions Y introduced in Table 2.2, the Eq. 2.1 can be expressed as Eq. 2.5 and can be expanded as Eq. 2.6.

$$\frac{dN_t y_i}{dt} = F y_i^F - L_i + N_t s_i, \quad i = 1, 2 \dots 4 \quad (2.5)$$

$$\begin{aligned} \frac{dN_t y_1}{dt} &= F y_1^F - L y_1 + N_t (-r_1 - r_3) \\ \frac{dN_t y_2}{dt} &= F y_2^F - L y_2 + N_t (-r_2 + r_3) \\ \frac{dN_t y_3}{dt} &= F y_3^F - L y_3 + N_t (+r_1 - r_4) \\ \frac{dN_t y_4}{dt} &= F y_4^F - L y_4 + N_t (+r_2 + r_4) \end{aligned} \quad (2.6)$$

By making use of the assumption of constant volume and constant total moles ($F = L$), the Eq. 2.6 can be written in dimensionless form as Eq. 2.7. Here, τ is the dimensionless residence time given in Table 2.2.

$$\begin{aligned} \frac{dy_1}{d\tau} &= (y_1^F - y_1) + \frac{N_t}{F} (-r_1 - r_3) \\ \frac{dy_2}{d\tau} &= (y_2^F - y_2) + \frac{N_t}{F} (-r_2 + r_3) \\ \frac{dy_3}{d\tau} &= (y_3^F - y_3) + \frac{N_t}{F} (+r_1 - r_4) \\ \frac{dy_4}{d\tau} &= (y_4^F - y_4) + \frac{N_t}{F} (+r_2 + r_4) \end{aligned} \quad (2.7)$$

In order to derive the dimensionless transition rates ρ_j , the Eq. 2.4 is written in an expanded form as given in Table 2.3. Here, the chemical potentials are nonlinear functions of the phase compositions as given in Eq. 2.8, where $a_i = \gamma_i x_i$ is the activity.

$$\mu_i = \mu_i^\theta + RT \ln a_i \quad (2.8)$$

Different activity coefficient models are available for non-ideal solutions. For simplicity the ‘one parameter Margules activity coefficient model’ is chosen (Eq. 2.9). In this activity model, A is the thermodynamic Margules parameter. This parameter describes the non-ideality of the system. If $A = 0$, the solution is ideal and the activities are equal to the corresponding concentrations (mole fractions). If $A > 0$, the solution is non-ideal. If $A > 2$, liquid phase splitting occurs.

$$\ln \gamma_1 = Ax_2^2, \ln \gamma_2 = Ax_1^2, \ln \gamma_3 = Ax_4^2, \ln \gamma_4 = Ax_3^2 \quad (2.9)$$

From Eq. 2.8 and Eq. 2.9 the chemical potentials can be expressed as Eq. 2.10 and Eq. 2.11 respectively.

$$\mu_i = \mu_i^\theta + RT \ln\{\gamma_i x_i\} \quad (2.10)$$

$$\begin{aligned} \mu_1 &= \mu_1^\theta + RT(\ln x_1 + Ax_2^2) \\ \mu_2 &= \mu_2^\theta + RT(\ln x_2 + Ax_1^2) \\ \mu_3 &= \mu_3^\theta + RT(\ln x_3 + Ax_4^2) \\ \mu_4 &= \mu_4^\theta + RT(\ln x_4 + Ax_3^2) \end{aligned} \quad (2.11)$$

The species A_1 and A_3 , A_2 and A_4 are the same, and that means the respective reference values of chemical potential are the same ($\mu_1^\theta = \mu_3^\theta, \mu_2^\theta = \mu_4^\theta$). From Table 2.3 and Eq. 2.11 the dimensionless transition rate of process 1, ρ_1 can be expressed as Eq. 2.12.

$$\begin{aligned} \rho_1 &= \frac{N_t}{F} r_1 \\ &= \frac{N_t}{F} k_1 \frac{(\mu_1 - \mu_3)}{RT} \\ &= \frac{N_t}{F} k_1 \frac{(\mu_1^\theta + RT(\ln x_1 + Ax_2^2)) - (\mu_3^\theta + RT(\ln x_3 + Ax_4^2))}{RT} \\ &= \frac{N_t}{F} k_1 \left[\ln \left(\frac{x_1}{x_3} \right) + A(x_2^2 - x_4^2) \right] \\ &= St_1 \left[\ln \left(\frac{x_1}{x_3} \right) + A(x_2^2 - x_4^2) \right] \end{aligned} \quad (2.12)$$

Here, St_1 is the Stanton number of process 1 (Eq. 2.13).

$$St_1 = \frac{N_t}{F} k_1 \quad (2.13)$$

Similarly, the other dimensionless transition rates are formulated and the model is finally given in fully dimensionless form as given in Eq. 2.14 - 2.17.

$$\frac{dy_1}{d\tau} = (y_1^F - y_1) - \rho_1 - \rho_3 \quad (2.14)$$

$$\frac{dy_2}{d\tau} = (y_2^F - y_2) - \rho_2 + \rho_3 \quad (2.15)$$

$$\frac{dy_3}{d\tau} = (y_3^F - y_3) + \rho_1 - \rho_4 \quad (2.16)$$

$$y_4 = 1 - y_1 - y_2 - y_3 \quad (2.17)$$

where

$$\rho_1 = St_1 \left[\ln \left(\frac{x_1}{x_3} \right) + A(x_2^2 - x_4^2) \right] \quad (2.18)$$

$$\rho_2 = St_2 \left[\ln \left(\frac{x_2}{x_4} \right) + A(x_1^2 - x_3^2) \right] \quad (2.19)$$

2.3.3 Separation factor

For the sake of analysis a separation factor is defined (Eq. 2.20), which will reflect the extent of phase transfer taking place in the system. It is an approximate measure how close the system has reached towards equilibrium, in a manner analogous to the Murphree tray efficiency.

$$\eta = \frac{\frac{x_1^F - x_1}{x_1^F - x_1^e} + \frac{x_3^F - x_3}{x_3^F - x_3^e}}{2} \quad (2.20)$$

In Eq. 2.20, x_i^F is the actual mole fraction in the feed of component A_i in the respective phases and x_i^e is the equilibrium mole fraction of component A_i for the given conditions. Note that the separation factor defined this way may sometimes exceed unity as the driving force is the difference in activities rather than the difference in composition and correspondingly the transfer rate is a nonlinear function of the composition whereas the separation factor is linear.

2.4 Simulation

The analysis is restricted only to the phase transfer process. Chemical reactions are presently not considered, i.e. $\rho_3 = 0$ and $\rho_4 = 0$. The parameters used in the bifurcation analysis are given in Table 2.4. The Stanton number in a stirred tank reactor is affected by changes in the residence time (fraction of hold up to flow rate) or by changes in temperature and pressure of the system (rate constant). Thus in practice St_j of a reactor can be changed by manipulating the above factors (flow rate, hold up, temperature and pressure), and obviously a change in St_1 is always associated with a corresponding change in St_2 . It may be practically not possible to change one particular Stanton number independently for a given system. They change linearly with respect to residence time and non-linearly with respect to temperature and pressure. To account for these facts a parameter Kr is introduced so that

$$St_2 = KrSt_1 \quad (2.21)$$

Kr can be regarded in a similar way as the differential selectivity for a parallel chemical reaction scheme as it basically gives the ratio of rate constants of two parallel transitions. In the present analysis Kr is assumed to be constant and this assumption here is reasonable because both of the Stanton numbers change linearly with respect to residence time and for small changes in temperature and pressure. This simplification is made to facilitate the fundamental analysis carried out here for the hypothetical model system, for a practical case the model can be customized according to the process conditions.

parameters	notation	remarks
Margules parameter	A	$A > 2$ phase splitting
Stanton numbers	St_1, St_2	if no chemical reaction takes place $St_3 = St_4 = 0$
feed composition	y_1^F, y_2^F, y_3^F	pseudo mole fractions of species A_1, A_2 & A_3

Table 2.4: Parameters

The Stanton numbers are normalized as given in Eq. 2.22

$$St_1 = \frac{St}{1 - St} \quad (2.22)$$

so that as $\lim_{St \rightarrow 1.0} St_1 = \infty$ and $\lim_{St \rightarrow 0} St_1 = 0$. That way the analysis is bounded between the limits of $St = 0$ and $St = 1.0$.

$St = 0$ represents the case that no phase transfer takes place, the feed is flowing out unchanged, and the steady state is unique (input = output). $St = 1.0$ represents the case that infinite time is given for the phase transfer process, and the exit stream is at equilibrium. Practically there is only one feasible steady state (equilibrium state).

The model is simulated in the dynamic simulation environment DIVA [79]. Its robust solvers and continuation algorithms are especially suitable for carrying out bifurcation analysis. To counter-check the results, complementary simulations were carried out using the open source bifurcation software AUTO [80]. Matlab was used for the calculation of the steady state solutions which served as good initial guesses.

2.5 Bifurcation analysis

Rigorous bifurcation analysis was carried out for different feed conditions but since the parameter space is very large, only the interesting regions in the parameter window of MSS for a fixed feed composition are presented. One parameter continuation was carried out to track the bifurcation diagram and to locate the limit points. Then the effect of different parameters was analyzed by performing a two-parameter continuation of the limit points.

2.5.1 One parameter continuation

At a feed composition of $Y^F = (0.4, 0.3, 0.2, 0.1)$, $A = 2.2$, and $Kr = 1.0$, the model was solved for steady state, and the bifurcation analysis was carried out with ‘ St ’ (Eq. 2.22) as the principal bifurcation parameter. The homotopy continuation method was used in the analysis. The continuation step sizes used in the simulation had a range from 10^{-1} to 10^{-8} .

Figure 2.2, 2.3 and 2.4 illustrates the bifurcation diagram for the aforementioned conditions. Figure 2.2 depicts the effect of the Stanton number on the molar phase fraction ϕ . This system is three dimensional and hence the bifurcation diagrams shown here are projections of one state variable. Therefore, they may look like crossing each other while actually they do not cross in three dimensions. The bifurcation points

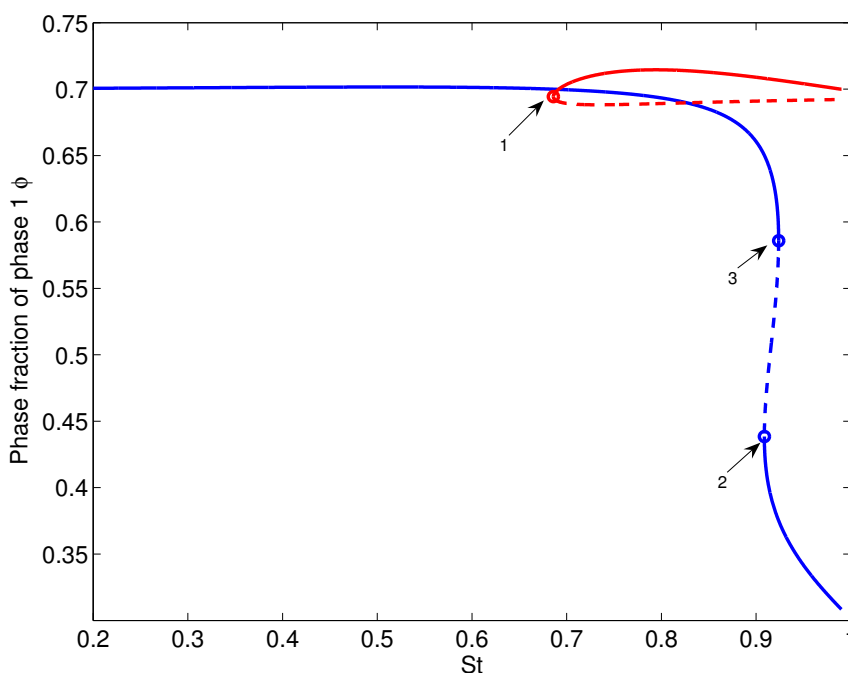


Figure 2.2: Bifurcation Diagram: phase fraction versus St ; red and blue curves indicate different branches of steady states. Solid lines (-) are stable steady states, broken lines (- -) are unstable

and stability of steady states are estimated from the characteristics of the eigenvalues. Three bifurcation points can be observed with a maximum of five possible steady states in a narrow window. The first bifurcation point is at $St = 0.686$ with the onset of bi-stability, the second one is at $St = 0.909$ with the onset of tri-stability and the third one is at $St = 0.924$ with the end of tri-stability.

Figure 2.3 gives the molar fractions of components A_1 and A_3 in their respective phases with St as the bifurcation parameter. It should be noted in the Figure 2.3 that when $St = 0$, only one steady state exists (input = output) and when $St = 1.0$ it seems from the figure that three steady states exist. Two of them are stable and one is unstable. If we observe Figure 2.3 carefully we can find that the two stable steady states at $St = 1.0$ are one and the same, they are exact mirror images of each other ($\phi_{ss1} = 1 - \phi_{ss2}$, $x_{ss1} = 1 - x_{ss3}$, $x_{ss2} = 1 - x_{ss4}$). This basically means that the same equilibrium point can be reached by two different paths during the transient period depending on the initial conditions. Furthermore, these steady states are not identical for even an infinitesimal departure from equilibrium.

The third unstable steady state at $St = 1.0$ is a trivial solution of the problem $x_{ss1} = x_{ss2} = (y_1^F + y_3^F)$. The trivial solution may not be important from a practical

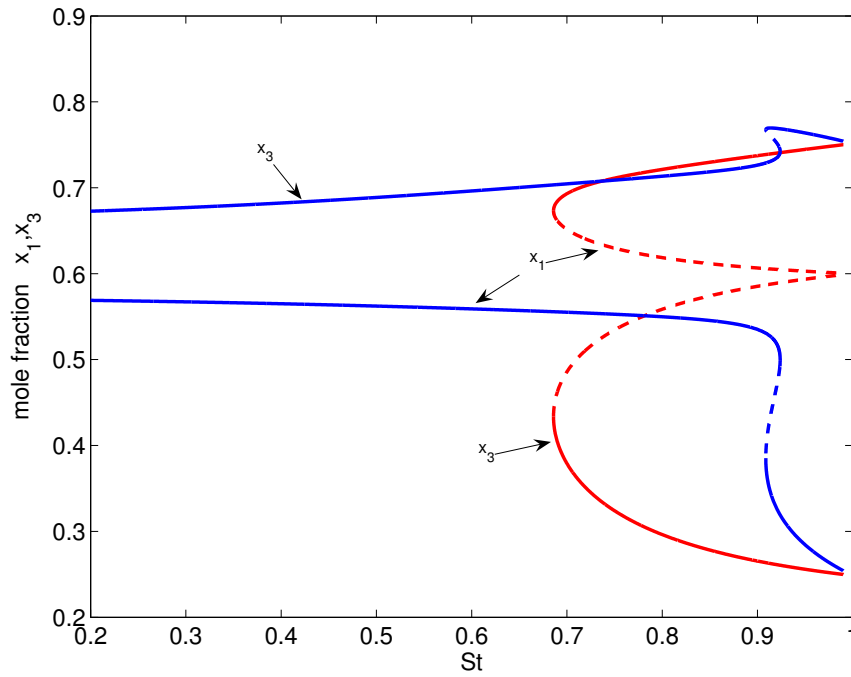


Figure 2.3: Bifurcation diagram: molar fractions of components A_1 and A_3 in their respective phases versus St

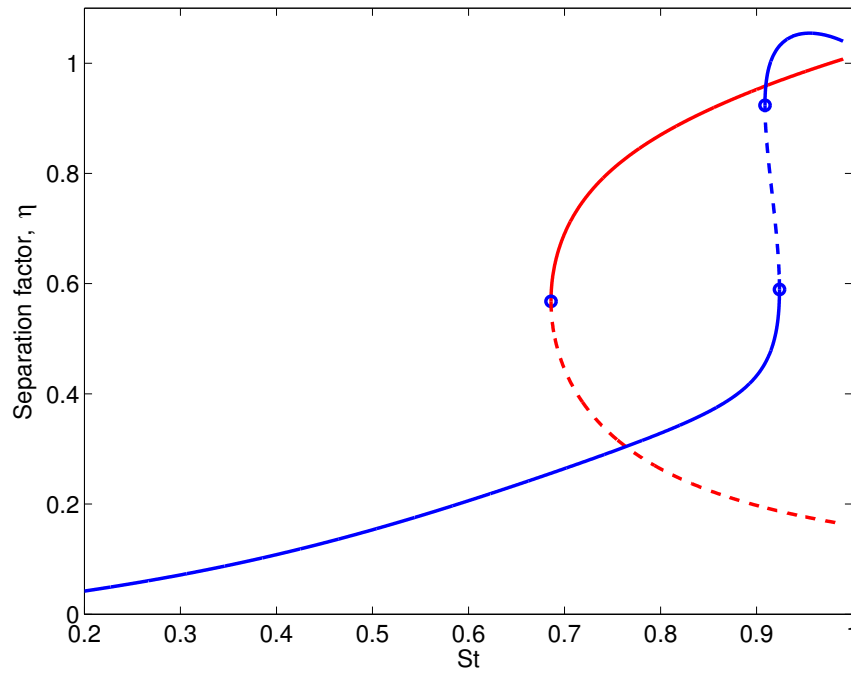


Figure 2.4: Bifurcation diagram: separation factor versus St

point of view, but it is this solution that connects itself to the second stable steady state originating at lower values of St , which means in the non-equilibrium region. It is interesting to note that MSS neither exist at very low values of St , nor at the equilibrium, but only for some intermediate values.

For the sake of analysis we defined a separation factor in Eq. (2.20). Figure 2.4 illustrates the course of the separation factor η of the steady states versus St . As mentioned before the separation factor defined this way may sometimes exceed unity because of its definition, but it gives us an approximate picture of the extent of separation ($\eta = 1.0$ means that the leaving stream is at equilibrium). Different stable steady states have different separation efficiencies, one may be better than the other and this could be important if the system involves competitive parallel reactions where selectivity issues come into play.

2.5.2 Two parameter continuation

Apart from St , the system has many other parameters as given in Table 2.4. The second most important parameter that can potentially influence the system behavior is the thermodynamic parameter ‘ A ’ which characterizes the type of chemical species, and is a strong function of thermodynamic variables such as, e.g., the temperature. Moreover, this parameter also characterizes the qualitative behavior of the system. If $A < 2$ there is no phase splitting, if $A > 2$ there will be phase splitting, and if $A \gg 2$ the difference in equilibrium compositions of the two phases is very large and vice versa (i.e. the closer the A is to 2 the smaller is the difference). For these reasons ‘ A ’ was chosen as the secondary bifurcation parameter and a two parameter continuation of the bifurcation points was carried out. Figure 2.5 gives the two parameter continuation diagram of the three bifurcation points we had previously observed. This analysis reveals further details of the dynamics of this system. The red curve indicates the locus of the first bifurcation point; the blue cusp indicates the locus of the other two bifurcation points.

The parameter space is divided into three regions; only one steady state exists in the lower region below the red curve, while the upper region can feature MSS, i.e. three or five. The cusp indicates a region of five steady states, and it exists within the range $2.0 < A < 2.375$. For $A > 2.375$, tri-stability is not present.

- Region I : The steady state is unique
- Region II : Three steady states (two are stable and one is unstable)
- Region III : Five steady states (three are stable and two are unstable)

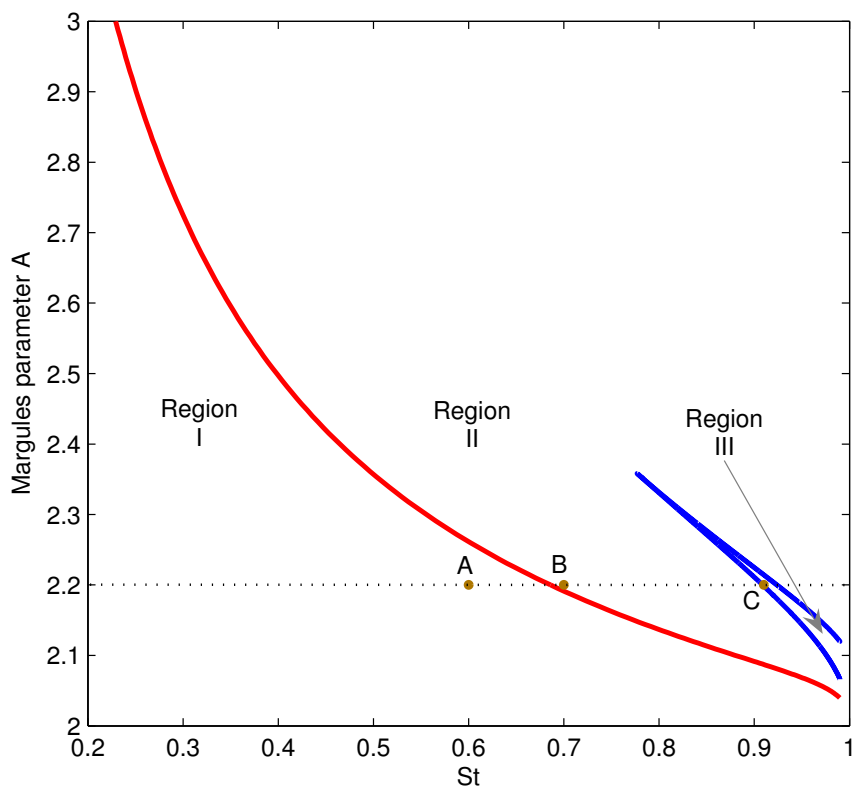


Figure 2.5: Two parameter continuation diagram of the limit points with respect to Margules parameter A , for $Kr = 1.0$, Red line indicates the bifurcation point in the red branch of Figure 2, blue cusp indicates the two bifurcation points in the blue branch of Figure 2.2

It can be observed that there is a critical bound for thermodynamic variables; in this case it is $2.0 < A < 2.375$, within which rich multiplicity exists. The five steady states appearing in this analysis occur within a small window of parameters near the critical solution value ($A = 2.0$). As the value of A is decreased, all the two parameter continuation diagrams asymptotically approach $St = 1.0$ (which means $St_1 = \infty$).

The present study is based on a hypothetical system that follows a simple one parameter Margules type non-ideality. In real systems which are rather to be represented by other activity models such as the NRTL method, the critical parameter analogous to A can be the temperature or any similar parameter that influences the solubility of the system.

The next parameter of interest is the ratio of the Stanton numbers $Kr = St_2/St_1$ (from Eq. 2.21). In real cases the transfer rate constants are based on the characteristics of different species. The effect of this difference on the MSS of the system is shown in Figure 2.6, which is a two parameter continuation diagram with Kr as

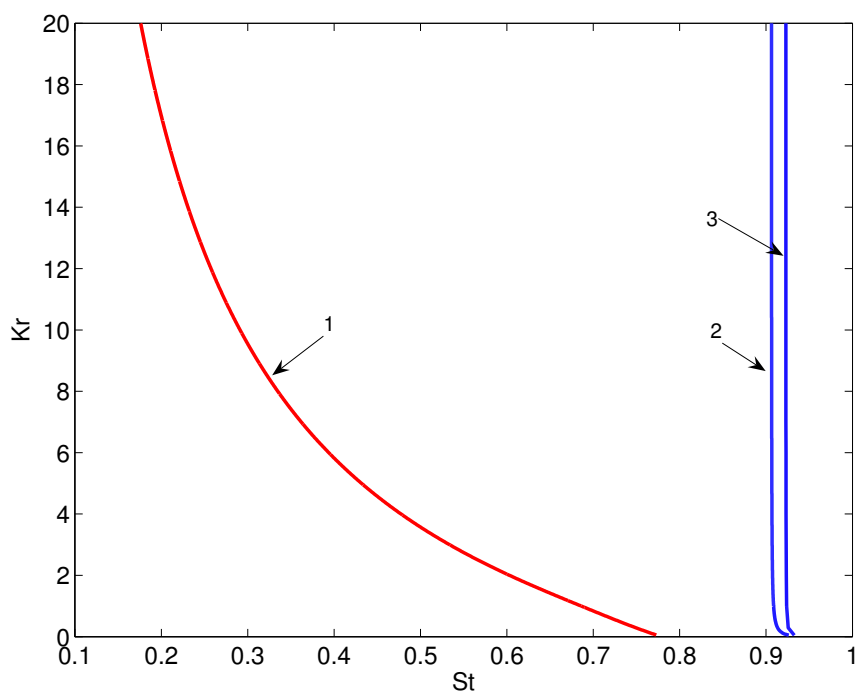


Figure 2.6: Two parameter continuation diagram of the limit points with respect to Kr , for $A = 2.2$. Red curve represents the course of the first bifurcation point and the two blue curves represent the course of the second and third bifurcation points located on the blue branch of Figure 2.2

a secondary bifurcation parameter at a constant value of $A = 2.2$. The red curve indicates the locus of the first bifurcation point, and the two blue curves correspond to the other two hysteresis type bifurcation points. It is quite evident that the first bifurcation point is also sensitive to Kr . Unlike in Figure 3, the second and third bifurcation points do not develop any cusp with Kr ; they are nearly insensitive to any changes in Kr .

To summarize, the two parameter continuation diagrams reveal that the MSS are sensitive to thermodynamic variables and species properties. Temperature and partial miscibility can play an important role in triggering MSS. This work justifies the observation of Schmitz and Amundson [62, 72–74] that MSS are more likely to exist in heterogeneous systems than in homogeneous systems, and mass transfer rates can play a critical role in the qualitative behavior of such systems. There are definitely other parameters which may also influence the system, for instance St_2 may not change linearly with respect to St_1 . Also, the effect of feed conditions may play a role. Since the parameter space is very large, the analysis carried out in this work has been restricted to the most important parameters.

2.5.3 Visualization of multiple steady states

The bifurcation analysis given in the previous section was carried out by making use of the solvers and continuation algorithms in DIVA [79], and counter checked with parallel simulations in AUTO [80] to ensure the consistency of the steady state solutions. In this section a geometrical visualization of how these MSS emerge is illustrated. The model equations of Eq. 2.14 - 2.17, at steady state can be written as

$$0 = (y_1^F - y_1) - \rho_1(y_1, y_2, y_3) \quad (2.23)$$

$$0 = (y_2^F - y_2) - \rho_2(y_1, y_2, y_3) \quad (2.24)$$

$$0 = (y_3^F - y_3) + \rho_1(y_1, y_2, y_3) \quad (2.25)$$

Substituting Eq. 2.23 into Eq. 2.25 yields

$$y_3 = y_3^F + y_1^F - y_1 \quad (2.26)$$

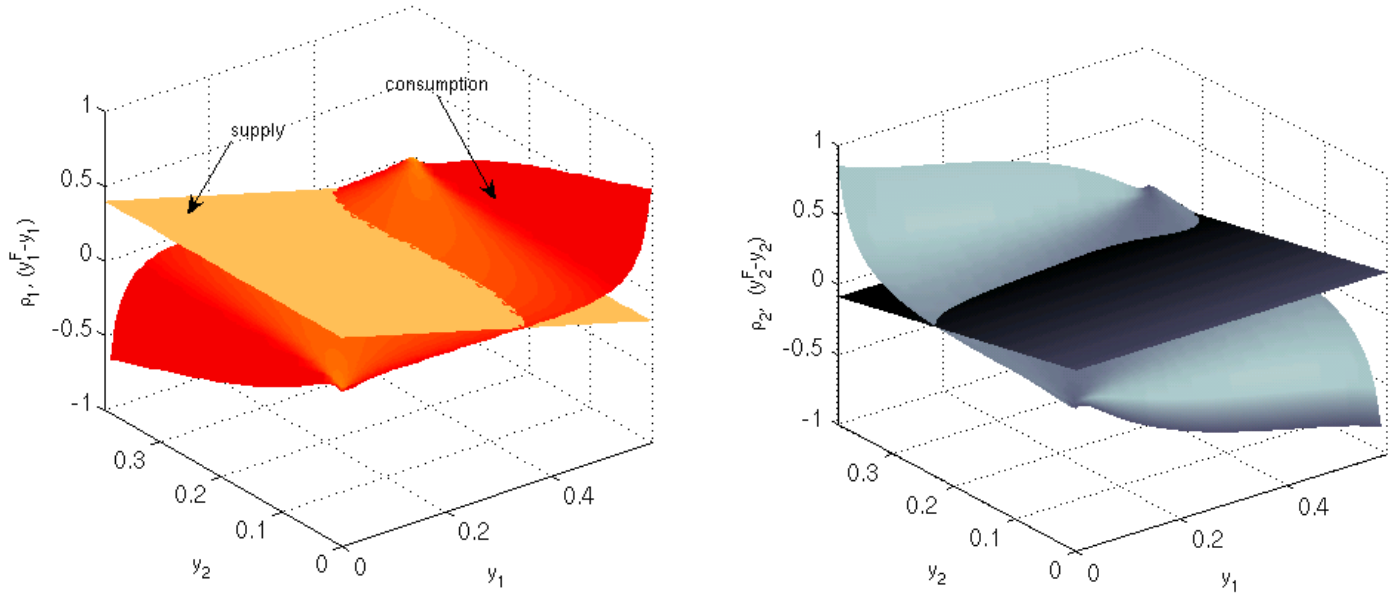
Eliminating the variable y_3 using Eq. 2.26 we are left with two equations

$$0 = (y_1^F - y_1) - \rho_1(y_1, y_2) \quad (2.27)$$

$$0 = (y_2^F - y_2) - \rho_2(y_1, y_2) \quad (2.28)$$

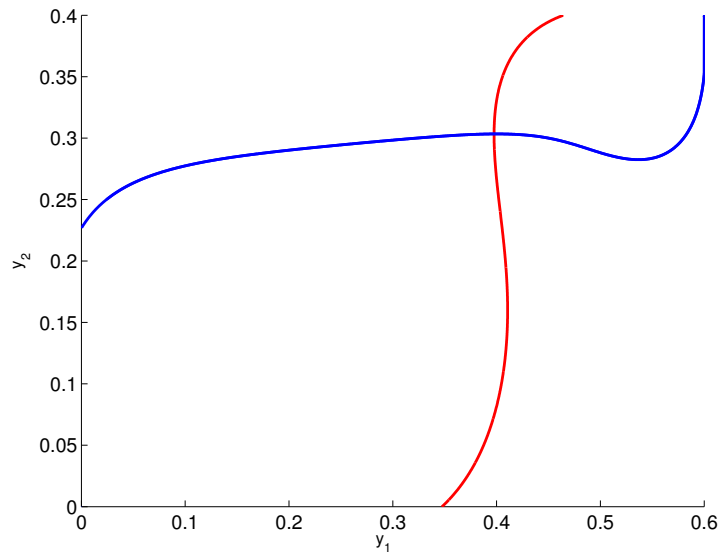
The first term $(y_1^F - y_1)$ in Eq. 2.27 represents the rate of supply of component A_1 visualized as a plane in a three dimensional view (Figure 2.7(a)). The second term $\rho_1(y_1, y_2)$ represents the rate of consumption of component A_1 visualized as a surface. Eq. 2.27 is satisfied at the intersections of this surface with the plane. Similarly, the other equation Eq. 2.28 is represented in Figure 2.7(b). These equations when projected on $y_1 - y_2$ plane (Figure 2.7(c)) make an intersection which is the solution/steady state of the system. In this case only one steady state exists as the parameters lie in region I.

Having explained the approach, a similar procedure can be repeated in the other regions of Figure 2.5. Three different points A, B, C were selected (Figure 2.5). The projections at point A are qualitatively similar to Figure 2.7(c) as it lies in the same region. The projections at points B and C are given in Figure 2.8(a) and 2.8(b) respectively. As predicted, the point B from region II features three steady states and point C from region III features five steady states.



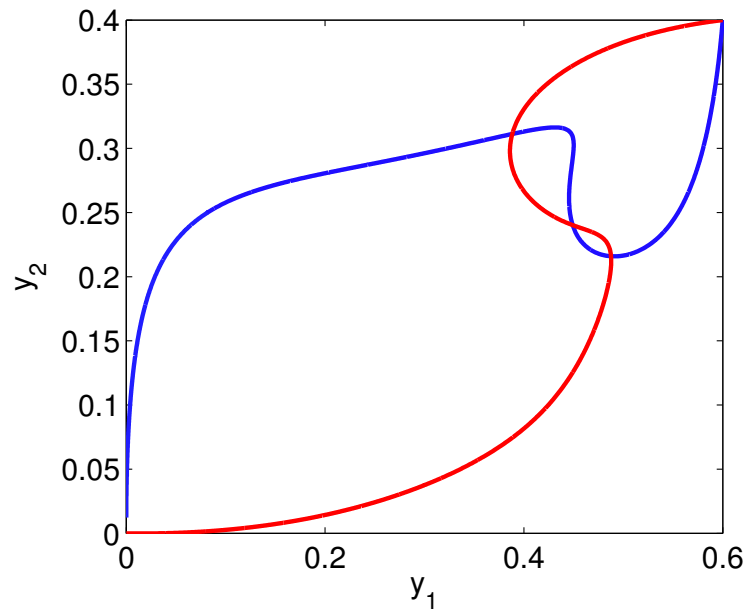
(a) supply $(y_1^F - y_1)$ vs. consumption ρ_1

(b) supply $(y_2^F - y_2)$ vs. consumption ρ_2

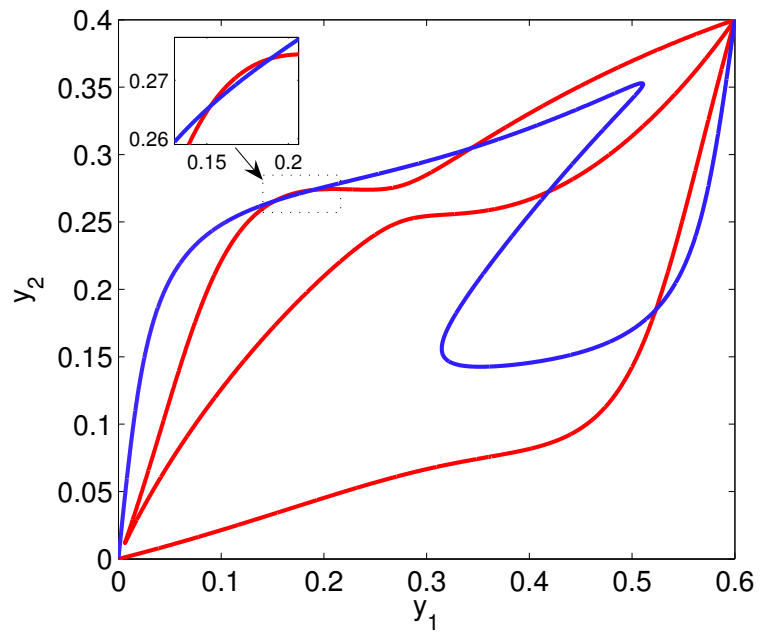


(c) projections of the intersections of source vs. consumptions on $y_1 - y_2$ plane representing one steady state

Figure 2.7: Geometrical representation of steady state, $St = 0.3$, $A = 2.2$, $Kr = 1.0$ (Region I)



(a) projections at point B ($St = 0.7$): three steady states



(b) projections at point C ($St = 0.91$): five steady states

Figure 2.8: Geometrical projections at the points selected in different regions of Figure 2.5

2.5.4 Physical explanation for multiple steady states

In non-linear dynamics, it is well-known that nonlinearity and feedback are the two important factors that cause complex dynamics of the system. Nonlinearity is mainly responsible for steady state multiplicity and feedback can induce oscillations. In more complex cases, oscillations pave the way to chaos. In the present system, the steady state multiplicity is caused by the nonlinearity in the activity models.

As we have not considered any transition process happening within a phase (non-reacting system) there is no actual feedback in the present case. However, the mass transfer from one phase to the other changes the composition of the phases, which in turn affects the mass transfer rate itself in a non-linear fashion. This can be regarded as an internal feedback. In fact, if there is some transition process taking place inside a phase, for instance a chemical reaction, then it certainly acts as a feedback which may induce oscillations or more complex behavior.

2.6 Summary of Chapter 2

In this chapter an overview of different sources of MSS in liquid-liquid systems has been presented. The effect of nonlinearity in the activity model on the MSS has been studied. A simplified non-equilibrium model based on Linear Thermodynamics of Irreversible Processes is presented for liquid-liquid systems. Bifurcation analysis was carried out to examine the effect of the nonlinearity in the activity models on MSS of the system. Unlike the studies that have been performed in previous works such as, e.g., Schmitz and Amundson [62, 72–74] and Abashar [75], the present study analyzes the liquid-liquid systems without the effect of reaction kinetics and thermal coupling. That way, the individual contribution of mass transfer on the dynamical behavior could be investigated. It is observed that a liquid-liquid system is more likely to exhibit MSS when it is in non-equilibrium state than in equilibrium state. This holds true even for an infinitesimal departure from equilibrium. Five possible steady states are reported even for the simplest non-ideal system. The existence of MSS was also verified by geometrical illustration. Two parameter continuation studies reveal that the MSS are sensitive to thermodynamic variables and species characteristics. There are some critical values of thermodynamic variables that can limit the MSS in the system.

Two important conclusions can be drawn from this fundamental study. The first one is that several different combinations of phase compositions can have equal transfer rate (if the chemical potential difference alone affects the transfer rate), which

forms the basis for the existence of MSS in the system. Secondly, the parameters that influence the solubility of the system (e.g. temperature) can play a critical role in determining the MSS in the system and they will be especially important from a control point of view which parameters to adjust as to reach the desired steady state with a preferred phase composition (e.g. in a settler/phase splitter).

The presented model that is based on the fundamental driving force of chemical potential difference with only the most important physics considered helps us to understand the origin of MSS induced in the phase splitting systems. The multiplicity in this case is caused by the nonlinearity in the activity model used to model the mass transfer rate. When the mass transfer model is changed, the behavior will be different because the transfer/consumption surfaces are different.

Chapter 3

Process concepts for the indirect hydration of cyclohexene to cyclohexanol

Direct/indirect hydration of cyclohexene exhibit liquid-liquid phase splitting. This makes these processes challenging as well as interesting to study. In the previous chapter we have learned that such liquid-liquid systems are more likely to exhibit multiple steady states. The chapter listed several sources of multiple steady states and it was found that even the nonlinearity in activity models can act as a source. Apart from these inherent limitations there are further challenges associated with the indirect hydration of cyclohexene. Particularly, the interplay of reactions, phase equilibrium, separation and feed back (recycle streams) should be understood. Therefore, this chapter is dedicated to a systematic development and study of different process concepts so as to realize the indirect hydration process route.

3.1 Introduction

The limitations of the conventional processes for the production of cyclohexanol were discussed in Chapter 1. A promising alternative process route developed by Steyer et al. [1, 2] is the indirect hydration of cyclohexene using formic acid as a reactive entrainer [56]. It is a two-step process route, in the first-step, formic acid and cyclohexene react to produce the ester, i.e. cyclohexylformate. In the second-step, the ester is hydrolyzed to produce cyclohexanol. The reactions are by orders of magnitude faster compared to the direct hydration and can be conducted at lower temperature. A comparison of these reaction rates can be found in the work of Steyer et al. [1]. They also proposed a coupled column reactive distillation process concept to realize the indirect hydration of cyclohexene [2].

Continuing the works of Steyer et al., a coupled column reactive distillation process concept was successfully demonstrated by Katariya et al. using extensive model based simulations [7, 8]. Furthermore, the process concept was validated by extensive pilot plant scale studies of Kumar et al. [9]. Nearly complete conversion of cyclohexene to cyclohexanol was possible. However, due to the very high complexity of the process system the operating window was strongly limited by multiple steady states. The hydrolysis step in particular was very complex due to multiple reactions, phase splitting, and mismatch between the reaction conditions and separation conditions. Furthermore, the energy requirement was very high. In order to overcome these limitations the underlying complexities of indirect hydration need to be understood. Therefore, a systematic development of process concepts is required to search for other promising alternatives to the coupled reactive distillation process concept. In this direction, the present chapter describes the development of several process concepts from the fundamentals. The challenges, the limitations, and the way forward for the indirect hydration of cyclohexene are addressed.

3.1.1 Formic acid vs Acetic acid

Olefins are known to be esterified using carboxylic acids [53–55]. In the literature formic acid (formic acid is comparable to a strong acid because of its high acidity value, i.e., a low pKa value of 3.77) and acetic acid were the first choices to be studied to produce cyclohexanol from cyclohexene [56, 81]. Among all other acids formic acid shows the highest reactivity with cyclohexene. Apart from the acidity, the thermodynamic factors should also be considered. The reactants have a very limited mutual solubility which leads to low effective reaction rates for direct hydration. The addition of a reactive entrainer changes the phase diagram which causes an increase in the solubility as well as an increase in the acidity. These effects leads to a higher effective reaction rate. Therefore, when comparing formic acid and acetic acid, not only the acidity but also the phase behavior of the resulting mixture must be considered.

As would be discussed in the next section, the system is thermodynamically limited by the phase splitting and temperature. The higher the temperature, the lower would be the attainable conversion per pass. The reactive entrainers such as formic acid or acetic acid have a thermodynamic and a kinetic effect on the reaction system. They speed up the overall reaction rate, but nevertheless the attainable conversion per pass remains limited by the operating temperature. The advantage of using formic acid is that at lower temperature (less than 353 K), the reaction rates are faster compared

to the reaction rate with acetic acid. The lower temperature is beneficial from a thermodynamic point of view as it provides a wider window to increase the overall conversion per pass.

In the intensified process concepts such as, e.g., reactive distillation or distillation with side reactors, it is important that the product is separable from the reaction zone. In the case of formic acid, in the hydrolysis step the reactant cyclohexylformate is an intermediate boiler and the product cyclohexanol is a high boiler. This makes the reactive distillation a feasible operation. In contrast, in the case of acetic acid, the ester is the high boiler, and the product cyclohexanol is an intermediate boiler which thus are difficult to be separated with high purity from the reaction zone. For the above reasons formic acid has been chosen. However, in the literature there have been some studies on the application of acetic acid [81]. Recently Kolah et al. [82] have studied the application of acetic acid as a reactive entrainer using advanced reactive distillation process concepts. Thus, while in principle acetic acid could also be an interesting process option, in this work formic acid was selected as the most promising reactive entrainer.

3.2 Thermodynamic analysis

In order to better understand the thermodynamic limitation of the direct hydration reaction, the analysis of the chemical equilibrium is necessary. The thermodynamic models form the basis for the calculation of chemical equilibrium.

3.2.1 Activity model

Activity models are required not only to calculate the chemical equilibrium but are also required for phase equilibrium calculations such as LLE, VLE and VLLE. In addition to that they are also used in the calculation of the reaction rates. An NRTL activity model [83] was used to calculate the activity coefficients required for the afore mentioned kinetics and phase equilibrium calculations. The NRTL model has been chosen because of the availability of NRTL parameters (estimated from VLE, LLE and VLLE experiments) for this system [57, 58]. The NRTL parameters are provided in the Appendix A.

3.2.2 Thermodynamic limitation of direct hydration

The direct hydration reaction shows a limited conversion per pass (maximum 15%). The reason for this limitation can be understood by studying the chemical

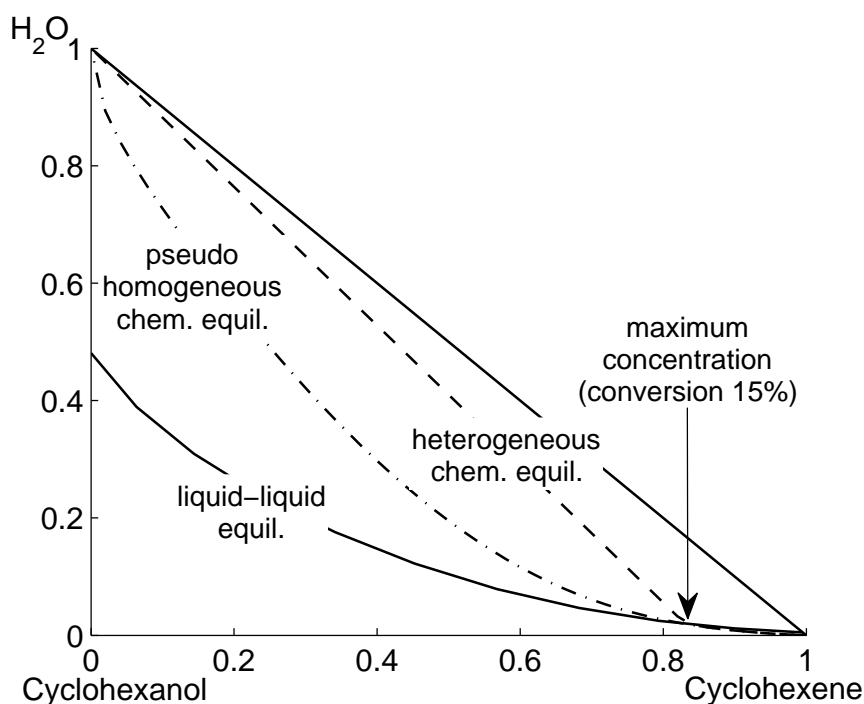


Figure 3.1: Direct hydration chemical equilibrium at 393 K

equilibrium surface as depicted in Figure 3.1. The chemical equilibrium represents the state of the system when infinite time is given for the system to react. It means that the forward and the reverse reaction rate balance each other so that there is no further change in the concentration of the species. In thermodynamical terminology the driving force for the reactions to proceed becomes zero (i.e. there is no further decrease in the Gibbs free energy because of the changes in the concentration). The driving force for the reactions is provided in the second half of the Eq. 3.1 given in the next section (reaction kinetics, Section 3.4). Here, the K_{eq} represents the chemical equilibrium constant, a thermodynamic quantity that can be evaluated from the property data such as the standard heat of formation, standard entropy of formation, specific heat capacity and temperature (refer to Section 3.7.4, Eq. 3.10 for the calculation details of K_{eq}).

The experimental values of the standard entropy of formation, specific heat capacities of the system are available in the literature [1] and are also provided in the Table 3.1. The experimental values of the heat of formation (HOF) data are also available but not for the ester (cyclohexylformate). Steyer et al. [1] estimated the heat of formation of the ester by fitting it to the reaction kinetic experimental data (refer Tables 3.1 and 3.3).

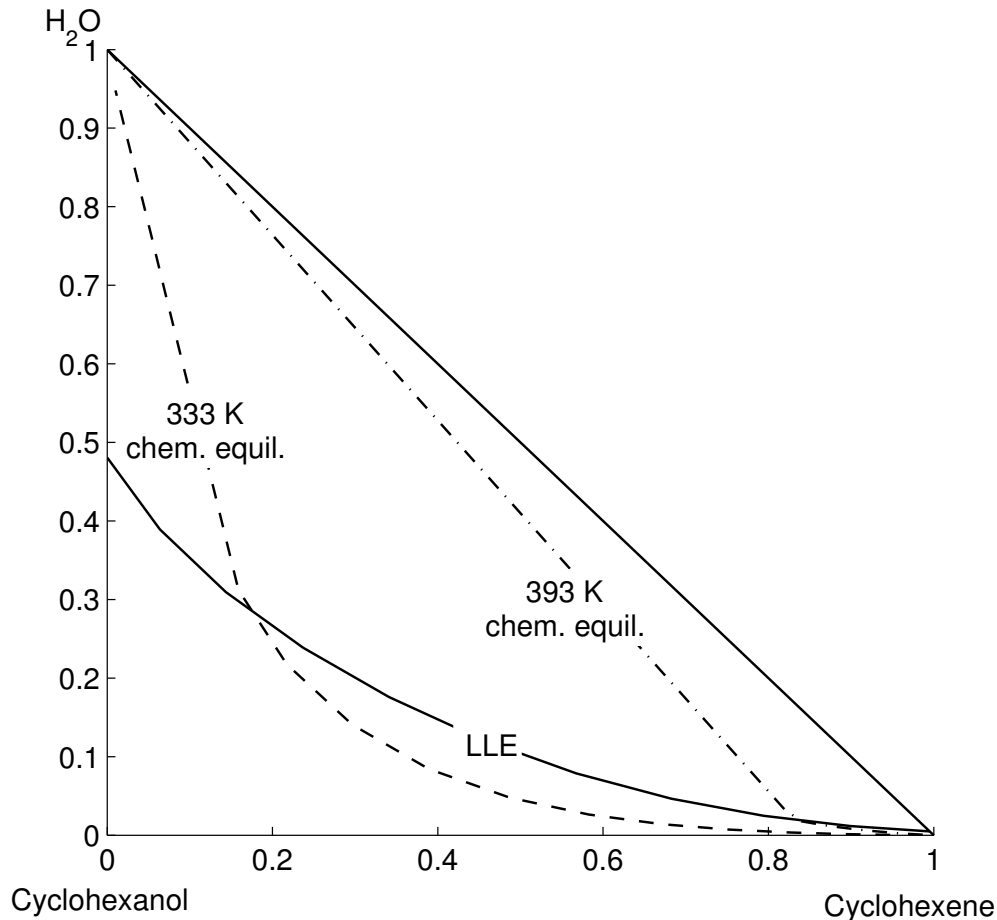


Figure 3.2: Effect of temperature on direct hydration chemical equilibrium

Using HOF values and activity model, the chemical equilibrium can be calculated. Figure 3.1 depicts three envelopes: phase equilibrium, pseudo-homogeneous chemical equilibrium and the heterogeneous chemical equilibrium. The first envelope, i.e. phase equilibrium, is the LLE diagram. The second envelope, i.e. pseudo-homogeneous chemical equilibrium, is defined on the basis of the assumption that the system is homogeneous and the activities are calculated at the overall mole fractions. In other words, it is the hypothetical chemical equilibrium that could have been reached if the system had been homogeneous. The third envelope, i.e. heterogeneous chemical equilibrium, is defined on the basis of the activities obtained from phase splitting calculations.

In the case of direct hydration at 393 K, most part of the chemical equilibrium exists inside the phase splitting zone (refer to Figure 3.1). In such cases where there is an overlap of chemical and phase equilibrium, the concentration of the species

are limited by the phase equilibrium to lie on the bounds of a unique tie line that passes through the intersection of the phase equilibrium and the pseudo-homogeneous chemical equilibrium. Further details on the subject are available elsewhere [68, 84]. No matter how large the reactor is, it would be not possible to get a conversion greater than 15% mol/mol. One possibility to overcome this bottleneck is to influence the phase equilibrium so as to minimize the miscibility gap (for example using solvents). Another possibility is to influence the chemical equilibrium (for example by changing the temperature) so that the intersection point of the chemical equilibrium with the phase equilibrium can be moved towards a higher conversion. This effect is depicted in the Figure 3.2. Lowering the temperature shifts the intersection point so that at 333 K, the conversion can be about four times higher than that at 393 K.

The former option, i.e. the use of solvents has been investigated in the literature, but the choice of solvent is important as the solvent can affect the protonation of cyclohexene that could bring down the reaction rate [49–52]. Many solvents are not inert in hydration conditions especially in the presence of a solid acid catalyst. Asahi investigated several solvents and patented the most promising solvents such as isophorone with a maximum conversion of 21.6% [85]. Recently Shan et al. [46] and Li et al. [47] have further investigated solvents and reported improvements in conversion, but an excessive amount of solvent is required (about 80% mol/mol) which will in turn lead to higher downstream costs. In the case of the other option, i.e. at lower temperature, the direct hydration rate is extremely low. Indirect hydration which follows a different mechanism helps to realize faster reaction rates at lower temperature, thereby increasing the overall conversion per pass.

3.3 Thermo-morphic solvents

As described above, the solvent based process concepts to improve the conversion of direct hydration reaction have limitations. The solvent recovery is energy intensive. From the works of the group of Prof. Behr at the Dortmund University [86, 87], the thermo-morphic effect of some solvent systems can be intelligently used to bring down the separation cost. The idea is to design a solvent based process system, so that the system is homogeneous at reaction temperature and while cooling down to a lower temperature, it splits into two liquid phases. In this way, the reaction occurs in a homogeneous mode without strong mass transfer limitations and then the lower temperature splitting into two phases brings down the downstream separation cost. For example, the reactants or the catalyst can be concentrated in one phase which

can be readily recycled after a decantation. The concept looks ideally suited for the direct hydration reaction provided a good solvent system can be designed.

In this direction, a search for a thermo-morphic solvent system for this direct hydration reaction system has been carried out in the present work. Water and cyclohexene have a large miscibility gap, that it takes a large amount of solvent to make the system homogeneous. Therefore, the solvents must have high solubility for both the components of widely different solubility nature. Furthermore, the solvent must also exhibit a good thermo-morphic behavior with the present system. A manual search of such a solvent is extensive and difficult. Therefore, a three level search was carried out in a systematic manner.

In the first level, a computer aided search is carried out using Hildebrand and Hansen's solubility parameters [88–90]. In this method each molecule is given three Hansen parameters:

- δ_d The dispersion forces between molecules
- δ_p The dipolar intermolecular force
- δ_{hb} The hydrogen bonding between molecules

The systems with like values of Hansen's solubility parameters are miscible with each other. The more different these values are, the more likely are they to exhibit immiscibility. These solubility parameters are available in the handbooks [90] for a large number of industrially relevant solvents.

In the computer aided search, the potential solvents are selected based on the Hansen's solubility distance, i. e., the sum of squares of the difference of Hansen's solubility parameters of the solvents compared to cyclohexene and water. The search narrows down from thousands of solvents to approximately 100.

Then in the second level, these solvents are analyzed based on LLE simulations using commercial softwares such as Aspen plus. At this stage, the solvents that are likely to be reactive under acidic conditions (for example amines, though amines are very good in solubility to dissolve water and cyclohexene) are carefully sorted out. As the binary interaction parameters required for the activity models were not available for many systems considered in the present search, the group contribution method UNIFAC [91, 92] was used to predict the LLE behavior. Studying the LLE solubility diagrams the best solvents are chosen (approximately 20).

In the third level, these solvents are studied for thermo-morphic property using LLE calculations at different temperatures. One of the important criteria during this

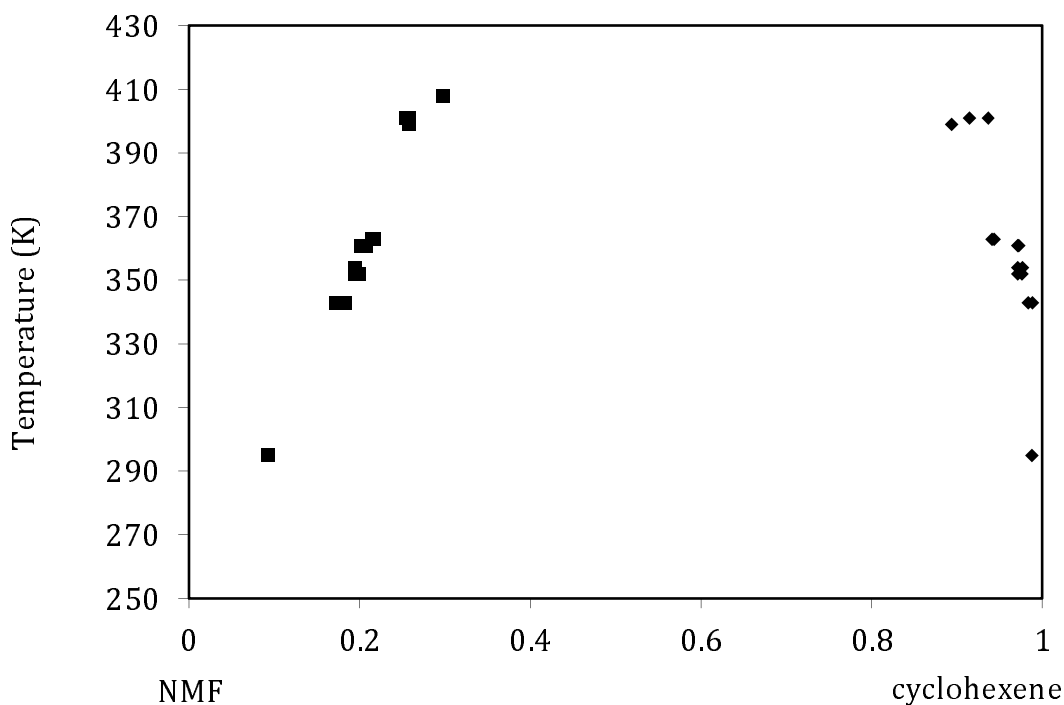


Figure 3.3: Binary LLE diagram, NMF-cyclohexene

search is, that the upper critical solution temperature (UCST) of the solvent with one of the components is within the range of the direct hydration reaction temperature, i.e., 393 K. Even though several better solvents were identified in the second level of search, in the third level many of them exhibited poor thermo-morphic behavior.

The most promising solvents from the third level of search (about 5) are then experimentally investigated. The LLE experimental setup is the same as the batch reactor experimental setup that is described in detail in the section 3.5.4. The sample probe is adjustable in immersion depth so that the samples from both the phases can be obtained. The samples are directly added to the standard solvent (internal standard in GC analysis) dioxane or isopropyl alcohol already present in the vials so that the phase-splitting effect while cooling it down to room temperature is avoided.

The experimental LLE data was agreeing well with the LLE prediction by group-contribution methods such as UNIFAC at room temperature. But at higher temperatures they do not. The deviations of the predicted upper critical solution temperature (UCST) values in some cases were as large as 100 K. This could be because most of the data bases that are used to estimate the UNIFAC parameters are usually in the range of 298-343 K. Therefore, during the experiments, the UCST of the solvents were observed to be far away from the predicted values. A few solvents showed an

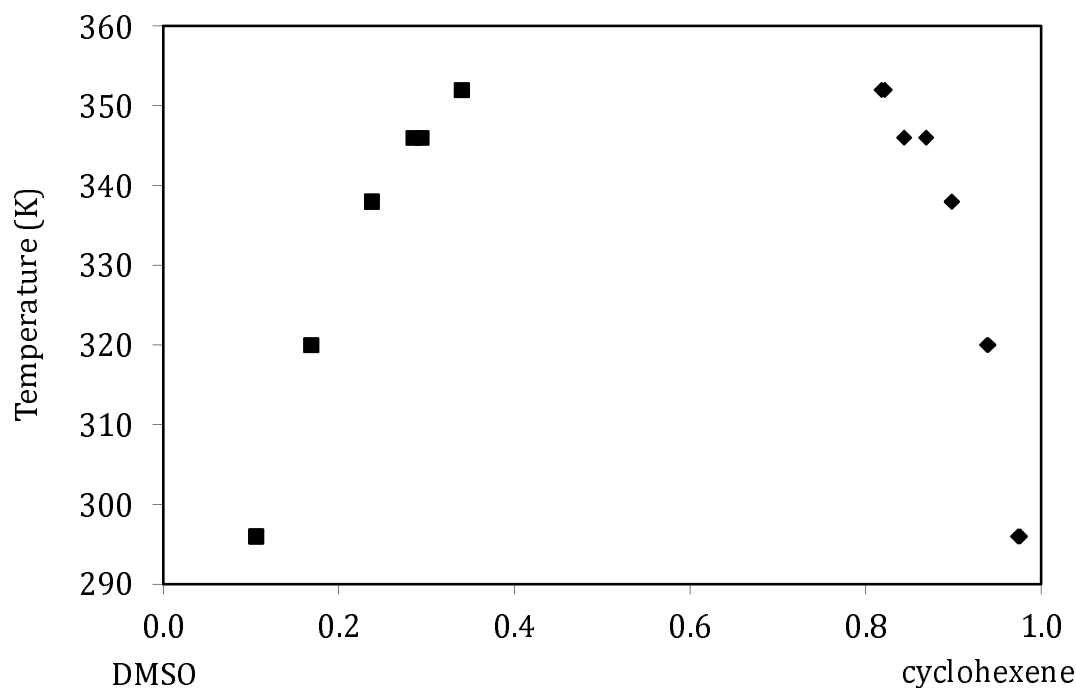


Figure 3.4: Binary LLE diagram, DMSO-cyclohexene

UCST close to the range of the reaction temperature of direct hydration.

One of them is N-methylformamide (NMF), that showed an UCST at around 415 K (about 20 K higher than the reaction temperature of direct hydration, refer to Figure 3.3). As dimerization of cyclohexene could be an issue at higher reaction temperatures, it would not be a good option to chose NMF.

Another solvent that showed a relatively good thermo-morphic property is Dimethyl sulfoxide (DMSO) (Figure 3.4). It showed an UCST at around 360 K (about 35 K below the reaction temperature of direct hydration). DMSO-cyclohexene-water system characterize a type III thermo-morphic behavior. In type III behavior [93], the solvent is totally miscible with one of the components but exhibits a thermo-morphic solubility with the other component. This behavior is desirable as it provides a good potential to recycle one of the reactants (including the solvent). In this case, DMSO and cyclohexene have a large miscibility gap at room temperature and they become completely miscible above 360 K (refer to Figure 3.4). This makes the system suitable for the direct hydration reaction that is usually carried out at 393 K.

The Figure 3.5 represents the ternary LLE experimental data describing the thermo-morphic behavior. Even though the thermo-morphic behavior with DMSO is interesting, the reaction kinetic experiments using Zeolite ZSM5 catalyst showed

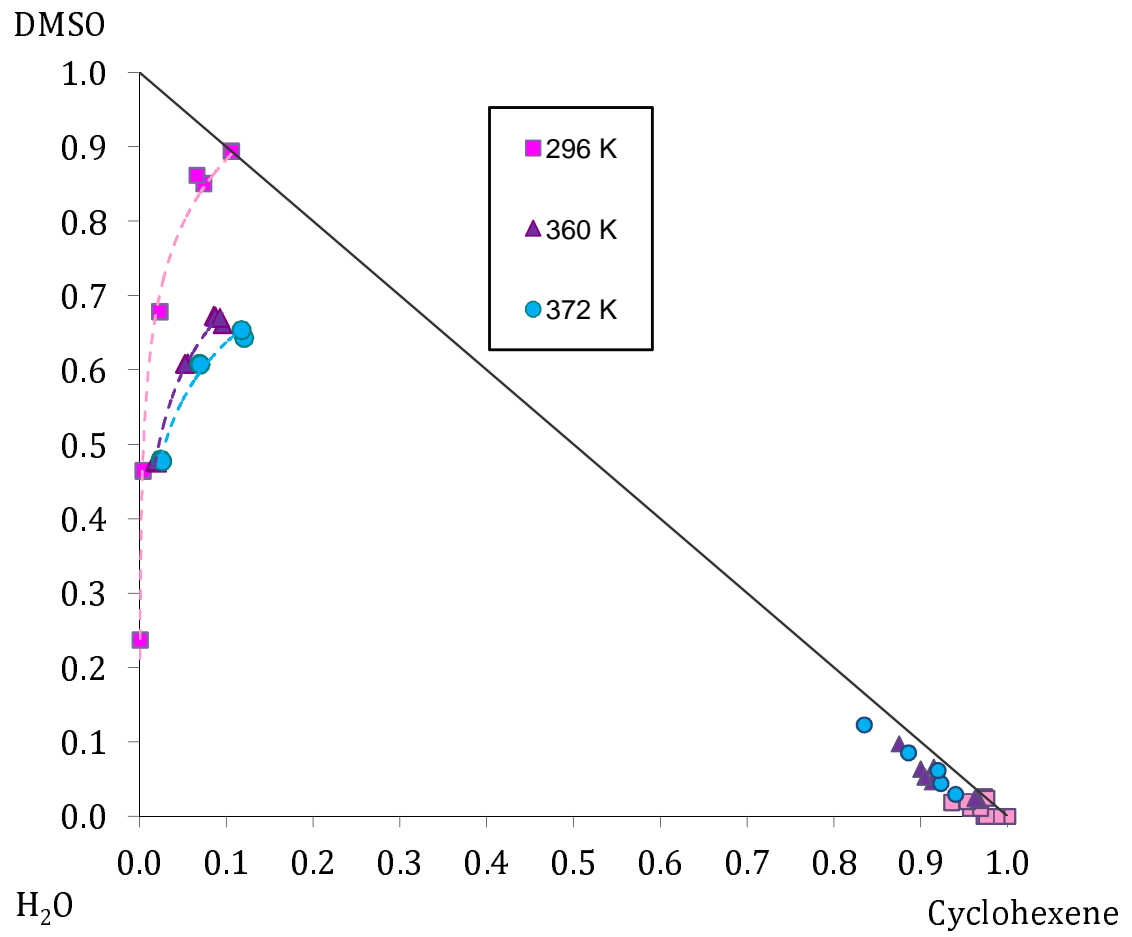


Figure 3.5: Ternary LLE diagram DMSO-cyclohexene-water

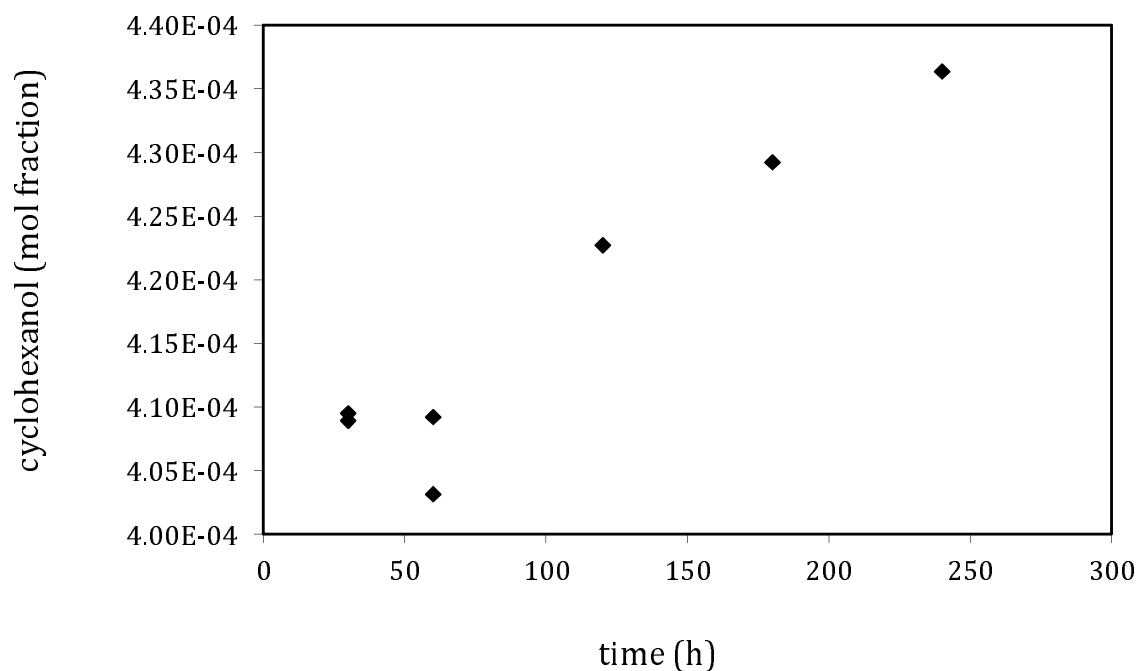


Figure 3.6: Batch kinetic experiment, direct hydration with DMSO as solvent, Zeolite 7g, water 4g, ene 20g, DMSO 50g, 393 K

extremely slow reaction rates (refer to Figure 3.6). This could be because of the effect of DMSO on the protonation of cyclohexene [49–52].

Due to the difficulties in reliably predicting the properties of solvents especially with regard to the effect on the reaction kinetics, the study of the concept of thermomorphic solvents for this system will no longer be pursued. But the above work presented a general strategy to identify suitable candidates which could be beneficial for the researchers working on solvent based methods for direct hydration.

3.4 Reaction kinetics

The generalized Langmuir-Hinshelwood type reaction rate model used to describe all the three reactions [1] is given in Eq. 3.1. The model is valid under the assumptions that a mono-molecular layer of chemical species is adsorbed, an active site can adsorb only one molecule at a time and that there are no interactions between the adsorbing species. The Amberlyst 15 catalyst used in the present work, swells in water and also the adsorption sites dissociate in water. Under these conditions, some of the aforesaid assumptions do not hold. But some experimental studies in the literature have suggested, that the Langmuir-Hinshelwood approach can be used to formally describe these type of solid catalyzed reactions [94]. A recent study [23] also suggests that the Amberlyst catalyzed reactions follow the Langmuir-Hinshelwood type reaction mechanism. The details of the derivation of the reaction rate Eq. 3.1 can be found elsewhere [95]. In general, the reaction rate has been subdivided into two parts. The first part is the heterogeneous part which is catalyzed by the solid catalyst. The second part is the homogeneous part that takes place without any external catalyst (for example, the reactant formic acid itself acts as a catalyst). The second bracket in the rate equation represents the thermodynamic driving force of the reaction.

$$r = \left[m_{cat} k_{f,0}^{het} e^{-E_A^{het}/R_{gas}T} \frac{K_{ads}(A) K_{ads}(B)}{[1 + \sum_i a(i) K_{ads}(i)]^2} + n_{FA} k_{f,0}^{hom} e^{-E_A^{hom}/R_{gas}T} \right] \left[\prod a^{reactants} - \frac{1}{K_{eq}} \prod a^{products} \right] \quad (3.1)$$

Component	$\Delta_f H^0$ ($Jmol^{-1}$)	S^0 ($Jmol^{-1}$)	C_p ($Jmol^{-1}K^{-1}$)	K_{ads}
cyclohexene	-37820	216.33	148.83	0.055396
cyclohexanol	-351831	203.87	213.59	0.92793
water	-285830	69.95	75.39	19.878
cyclohexylformate	-487129	275.5	219.5	3.7942
formic acid	-425379	129	99.84	2.856810 ⁷

Table 3.1: Thermodynamic data and Langmuir-Hinshelwood adsorption parameters of Steyer et al. [1]

In this equation m_{cat} denotes the catalyst amount used, $k_{f,0}^{het}$ and $k_{f,0}^{hom}$ are the frequency factors of the heterogeneous and homogeneous reactions respectively. E_A^{het} and E_A^{hom} are the according activation energies. The K_{ads} are the adsorption equilibrium constants. K_{eq} is the chemical equilibrium constant. The $a(i)$'s are the activities of the chemical species. n_{FA} is the molar amount of formic acid (the homogeneous catalyst). R_{gas} is the universal gas constant, and T is the temperature in K. The kinetic parameters obtained from Steyer et al. [1] are provided in the Table 3.2 as most of these kinetic parameters are used in the simulations.

3.5 Kinetic experiments

The kinetic measurements of Steyer et al. [1] were designed for a reactive distillation (RD) process operating at a relatively low temperature and low concentrations of product. The process concepts that are discussed in this thesis have a wide variation in concentration and temperature ranges. The reliability of the kinetic model for wider ranges of temperature and concentration requires new kinetic measurements and parameter estimation. Furthermore, the experimental heat of formation (HOF) data of cyclohexylformate is not available in the literature. Steyer et al. [1] estimated the HOF of the ester by fitting it to the kinetic experiments. As already mentioned, the experiments were designed to suit the conditions of a low temperature, low pressure reactive distillation operation, and were not designed to accurately estimate the HOF.

Chemical equilibrium is known to be sensitive to the HOF values, this is due to the fact that the HOF exists in an exponential function (refer to Eq. 3.9 and 3.10). An accurate value for the HOF is very important to thermodynamically define not only the chemical equilibrium, but also the enthalpy balances in distillation column modeling. Therefore, experiments specifically meant to accurately evaluate the HOF

Reaction	$k_{f,0}^{hom}$ (s^{-1})	E_A^{hom} ($Jmol^{-1}$)	$k_{f,0}^{het}$ ($molkg_{cat}^{-1}s^{-1}$)	E_A^{het} ($Jmol^{-1}$)
cyclohexene hydration	-	-	7.7083×10^{12}	93687
cyclohexene esterification	1.7089×10^{11}	95467	4.5701×10^{25}	114395
ester hydrolysis	7.2738×10^5	52287	1.2148×10^{16}	100240

Table 3.2: Reaction kinetic parameters of Steyer et al. [1]

have to be carried out.

In order to meet the above requirements, the present section describes the details of experiments carried out and discusses the experimental results that are required for further model based simulation and analysis of process concepts.

3.5.1 Materials

The chemicals used in the experiments viz. cyclohexene, formic acid and cyclohexanol were acquired in synthesis quality (> 99%). The formic acid during the storage might potentially decompose into CO and water. Therefore, it is always analyzed using GC prior to be used in the experiments (usually it contained about 2% water mol/mol). Cyclohexene was distilled twice using a rotary evaporator under vacuum to purify it from high boiling stabilizer. A deionizer of type Millipore Milli-Q was used to produce pure water which was then used in the experiments. The catalysts used were Amberlyst 15 and Zeolite ZSM5. Amberlyst 15 is pre-dried in the oven for 6 to 7 hours prior to use.

The ester cyclohexylformate was not commercially available and therefore had to be prepared in the laboratory. It is prepared by the esterification of cyclohexene and formic acid using Amberlyst 15 as catalyst (approximately 5% w/w). The reaction is carried out in a rotary evaporator for 4 hours at 333 K rotating at a speed of 90 rpm at atmospheric pressure. After the 4 hours period, the temperature was raised to 353 K for another two hours. As the reaction proceeds, the miscibility gap decreases due to the solvent effect of the ester being formed, and after some time the system becomes homogeneous. At the end of the experiment a brownish green solution is obtained which is washed with water several times to remove the residual formic acid that may catalyze the reverse reaction during the purification of ester. After the water wash the liquid remained yellow in color. This is then distilled in a rotary vacuum distiller at a reduced pressure of 90mbar to remove the light boiling cyclohexene. Then the residual mixture is distilled again at 20mbar to remove the high boilers responsible for the yellow color. The amount of these high boilers was in traces only and no significant peak could be observed during GC-MS analysis. The produced ester is then again distilled for about 5 to 6 hours in a total reflux vacuum distiller at 20mbar. At this pressure the vacuum condenser cannot condense cyclohexene, therefore the cyclohexene is condensed by another glass condenser fitted to the exit of the vacuum pump. The cyclohexylformate produced by this procedure has a purity of about 98% with traces of cyclohexene and cyclohexanol (cyclohexanol was formed due to the traces of water that was present with the formic acid).

3.5.2 Choice of catalyst

The direct hydration reaction is catalyzed by strong acids. Studies using sulphuric acid as homogeneous catalyst have been carried out in the literature [5]. The sulphuric acid being a high boiler accumulates in the bottom of the column along with cyclohexanol catalyzing the reverse reaction, thereby decreasing the overall conversion. Furthermore, the sulphuric acid is also known to catalyze unnecessary side reactions bringing down the selectivity [5]. A heterogeneous catalyst is advantageous as it gives a good control to limit the reaction zones. In this work, Amberlyst 15 catalyst was chosen for the experiments. The choice of Amberlyst 15 was made because the kinetic data is already available in the literature as the emphasis of the present work is more on the process concepts development. However, Zeolite ZSM5 catalyst was also used in some experiments so as to compare it with the performance of Amberlyst 15.

3.5.3 Measurement and analysis

Composition analysis was performed by gas chromatography using one of two gas chromatographs. The first of these was a Hewlett Packard 6890 with FID and TCD detectors. The column used is a 30 m \times 250 μm \times 0.25 μm INNOWAX column (it can tolerate formic acid measurement). This column is mainly used for quantification purposes. The other one was a GC/MSD with a 60 m \times 250 μm \times 0.1 μm DB5ms column. This GC is mainly used for substance identification (Type Hewlett Packard 6890 or Agilent 6890N respectively).

The columns were calibrated using samples of known composition. The methods used to perform the GC operation had a temperature ramp from 353K to 473K, to get a better resolution of the peaks. The calibration was repeated several times to ensure the reproducibility of the measurements. Furthermore, separate calibration was done especially to measure the dilute concentrations. Solvents dioxane and isopropylalcohol were used as internal standard during the GC calibrations. The solvent was weighed and added to GC vials before sampling. These vials now containing known amount of solvent were used to take samples from the experiments.

3.5.4 Experimental setup

The reactor is a 100 ml glass reactor from Büchiglas Uster (type Miniclave Drive) designed for pressures up to 10 bar. The schematic diagram is presented in Figure 3.7. The reactor is stirred using a propeller stirrer also from Büchi (using a type

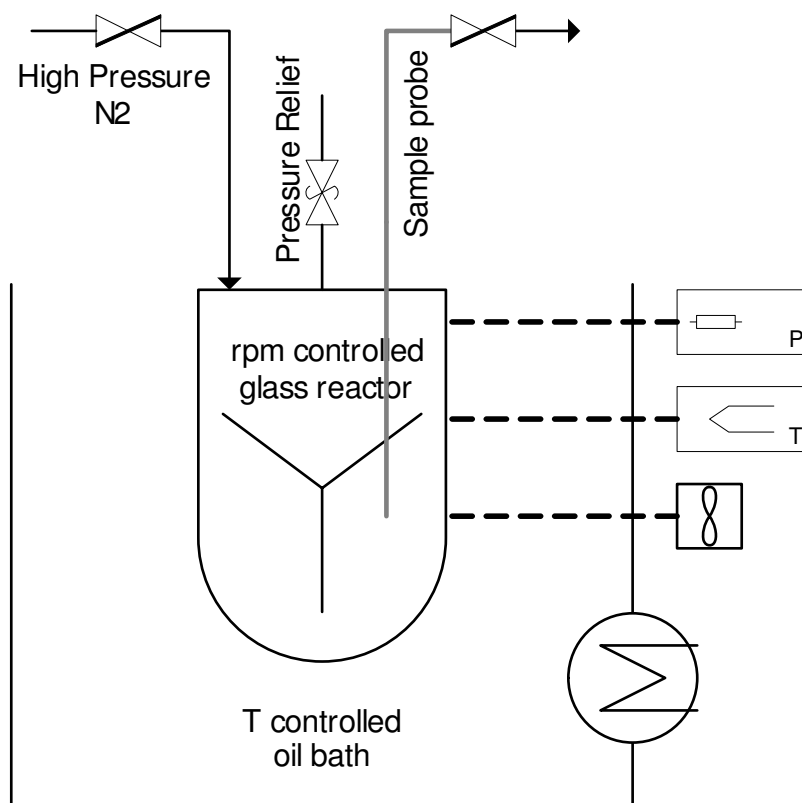


Figure 3.7: Schematic representation of experimental setup.

cc075 controller for adjustment and a hall sensor for stirrer speed measurement of type sm94). It allows adjusting stirring speeds from 200 rpm up to 3000 rpm. The reactor is equipped with a Pt100 temperature sensor and a pressure sensor which are attached to appropriate electronic indicators (Büchi types te94 and pr94 with resolutions of 0.1 K and 10 mbar, respectively). The reactor temperature was adjusted by immersing the reactor in a water or oil bath (type Haake C40) whose temperature was set slightly above the desired reactor temperature and whose temperature control allowed a setting accuracy of 0.1 K. To ensure that the heterogeneous catalyst stayed within the reactor during the experiments the sample probe was shielded behind a wire mesh with 140 μm holes. To be able to pressurize the reactor it was attached to an 8 bar technical nitrogen line by another valve. For a safe operation of the reactor, a safety valve was mounted whose pressure setting can be adjusted. The whole reactor is mounted on a jack so that the depth of immersion can be adjusted. This provision allowed a rapid adjustment of the reactor temperature. Furthermore, when the bath is filled with oil, it makes the handling a lot safer and easier. The oil used was Detherm hot oil from BASF. It is non volatile and can be used safely to heat as high as 573K.

3.5.5 Batch kinetic reaction measurement

Reaction kinetics can be conveniently measured using batch reactor experiments or continuous stirred tank reactor (CSTR) experiments while in principle, a plug flow reactor can also be employed except that the temperature control could be difficult. The reaction rates in the present composition ranges were slow, which would require a very large CSTR. Therefore, batch reactor experiments are used to evaluate the reaction kinetics. Batch reactors are also best suited to measure a wide range of operating conditions.

The batch reactor model equations used in the simulations are given in Eq. 3.2-3.4

$$\frac{dN_t}{dt} = \sum_{j=1}^{NR} \nu_j^T r_j \quad (3.2)$$

$$\frac{dx_i}{dt} = \frac{1}{N_t} \sum_{j=1}^{NR} (\nu_{ij} - \nu_j^T x_i) r_j \quad i=1,2,\dots,NC-1 \quad (3.3)$$

$$\sum_{i=1}^{NC} x_i = 1 \quad (3.4)$$

The reactor is initially loaded with a measured amount of catalyst and then a measured amount of polar phase is added. Then the apolar phase is added. The bath is heated to the required temperature. The reactor is pressurized to about 3-4 bar using high pressure technical nitrogen so that the evaporative losses are not significant. The reactor is immersed in the bath by adjusting the jack. When the reactor temperature has reached the desired level, the stirrer is switched on and immediately the stop watch is started. A sample is also taken so that the initial composition is recorded. Samples of the organic phase alone is taken. This is because it is impossible to get an exact representation of the phase ratio in the kinetic experiments and therefore the overall mole fraction is not measured experimentally. It can, however, be back calculated by simulations using the phase equilibrium calculations with the assumption that the reactions are not mass transfer controlled. The effect of mass transfer was studied by Steyer et al. [1] with several experiments by increasing the stirrer speed and no significant difference at higher stirrer speeds (above 900 rpm) was reported. However, significant attrition of catalyst particles was noticed above 1600 rpm. Therefore, the experiments were performed usually at a stirrer speed of about 1400 rpm.

3.5.6 Parameter estimation

Parameter estimation was carried out to update the kinetic parameters by fitting them to the experimental data. As the reaction kinetic data of Steyer et al. [1] were measured with considerable variation of temperature (298-333K), the activation energies of Steyer et al. [1] were considered reliable and were therefore not updated in the present work. The pre-exponential factors of all the reactions have been updated. In addition to that the adsorption coefficients of ester is also updated.

The experiments are carefully designed so that only one of the reactions dominates at a time. Therefore, the number of parameters needed to be evaluated per simulation was less (a maximum of 4). The parameter estimation packages available in the in-house software DIVA was employed for the parameter estimation problem. The objective function used was a least square sum of the absolute deviations from the experimental data.

3.5.7 Experimental data

The batch kinetic experiments that have been carried out in this work can be categorized into 4 groups. The first set of experiments are long time esterification experiments carried out to evaluate the HOF of ester. The second set are esterification experiments carried out to update the esterification kinetics. The third set are ester hydrolysis and reverse hydrolysis experiments carried out to update the ester hydrolysis reaction kinetics. The fourth set of experiments are comparison of Amberlyst 15 with Zeolite ZSM5.

Some general clarifications are given below regarding the experimental conditions. As the experimental temperatures were not very high, the amount of side products such as, e.g., dimers, was very low (less than 1% by mass). The activity of the catalyst was checked before and after the experiments, and significant deactivation was not observed. Further details can be found elsewhere [1]. The ion exchange resin catalyst is totally anhydrous, as it was pre-dried in an oven for several hours before use. During the startup of experiments, the polar phase is added first to the catalyst. Therefore, in the esterification experiments, formic acid is added first. Since formic acid is only 98% pure, there is always some water present during the esterification experiments.

ref	heat of formation (J mol ⁻¹)
Steyer et al. 2007 [1]	- 487129
Vatani et al. 2007 [96]	- 495520
estimated from current experiments	- 494898

Table 3.3: Heat of formation of cyclohexylformate

3.5.7.1 Experiments to evaluate the heat of formation of ester

As already stated the chemical equilibrium is highly sensitive to the HOF values, because the equilibrium constant K_{eq} is an exponential function of the HOF. Therefore, even a small difference in the estimation of the HOF could largely affect the chemical equilibrium. Steyer et al. estimated the HOF of ester by fitting it to the kinetic experiments, which, however, were not designed to evaluate the HOF, but only to estimate the general kinetics.

It is important to ensure that the value of the HOF is precise, as these values thermodynamically define the state of a system. To achieve this, long time batch kinetic esterification experiments were performed. The reaction is carried out for very long time (about 300 hours) in order to allow the system to approach as close to the chemical equilibrium as possible. The reactions are carried out at a low temperature of 333 K, to avoid the decomposition of formic acid. The experimental setup is carefully monitored so that there is no loss of contents due to leakage. High pressure nitrogen is passed in the reactor to minimize the evaporative losses.

The results of these batch experiments are presented in Figure 3.8. It shows the sensitivity of the chemical equilibrium to the HOF. The Figure 3.8 contains three equilibrium curves. The first one is an LLE phase equilibrium of formic acid-cyclohexene-cyclohexylformate ternary system at 333K. The second and the third curves are chemical equilibrium curves calculated for two different values of HOF of ester. The first value is that of Steyer et al. [1]. The other HOF value is that of Vatani et al. [96] who predicted the HOF value of cyclohexylformate using group contribution methods. These HOF values along with what is estimated from the current experiments are provided in the Table 3.3.

Even though the difference between the HOF predicted by Vatani et al. [96] and that previously estimated by Steyer et al. [1] is very small (8 kJ mol⁻¹) (refer to Table 3.3), the chemical equilibrium is considerably different. The end points of long time esterification experiments are also presented in Figure 3.8. The experimental data

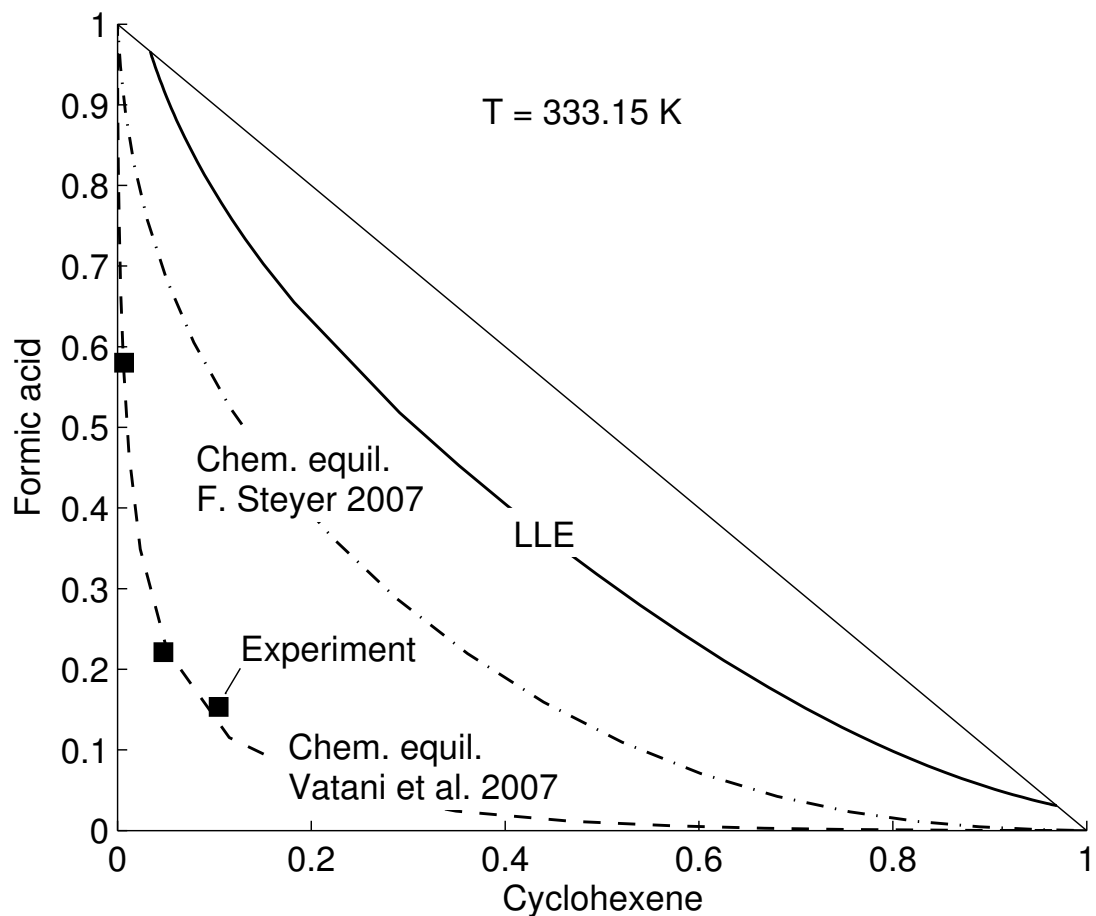


Figure 3.8: Sensitivity of esterification chemical equilibrium to the heat of formation of cyclohexylformate

agrees well with the HOF predicted by Vatani et al. [96].

Due to this sensitivity of chemical equilibrium, it can be observed that there is marked difference in the attainable conversion in a batch reactor predicted by different HOF values. The present long time experiments were exhaustive but necessary for providing an accurate estimation of the HOF of cyclohexylformate. The complete data of long time batch reactor esterification experiments are given in Figure 3.9.

3.5.7.2 Esterification experiments

The esterification of cyclohexene by formic acid is catalyzed by both the solid catalyst and formic acid. Therefore, experiments were performed with and without the catalyst. Due to very less water present (the 2% that came along with formic acid), the other two reactions viz. the direct hydration and ester hydrolysis occur at very slow rates. Therefore, only the esterification parameters have to be estimated. Furthermore, the experiments without the catalyst were separately used to fit the homogeneous part of the kinetics. The experiments with the catalyst were used to fit the heterogeneous part of the kinetics (considering the estimated homogeneous kinetic parameters in the simulation).

In order to have a wide variation in the compositional space, the experiments were conducted at different stoichiometric ratios such as cyclohexene to formic acid in the ratios of 1:1, 1:2 and 1:3. The experimental data are provided in Figure 3.9 and 3.11.

From the Figure 3.9 it can be observed that the reaction rate is faster initially (as predicted by Steyer et al.), but very soon it slows down rapidly. As already stated in the Chapter 1, the experiments of Steyer et al. were designed to suit a reactive distillation operation where the ester is continuously removed from the reaction zone. Therefore, those experiments only covered a narrow concentration range of either at very low ester level (typically less than 0.001 mol/mol) or at very high ester level (typically greater than 0.98 mol/mol).

From the present experiments, it is observed that as soon as the ester level increases, the overall reaction rates were much slower than those predicted by previous kinetics [1]. This could be due to the effect of adsorption of ester on the active sites of the catalyst. Therefore, the adsorption coefficient of ester was also taken into account in the fitting during the parameter estimation.

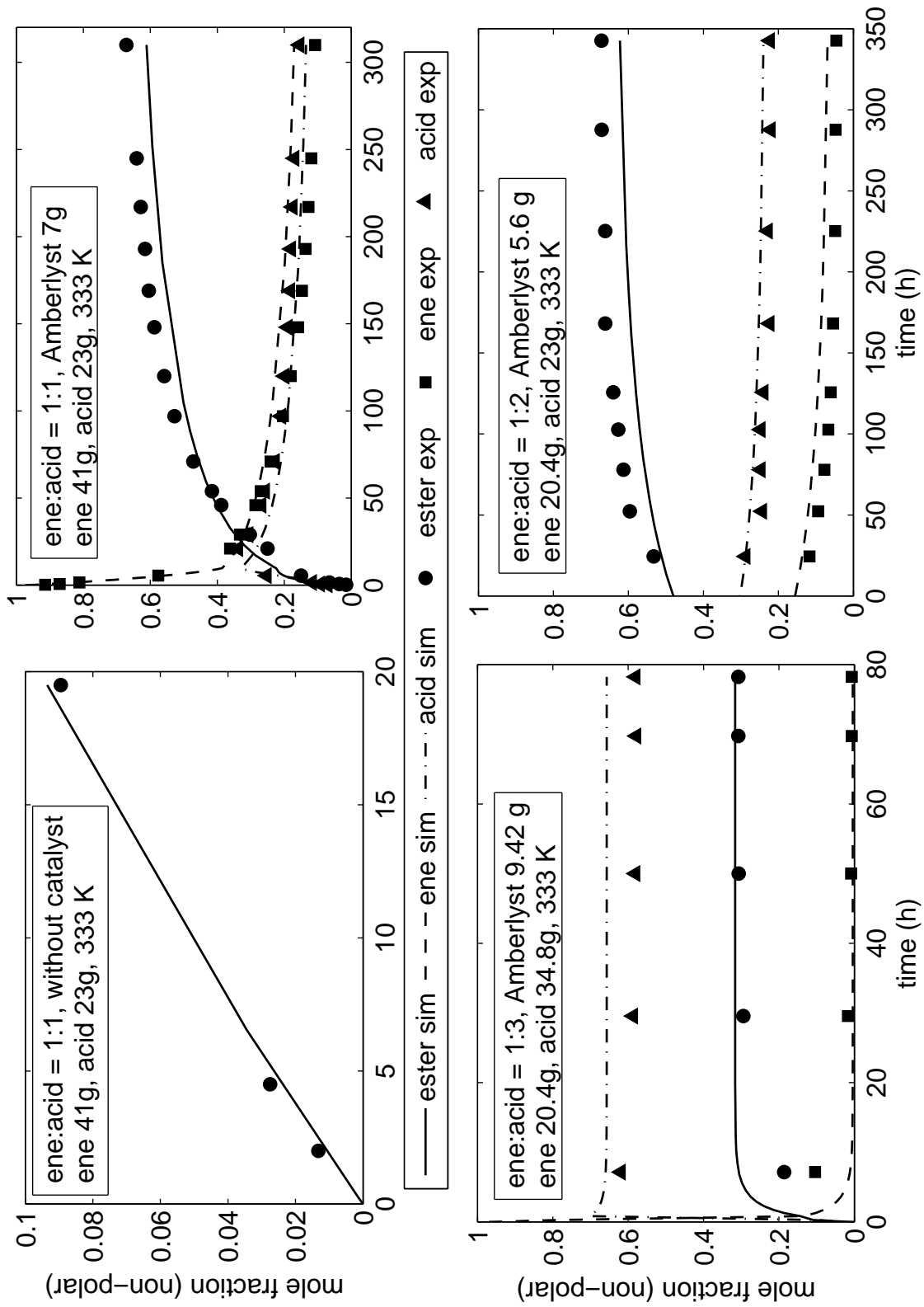


Figure 3.9: Esterification experiments and simulations with fitted parameters.

3.5.7.3 Hydrolysis experiments

Similar to the esterification experiments, the hydrolysis of ester is also performed so that the reaction is carried out at wide variations of compositional space. To fit the kinetic parameters of the hydrolysis reaction two types of experiments were performed. The first one is the hydrolysis of ester, the other one is the reverse of hydrolysis, i.e., the reaction between cyclohexanol and formic acid to produce the ester.

The hydrolysis experiments require a large amount of pure ester. As already stated, the ester cyclohexylformate is not commercially available and therefore has to be prepared in the laboratory through a lengthy procedure. Considering the limited availability of pure ester, fewer hydrolysis experiments were carried out. On the other hand, the reverse hydrolysis experiments of cyclohexanol with formic acid were performed at wide variations of compositional space. The reverse hydrolysis reaction is also faster and therefore more experiments can be performed at different experimental conditions. Similar to the esterification experiments, the hydrolysis experiments have been also performed with and without catalyst in order to distinguish the homogeneous and heterogeneous part of the kinetics. The experimental data with fitted parameters are given in Figure 3.10 and 3.12.

3.5.7.4 Comparison of Amberlyst 15 and Zeolite ZSM5

As discussed later, because of the slower reaction rates, the process concepts require a very large reactor, and there is a need to improve the reaction conditions. To improve the reaction rates, the temperature of the experiments was increased to 343 K. Decomposition of formic acid could be a problem above 333 K [1]. But when considerable amount of water is present, as is the case with certain process concepts, the decomposition of formic acid is hindered [97]. Therefore, higher temperature experiments were performed, so as to analyze the possibilities to improve those process concepts. In addition to temperature effect, the effect of catalyst type was also studied by employing Zeolite ZSM5 in comparison to Amberlyst 15 as this catalyst seemed promising from previous publications [4–6, 41]. The experimental method is the same for both the catalysts, except that the zeolite being fine powder gets dispersed in the liquid and must be filtered out before the samples are analyzed in the GC.

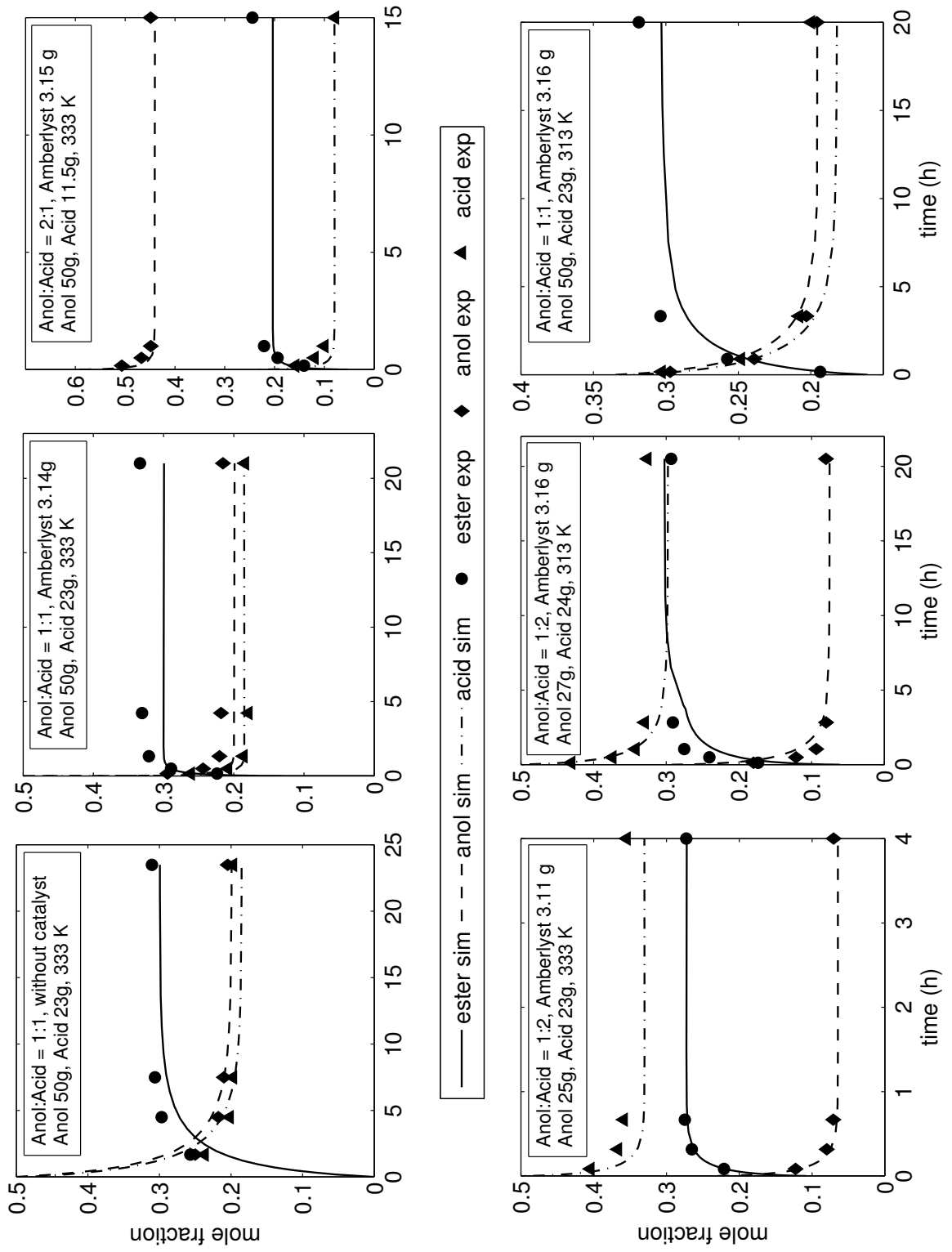


Figure 3.10: Reverse hydrolysis experiments and simulations with fitted parameters

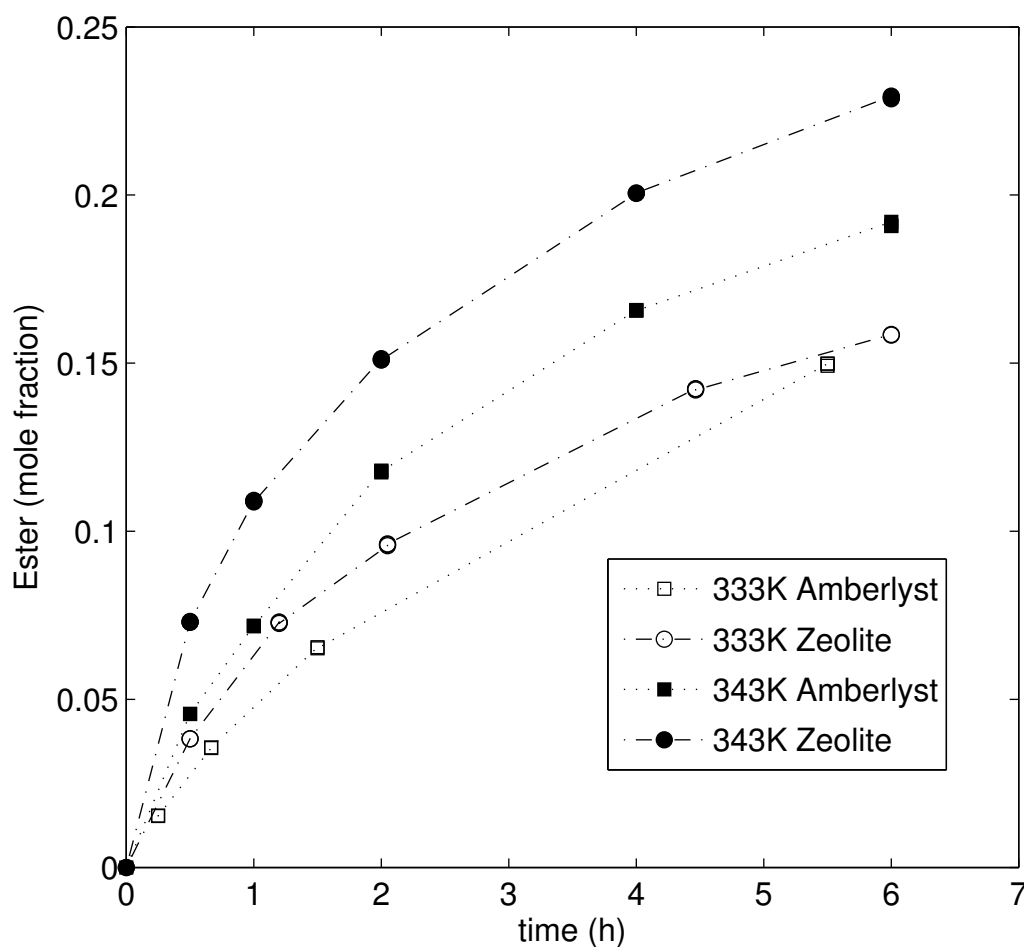


Figure 3.11: Esterification experiments. Zeolite ZSM5 vs. Amberlyst 15 (catalyst 7g, cyclohexene 41g, formic acid 23g)

Figure 3.11 and 3.12 compare the performance of Zeolite ZSM5 and Amberlyst 15. The performance of the two catalysts were similar during esterification at 333 K. At 343 K Zeolite ZSM5 performed better than Amberlyst 15. This could be due to a significant difference in the activation energies of esterification reaction catalyzed by Zeolite ZSM5 and that by Amberlyst 15. Furthermore, there was a dark green high boiler observed in very small amounts during esterification using Amberlyst 15. This discoloration was not noticed with Zeolite ZSM5.

The active surface areas of different catalysts are different. If it is only a factor of the number of active sites then the performance enhancement of Zeolite ZSM5 should be similar for the case of ester hydrolysis. On the other hand, the hydrolysis reaction catalyzed by Zeolite ZSM5 was much slower than that catalyzed by Amberlyst 15 (refer to Figure 3.12).

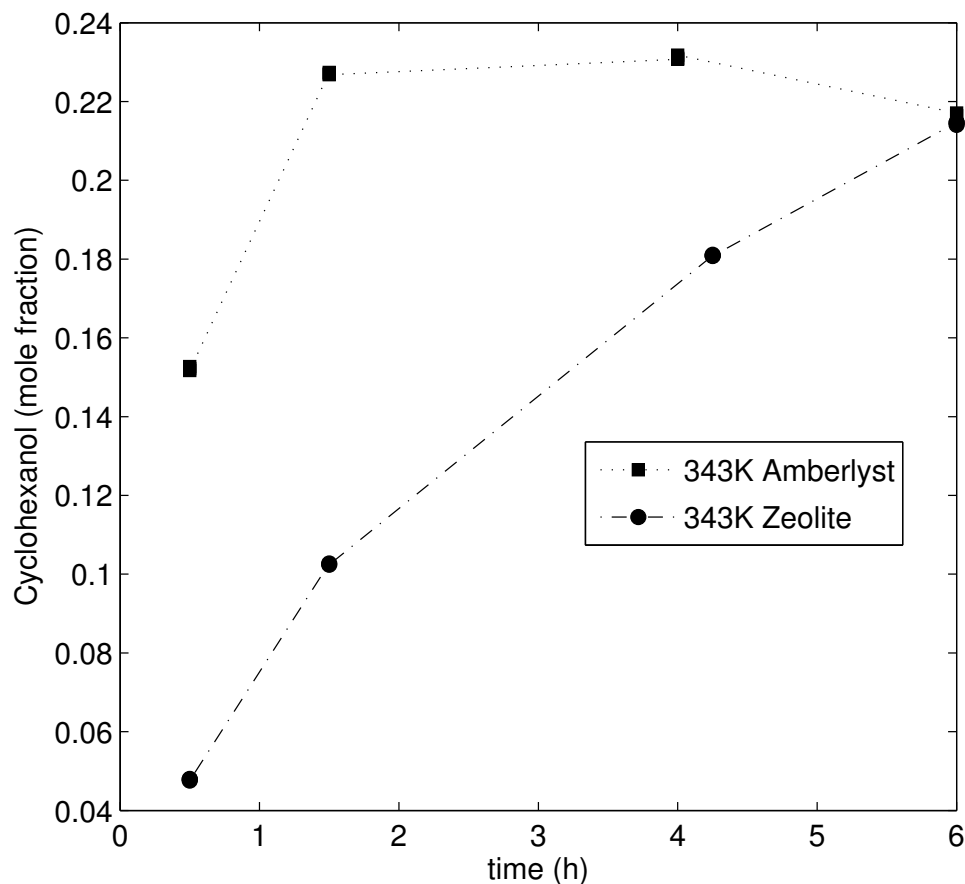


Figure 3.12: Hydrolysis experiments. Zeolite ZSM5 vs. Amberlyst 15 (catalyst 7g, ester 32g, water 9g)

Further studies are needed to understand the important factors that affect the performance of the catalyst. For example, the adsorption of water and other components on the surface of the catalyst can affect the performance significantly. A systematic study is required to design an efficient catalyst for this reactive system. For example, the Si:Al ratio of zeolites can be tuned to modify the hydrophilicity of the surface.

3.5.7.5 Updated kinetic parameters

A list of all the updated parameters is provided in the Table 3.4. In addition to this, the HOF of ester that was also estimated is provided in the Table 3.3. The rest of the kinetic parameters that are used during the simulations are the same as that of the previously estimated kinetics of Steyer et al. (Table 3.2) [1].

Reaction	T range (K)	$k_{f,0}^{hom}$ (s^{-1})	$k_{f,0}^{het}$ ($\text{mol kg}^{-1} s^{-1}$)	$K_{ads}(ester)$
Cyclohexene hydration	313-343	-	$7.708 \times 10^{+11}$	
Ester from cyclohexene	313-343	$2.2157 \times 10^{+9}$	$3.246 \times 10^{+23}$	0.9
Ester hydrolysis	313-343	$8.1296 \times 10^{+3}$	$2.649 \times 10^{+14}$	

Table 3.4: Updated kinetic parameters

3.6 Process concepts: overview and description

In the previous sections of this chapter, the thermodynamic data and reaction kinetic data were presented. These data are used to simulate, analyze and evaluate different process concepts for the indirect hydration of cyclohexene. This section presents an overview of the different process concepts studied in this thesis.

The process concepts can be categorized under two broad sections viz. RS process concepts and R1S1+R2S2 process concepts as represented in Figure 3.13. Figure 3.13 also includes the Asahi process concept as a reference. Here RS refers to reactor section followed by separator section. R1S1+R2S2 refers to two reactor sections and each of them is followed by a separator section. The concepts will be explained in detail in the next sub sections. The benchmark reference process, i.e. the Asahi direct hydration process concept, is explained first and then the two categories of process concepts for indirect hydration are explained.

In the Asahi process, the cyclohexene is purified prior to the direct hydration. As the present work focuses on an evaluation of process alternatives to the Asahi process (the hydration of cyclohexene), a pure cyclohexene feed stream is assumed. Cyclohexane is the most likely inert that could be present in the feed stream. The influence of cyclohexane adds another dimension of complexity to the design problem. It would require a separate study to address this case, and it is not the focus of the present work. Nevertheless, some potential directions of this case are addressed in the outlook part of this Thesis (Refer to Section 4.2).

3.6.1 Asahi benchmark

As already discussed, the Asahi process for direct hydration utilizes a zeolite catalyst of type ZSM5 [4–6, 41]. The catalyst is a fine powder so as to have greater surface area and active sites. Still, a very large amount of catalyst must be employed in a slurry type reactor to achieve appreciable reaction rates. The amount of water

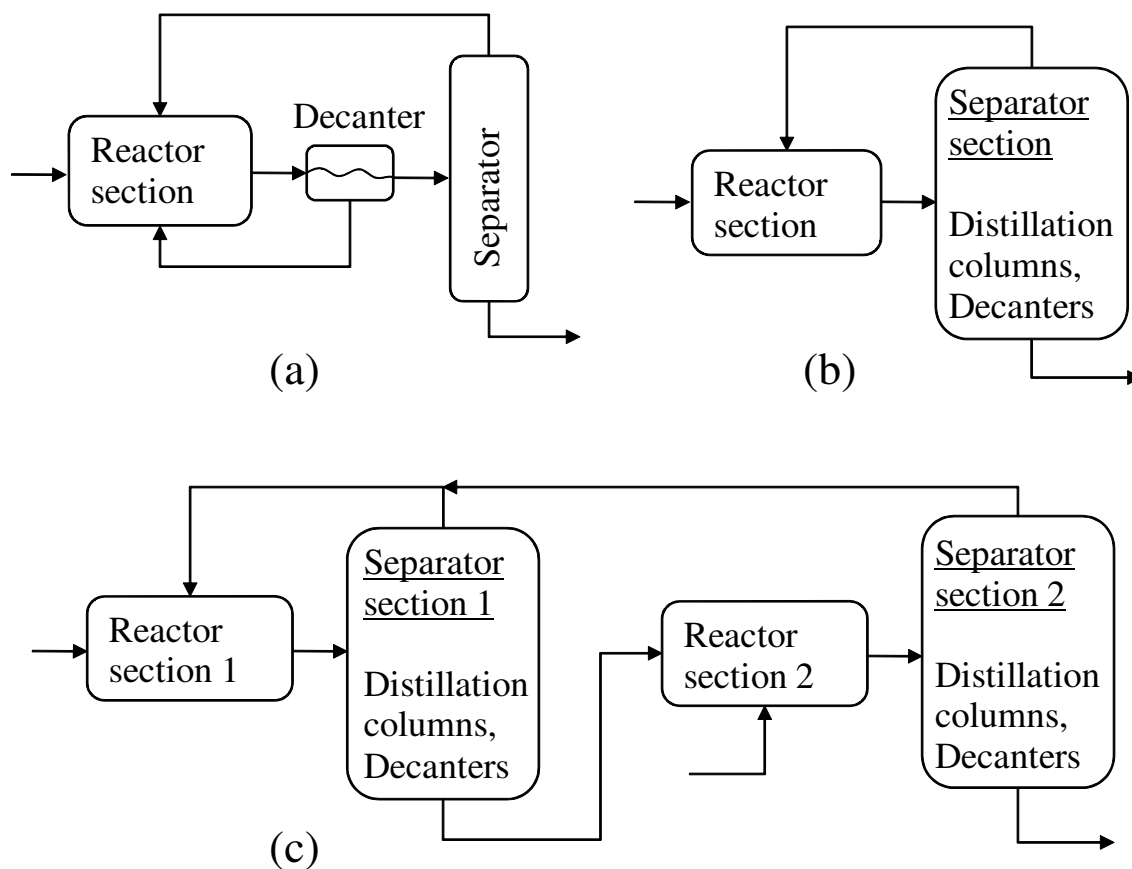


Figure 3.13: Process concepts overview; (a) Asahi process (direct hydration), (b) RS process concept (indirect hydration), (c) R1S1+R2S2 process concept (indirect hydration)

in the reactor is about an order of magnitude in excess to the stoichiometric amount. This amount of water is required to hold the large amount of catalyst used in the reactor (about 30% of the aqueous phase). The catalyst is designed such that it stays in the aqueous phase and therefore can be readily decanted and recycled back to the reactor. The organic phase that is richer in product is subsequently purified by distillation. The excess cyclohexene and some water are recovered from the top of the column and recycled back to the reactor. The Asahi process being the most recent commercial process route, is chosen as a benchmark reference case to evaluate the developed process concepts. The reference production rate is 100 kt/a of cyclohexanol of purity 99%. The simulation details of the benchmark case will be discussed later in Section 3.8.

3.6.2 RS process concepts

In this class of process concepts cyclohexene, water and formic acid are fed all together into a reactor section followed by a product recovery section and subsequent recycle of reactants. All the three reactions, namely the direct hydration, esterification and hydrolysis proceed at comparable rates. In this type of approach the mutual benefits between different reactions can be harvested. For example, the esterification reaction produces ester thereby enhancing the hydrolysis reaction. In the vice versa case, the hydrolysis reaction consumes the ester thereby enhancing the esterification reaction. The reactor can be a PFTR or a CSTR or a series of CSTRs, or countercurrent CSTR decanter cascades. An extraction step can be also employed to enhance the product composition. The separator can be a combination of distillation columns and decanters that achieve a given separation of the product stream. The excess reactants are recycled back. The details of different variations of this category of process concepts are discussed in the later sections of this chapter.

3.6.3 R1S1+R2S2 process concepts

In this class of process concepts the esterification and hydrolysis reactions are carried out separately in two steps R1S1 and R2S2, where R1 and R2 correspond to the esterification and hydrolysis reaction sections respectively. Similar to the previous case (RS), the reactors can be of different configurations. S1 and S2 correspond to the separator sections which follow R1 and R2 respectively. S1 purifies the ester, and S2 separates the product cyclohexanol as well as recovers formic acid to be recycled to R1. The segregated reaction zone approach allows the reactors to operate at the best conditions for the desired reaction, and that way higher reaction rates can be realized.

3.7 Modeling and simulation fundamentals

In this section, the details of model equations used to analyze the process concepts are presented. From an overall point of view, all the process concepts consist of one or more reactor sections that contain series of multiphase reactors, decanters and one or more separator sections that contain decanters and distillation columns. The reactors can be a PFTR or a series of CSTRs or a series of CSTR-decanter cascades.

In this section the modeling details of PFTR and the CSTR-decanter cascades (i.e. reactive-extraction) are presented as they cover most of the important modeling aspects of all the process concepts.

The distillation column is modeled with assumptions of constant molar overflow (CMO) approximation, equilibrium stage, ideal vapor phase, non-ideal liquid phase, and constant pressure. Further details of the mass-equilibrium-summation-enthalpy (MESH) equations can be found elsewhere [98–102]. The description of the distillation column model is not elaborated here as it is available in standard textbooks of separation processes.

3.7.1 General modeling strategy

The general assumptions are, that all the reactors are modeled at isothermal conditions and the energy balance was not considered in the modeling of the reactors because of the comparably little heat of reaction and negligible heat of mixing. The effect of catalyst swelling was also not considered, as the scope of this work is to identify promising conceptual process options. The reaction system is kinetically limited (due to slow reaction rates). Therefore, the mass transfer effect has been neglected and the system is assumed to be in phase equilibrium. The effects of catalyst swelling and mass transfer limitations shall be considered during the detailed design of the most promising process concepts. The general modeling strategy of the studied sets of problems is provided in Figure 3.14. For a given temperature and pressure the chemical equilibrium constant K_{eq} is calculated using Eq. 3.10. The liquid phase activities of the components are calculated at every point (at every step of iterative calculations) in the simulation. The activities as well as the phase equilibrium calculation are performed using an external subroutine which is used to decouple phase splitting calculations from general model equations. This strategy reduces the size of the problem and therefore enables better convergence which otherwise is extremely difficult to achieve. Refer to Steyer et al. and Gangadwala [103, 104] for further details of the decoupled phase splitting calculations strategy.

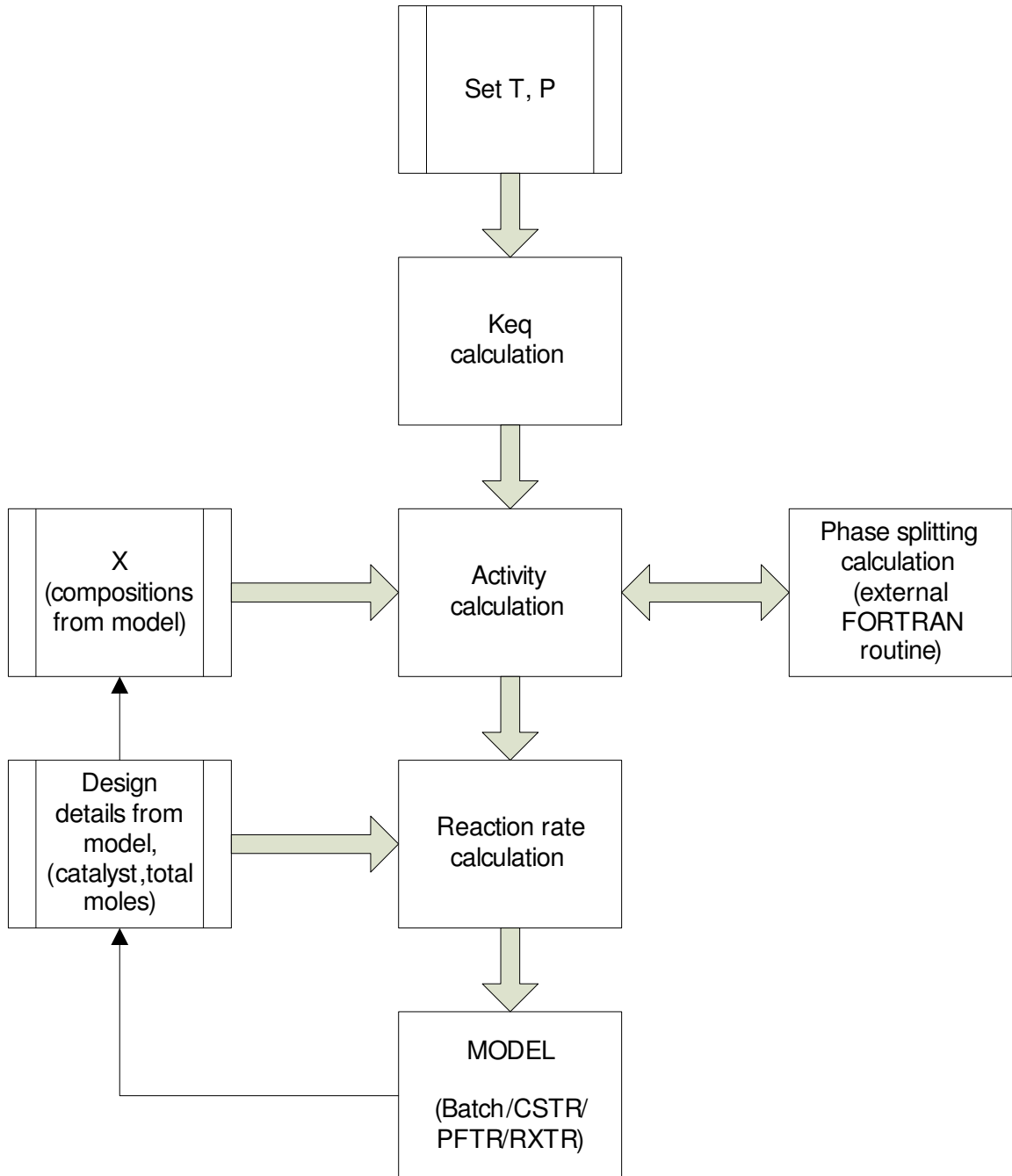


Figure 3.14: Modeling Strategy

3.7.2 Phase equilibrium calculations

As the system exhibits extensive phase splitting over wide compositional space, a phase splitting calculation is required in all the simulations. In addition to calculating the equilibrium compositions, liquid phase activities are required to calculate the reaction rate and they are also required for calculating VLE in the distillation column simulations. A robust methodology is required to effectively calculate the LLE. A comprehensive discussion on various methodologies to calculate LLE can be found elsewhere [78].

The most effective methodologies are the homotopy continuation method of Bausa and Marquardt [105] and the rate based method of Sundmacher [78]. While both these methods are efficient, the latter method is relatively more robust and converges faster. Further advantages of the rate based methodology such as the versatility to calculate complex multi-phase equilibria has been investigated by Ye et al. [106, 107].

The rate based approach suggested by Sundmacher [78] is based on non-equilibrium thermodynamics of irreversible processes that is similar to the approach that was discussed in the Chapter 2. The idea is to model the dynamic behavior of a system when there is a local concentration inhomogeneity. As per Kondepudi and Prigogine [61], such an inhomogeneity will cause the system to go back to the stable node if the one phase solution is stable. In the case of phase instability, the system will progressively grow into a multi-phase system. This behavior is modeled in a simplified manner (given in Eq. 3.5 and 3.6.) that captures the essential aspects of non-equilibrium thermodynamics.

$$\frac{dn_i^{org}}{dt} = \frac{k}{RT} A(\mu_i^{aq} - \mu_i^{org}) = kA \ln \left(\frac{a_i^{aq}}{a_i^{org}} \right) \quad (3.5)$$

$$\frac{dn_i^{aq}}{dt} = -\frac{k}{RT} A(\mu_i^{aq} - \mu_i^{org}) = -kA \ln \left(\frac{a_i^{aq}}{a_i^{org}} \right) \quad (3.6)$$

Assuming spherical droplets the inter-facial area A in the above equations are modeled as mole fraction of the minor phase to the power of $2/3$. The kinetic constant k here represents the mass transfer coefficient which is usually assumed to be some convenient value as the current objective is only to find the final composition and not the exact path of convergence. These equations are integrated until the steady state is reached which actually represents the equilibrium compositions. This is because mathematically the single phase solution is an unstable node. Therefore, the integrator always converges to the two phase solution. Once the solution is close

to the steady state point, it can serve as a good initial guess for Newton solution method that can quickly solve the phase equilibrium problem.

In most of the simulations the rate based methodology has been used to calculate the phase equilibrium. Nevertheless the homotopy continuation methodology has also been employed in the early stages of simulations which was before the implementation of the rate based methodology. The algorithm has been implemented as a subroutine in FORTRAN 77, and it uses dgesv solver from the LAPACK library. The subroutine is called in-line in the simulation environment DIVA. All the simulations have been carried out on a PC with Linux based Ubuntu kernel as operating system.

3.7.3 Simulation environment

The simulations were carried out using an in-house software DIVA [79]. DIVA provides a modular environment to solve DAE problems. For example, a reactor, a decanter, or a distillation column can be programmed as separate modules which can be connected and simulated together as a whole plant. DIVA is a solution environment that provides a platform to solve complex DAE problems using robust solvers. Built-in continuation algorithms can be employed to analyze the problems efficiently. It can be also linked to external subroutines such as FORTRAN. While the simulations are performed in DIVA, the data are plotted using MATLAB. Aspen plus software was also used particularly to perform distillation column simulations, when Aspen plus can provide a good starting guess for the simulations in DIVA.

3.7.4 Chemical equilibrium constant

The chemical equilibrium constant is calculated by the following equations.

$$\Delta H_{rxn}^j = \sum_{i=1}^{NC} \nu_{ij} \Delta_f H_i^0 + \sum_{i=1}^{NC} \nu_{ij} C_{p,i} (T - T_{ref}) \quad \dots j = 1, 2 \dots NR \quad (3.7)$$

$$\Delta S_{rxn}^j = \sum_{i=1}^{NC} \nu_{ij} S_i^0 + \sum_{i=1}^{NC} \nu_{ij} C_{p,i} \ln \left(\frac{T}{T_{ref}} \right) \quad \dots j = 1, 2 \dots NR \quad (3.8)$$

$$\Delta G_{rxn}^j = \Delta H_{rxn}^j - T \Delta S_{rxn}^j \quad \dots j = 1, 2 \dots NR \quad (3.9)$$

$$\ln K_{eq}^j = \frac{-\Delta G_{rxn}^j}{R_{gas} T} \quad \dots j = 1, 2 \dots NR \quad (3.10)$$

The stoichiometric coefficient ν_{ij} is given in Table 3.5. The values of $\Delta_f H_i^0$, S_i^0 and $C_{p,i}$ are available in Table 3.1. The reference temperature T_{ref} is 298 K.

Species i	Reaction j		
	Direct hydration	Esterification	Hydrolysis
Cyclohexene	-1	-1	0
Cyclohexanol	1	0	1
Water	-1	0	-1
Formic acid	0	-1	1
Cyclohexylformate	0	1	-1
Total molar change ν_j^T	-1	-1	0

Table 3.5: Stoichiometric coefficient ν_{ij}

3.7.5 Dimensionless formulation of PFTR model

In Section 3.6 the RS process concept was presented. As discussed later, in the ideal case of RS process concept a multi-phase plug flow tubular reactor (PFTR) is studied. This PFTR is modeled in a dimensionless form so as to estimate the full potential of the process concept. A one dimensional PFTR model is schematically represented in Figure 3.15. The catalyst swelling is assumed to be negligible so that the hold up (void volume) in the reactor is constant. In the case of liquid-liquid phase splitting, both the phases are assumed to be uniformly dispersed and there is no channeling of one phase relative to the other. Under these assumptions, the model equations in dimensionless form are given in Eq. 3.11 - 3.13. These dimensionless equations can be derived from mass and component balances.

$$\frac{df}{d\zeta} = \sum_{j=1}^{NR} \nu_j^T r'_j \quad (3.11)$$

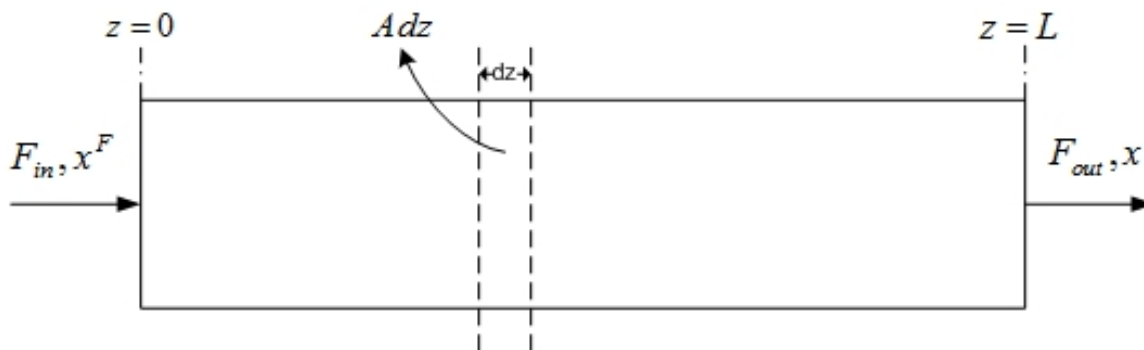


Figure 3.15: PFTR model

$$\frac{dx_i}{d\zeta} = \frac{1}{f} \sum_{i=1}^{NC} (\nu_{ij} - \nu_j^T x_i) r'_j \quad i = 1, 2 \dots NC - 1 \quad (3.12)$$

$$\sum_{i=1}^{NC} x_i = 1 \quad (3.13)$$

In Eq. 3.11 & Eq. 3.12, f is the dimensionless flow rate $f = F/F_{in}$, here F is molar flow rate at any given point and F_{in} is the feed molar flow rate, ζ is the dimensionless distance (length) of PFTR, $\zeta = z/L$, r'_j is the dimensionless rate of reaction j given in Eq. 3.14, ν_j^T is the total molar change of a reaction j given in Table 3.5

$$r'_j = \left[Da_j^{het} \frac{K_{ads}(A) K_{ads}(B)}{\left[1 + \sum_i^{NC} a(i) K_{ads}(i)\right]^2} + Da_j^{hom} \frac{\rho_{avg} x_{FA}^{ref}}{\rho_{avg} x_{FA}^{ref}} \right] \left[\prod a^{reactants} - \frac{1}{K_{eq}} \prod a^{products} \right] \quad (3.14)$$

$$Da_j^{het} = \frac{V}{F_{in}} (1 - \varepsilon) \rho_{cat} k_{f,0,j}^{het} e^{-E_{A,j}^{het}/R_{gas}T} \quad (3.15)$$

$$Da_j^{hom} = \varepsilon \frac{V}{F_{in}} \rho_{avg} x_{FA}^{ref} k_{f,0,j}^{hom} e^{-E_{A,j}^{hom}/R_{gas}T} \quad (3.16)$$

The reference temperature here is 393 K. This is because the reference Da as defined below is based on the direct hydration rate constant. The reference composition required for dimensionless formulation of the homogeneous reaction rate is chosen as pure formic acid. The following formulation helps to narrow down to one parameter Da instead of six.

$$Da = Da^{ref} = \frac{V}{F_{in}} (1 - \varepsilon) \rho_{cat} k_{f,0,1}^{het} e^{-E_{A,1}^{het}/R_{gas}T_{ref}} \quad (3.17)$$

$$Da_j^{het} = \frac{k_{f,0,j}^{het} e^{-E_{A,j}^{het}/R_{gas}T}}{k_{f,0,j}^{het} e^{-E_{A,j}^{het}/R_{gas}T_{ref}}} Da \quad (3.18)$$

$$Da_j^{hom} = \frac{\varepsilon}{(1 - \varepsilon)} \frac{k_{f,0,j}^{hom} e^{-E_{A,j}^{hom}/R_{gas}T}}{k_{f,0,j}^{het} e^{-E_{A,j}^{het}/R_{gas}T_{ref}}} \frac{\rho_{avg} x_{FA}^{ref}}{\rho_{cat}} Da \quad (3.19)$$

3.7.6 Reactive extraction model

In most of the process concepts, the reactor section consists of a series of CSTR (with phase splitting) or a cascade of CSTR and decanters operating in both cocurrent and countercurrent mode. All these process operations are theoretically a reactive extraction process. A countercurrent reactive extraction stage model is described here as an example. The schematic diagram of countercurrent reactive extraction is given in Figure 3.16. The co-current case, as well as all other cases with different recycle streams, can be similarly derived.

3.7.6.1 Total material balance (TMB)

The TMB for the stage 1 is

$$F_{aq} + E_2 - E_1 - R_1 = \sum_{j=1}^{NR} \nu_j^T r_{j,1} \quad (3.20)$$

In Eq. 3.20, E_k and R_k refer to the extract and raffinate stream of stage k respectively. $r_{j,k}$ is the rate of reaction j at stage k .

The TMB at stage k is

$$R_{k-1} + E_{k+1} - E_k - R_k = \sum_{j=1}^{NR} \nu_j^T r_{j,k} \quad (3.21)$$

At stage NS it is

$$F_{org} + R_{NS-1} - E_{NS} - R_{NS} = \sum_{j=1}^{NR} \nu_j^T r_{j,NS} \quad (3.22)$$

E_k for all the stages can be obtained from phase equilibrium calculation (refer to Eq. 3.23). As already mentioned the phase equilibrium calculation is carried out for every stage using a separate external FORTRAN routine.

$$E_k = R_k \frac{\phi_k}{(1 - \phi_k)} \quad (3.23)$$

ϕ_k is the phase fraction of the organic phase.

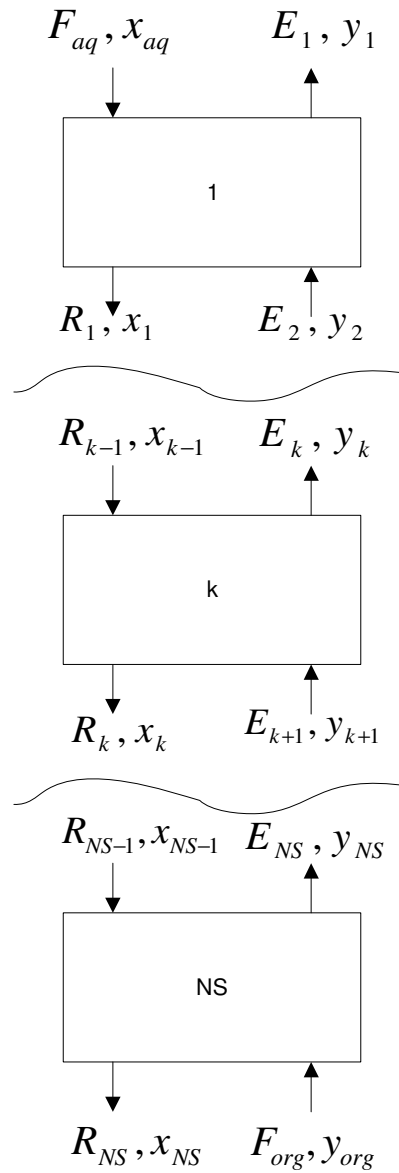


Figure 3.16: Countercurrent reactive extraction model

3.7.6.2 Component material balance (CMB)

The CMB for the stage 1 is

$$\frac{dx_1^i}{dt} = \left(\begin{array}{l} F_{aq}(x_{aq}^i - x_1^i) + E_2(x_{eqI,2}^i - x_1^i) - R_1(x_{eqII,1}^i - x_1^i) \\ -E_1(x_{eqI,1}^i - x_1^i) - \sum_j (\nu_{i,j} - \nu_j^T x_1^i) r_{j,1} \end{array} \right) \frac{1}{Nt_1} \quad (3.24)$$

$$i = 1, 2 \dots NC - 1$$

In Eq. 3.24, Nt_k is the molar hold up of stage k . $Nt_k = \rho_{avg,k} V_k$ and V_k is the volumetric hold up of the stage. $x_{eqI,k}^i$ and $x_{eqII,k}^i$ are the phase equilibrium compositions of the organic and aqueous phase respectively.

The CMB for the stage NS is

$$\frac{dx_{NS}^i}{dt} = \left(\begin{array}{l} F_{org}(y_{org}^i - x_{NS}^i) + R_{NS-1}(x_{eqII,NS-1}^i - x_{NS}^i) - \\ R_{NS}(x_{eqII,NS}^i - x_{NS}^i) - E_{NS}(x_{eqI,NS}^i - x_{NS}^i) - \sum_j (\nu_{i,j} - \nu_j^T x_{NS}^i) r_{j,NS} \end{array} \right) \frac{1}{Nt_{NS}} \quad (3.25)$$

$$i = 1, 2 \dots NC - 1$$

And for the stage k it is

$$\frac{dx_k^i}{dt} = \left(\begin{array}{l} E_{k+1}(x_{eqI,k}^i - x_k^i) + R_{k-1}(x_{eqII,k-1}^i - x_k^i) - \\ R_k(x_{eqII,k}^i - x_k^i) - E_k(x_{eqI,k}^i - x_k^i) - \sum_j (\nu_{i,j} - \nu_j^T x_k^i) r_{j,k} \end{array} \right) \frac{1}{Nt_k} \quad (3.26)$$

$$i = 1, 2 \dots NC - 1$$

The equation for the summation constraint is given below.

$$\sum_{i=1}^{NC} x_k^i = 1 \quad \dots \quad k = 1, 2 \dots NS \quad (3.27)$$

In addition to the state variables described in the TMB and CMB equations, the feed flow rates of water, cyclohexene, and formic acid makeup are also considered as state variables. This is because the feed has to be calculated in the simulations in order to fulfill the design production rate of cyclohexanol (100 kt/a). The cyclohexene feed rate is accounted for by the production rate constraint. The water feed rate is accounted for by fixing the Ene:Water ratio at a fixed point in the reactor for example the first reactor R_1 . The acid makeup is accounted for by fixing Acid:Water

or Acid:Ene ratios at R_1 . Further explanation on these ratios is given in a later Section 3.8.2.1.

3.8 Process Simulations

The thermodynamic data, kinetic data and modeling details have been presented in the previous sections of this chapter. In this section these information are applied to study the various process concepts from model based analysis. The benchmark for the evaluation of different process concepts is the Asahi process for direct hydration of cyclohexene (Table 3.6). All the process simulations are carried out for a design production rate of 100 kt/a of cyclohexanol. In the case of esterification reaction, the molar production rate of ester is the same as the molar production rate of cyclohexanol.

Simulation parameters	values
Production rate	100 kt/a
Feed condition	Saturated liquid
Column pressure	1 atm
Bottom purity	99% mol/mol
Reflux ratio	0.3
Cyclohexanol recovery	99% mol/mol
Number of stages	100
Feed stage	50
Reflux return stage	2
Condensor type	Total
Reboiler duty	7.5 MW

Table 3.6: Asahi benchmark

The design details of the optimum Asahi process are not available in the open literature. Therefore, assumptions had to be taken, and a 12 wt% cyclohexanol in the organic phase of the reactor outlet is assumed to be reasonable. To calculate the energy requirement of the Asahi process, distillation column simulations were performed using Aspen plus with user defined NRTL parameters [57, 58]. A large number of stages (100) is assumed to estimate the maximum energy potential of the process. The benchmark conditions are given in the Table 3.6. For a production rate of 100 kt/a of cyclohexanol of purity 99% with more than 99% recovery, the energy requirement was 7.5 MW. The separator in this case only includes a distillation for cyclohexanol/cyclohexene separation. It is likely that the reality is more complex

than that. One reason is the possibility of inerts in the feed such as cyclohexane. Furthermore, the hydration reaction is reported to be carried out in a series of reactors [13] (perhaps operating at different temperatures and with inter connected streams with the separator).

In the following sub sections the RS set of process concepts are discussed first and then the R1S1+R2S2 set of process concepts are presented.

3.8.1 Ideal RS process concept

As previously discussed in section 3.6, in the RS set of process concepts, all the reactants namely cyclohexene, formic acid and water are fed together into the reactor section. All the three reactions occur simultaneously which is done to harvest the mutual benefits between the reactions.

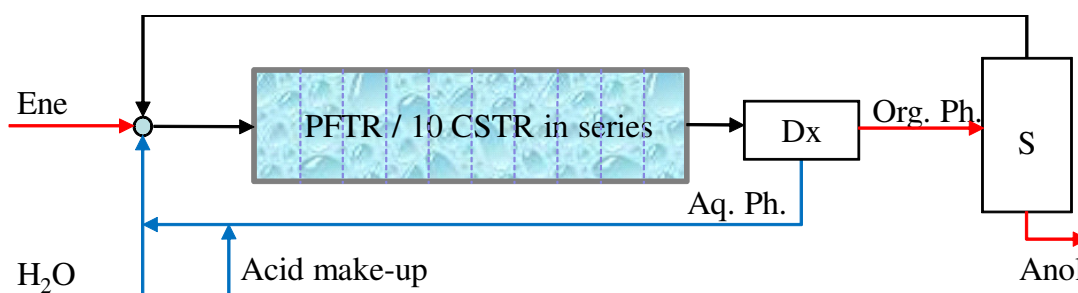


Figure 3.17: RS process concept: ideal (PFTR), real (finite 10 CSTR in series). Anol = cyclohexanol, Ene = cyclohexene, Acid = formic acid, Dx = decanter, S = separator

The ideal case of RS concept would be to study a PFTR coupled to an ideal distillation column without limiting it to any particular size (refer to Figure 3.17). In this regard, a one dimensional PFTR model was formulated in dimensionless form. The model formulation has been discussed in the previous section. The reactor is then analyzed in terms of the Damköhler number. The Damköhler number represents the ratio of the reaction time (i.e. the residence time) to the time constant of the reaction.

Figure 3.18 depicts the performance of this ideal case at different temperatures. Very high conversion of cyclohexene to cyclohexanol is theoretically possible. It could be a hypothetically large reactor, but the analysis provides the maximum performance limit achievable through the RS process concept. Ideally, at 333 K this process concept would require only about one fourth of the energy consumption of the Asahi process.

The energy saving in this case is because the temperature dependency of chemical equilibrium enables a several times higher conversion than the Asahi process.

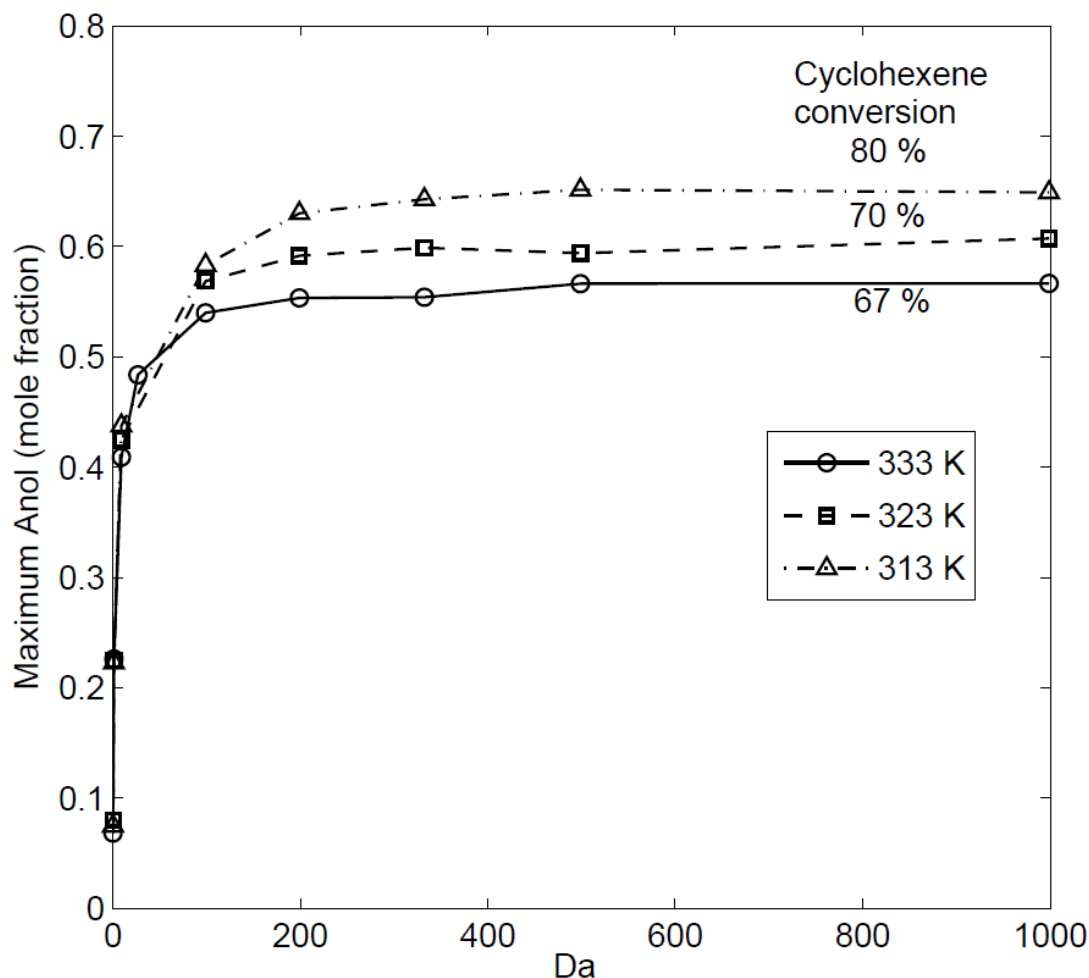


Figure 3.18: Performance of the ideal RS case

3.8.2 Real RS process concept

For a practical application of the RS process concept, the PFTR is approximated by a series of 10 CSTR of finite sizes. A schematic representation of the concept is provided in Figure 3.17. The reactor section is followed by a decanter where the aqueous phase is recycled back. The organic phase is then distilled. The number of stages considered in the distillation column simulation was very high (100). This was assumed in order to operate close to the minimum reflux ratio. If the formic acid level is kept low, a single distillation column was sufficient to recover up to 97% of cyclohexanol produced with a purity of 99.99%. Water is usually used in excess, and

therefore the system is always bi-phasic, the decanter at the end of the reactor section enables the aqueous stream to be recycled back.

3.8.2.1 Design parameters

In the previous section 3.7.6.2, it was discussed that a few design parameters were required to account for the water and acid feed to the system. This is due to the fact that the final product stream of cyclohexanol though 99.99% pure has that trace 0.01% whose composition is unknown. The design parameters bring closure to the system of equations to account for these unknown compositions and thereby enable the model to calculate the amount of water feed and formic acid makeup. In addition to that, these design parameters also enables one to study the effect of important factors such as the aqueous to organic phase ratio, total acid hold up etc. These parameters are defined below as they are important during the analysis of the process concepts.

- **Ene:Water ratio** - This parameter represents the molar ratio of cyclohexene to water in the first reactor. It basically represents the organic to aqueous phase ratio in the reactor.
- **Acid:Ene ratio** - This parameter represents the molar ratio of (acid+ester combined) to cyclohexene. It gives an idea about the amount of formic acid used in the process.
- **Acid:Water ratio** - This parameter gives the effective acidity of the system.
- **Catalyst loading** - This parameter refers to the volume fraction of catalyst in the reactor. The mass of the catalyst is internally calculated using the catalyst density.

3.8.2.2 Effect of catalyst loading

Figure 3.19 gives a picture of the typical reactor size requirement of the RS process concept. The production rate is the same as the reference benchmark (Table 3) for all the simulations. The increase in the catalyst loading decreases the reactor size required for a given conversion. For the cyclohexanol production a reasonable maximum for reactor size is 1000 m^3 . In this measure, despite extremely high catalyst loading of 30% (v/v) the reactor size requirement is very high if a reasonable conversion has to be obtained.

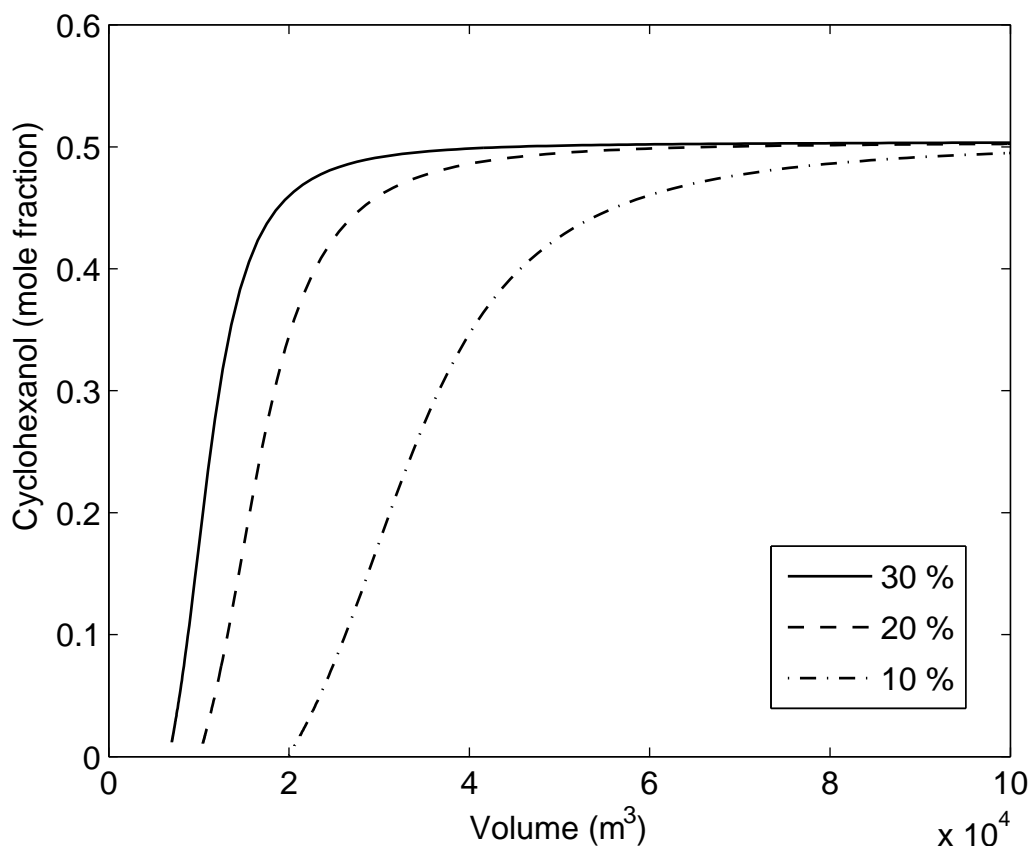


Figure 3.19: Effect of catalyst loading (v/v) for real RS process concept. 343K, Acid:Ene = 0.1, Ene:Water = 0.1

3.8.2.3 Effect of Ene:Water ratio

Figure 3.20 depicts the effect of Ene:Water ratio (as the aqueous phase is decanted and recycled, the product stream composition in Figure 3.20 refers to the organic phase). The ratio is varied from 0.05 to 0.2. It cannot be increased further due to homogeneous conditions that bring down the cyclohexanol level in the product stream. The ratio did not have a significant effect on the performance. This could be because of the use of excess water (required to maintain phase split) and also due to the large adsorption coefficient of water [1].

3.8.2.4 Effect of Acid:Ene ratio

Figure 3.21 depicts the effect of Acid:Ene ratio. The acid distribution between the two phases is nearly equivalent. Formic acid is soluble in cyclohexanol and ester.

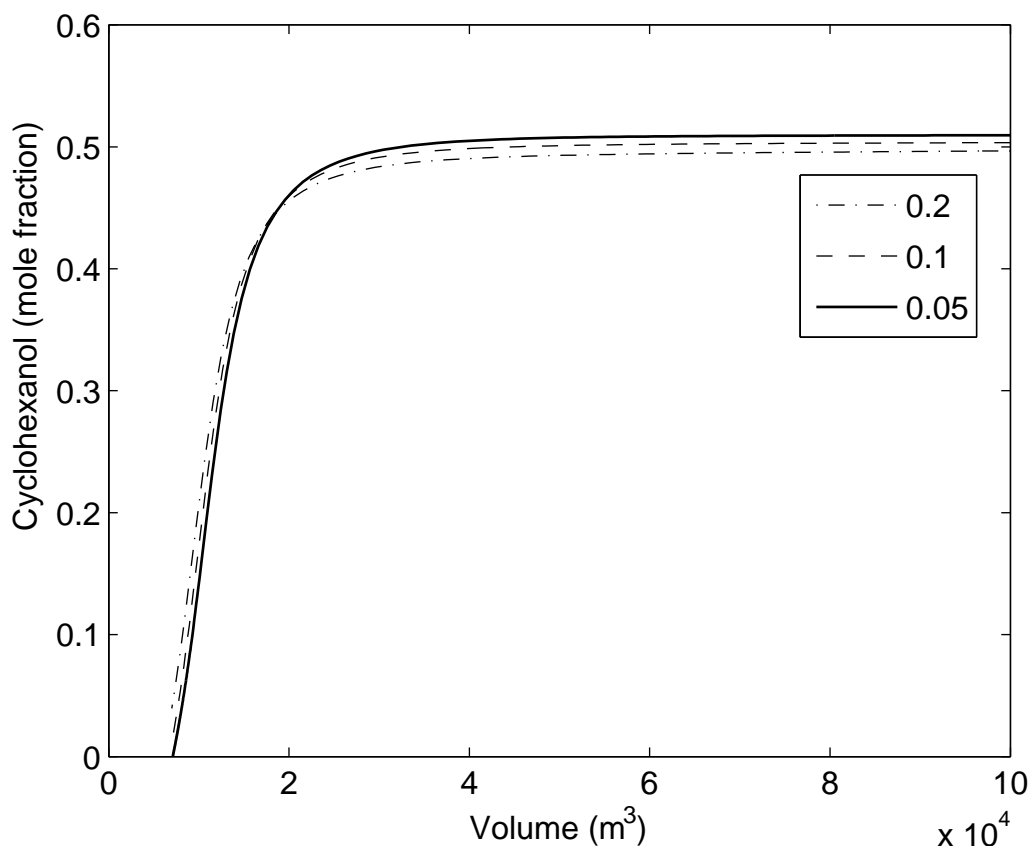


Figure 3.20: Effect of Ene:Water ratio for real RS process concept. 343K, catalyst loading 30%, Acid:Ene = 0.1

Therefore, the distribution of formic acid is equivalent in both the aqueous and the organic phase (possibly slightly higher in the aqueous phase). A high Acid:Ene ratio results in a faster reaction rate and therefore a smaller reactor size requirement. On the other hand it also causes higher ester levels in the product stream which in turn affects the separation cost. Therefore, the Acid:Ene ratio is an important optimization parameter in the detailed design of the process concept.

3.8.2.5 Effect of temperature

The sensitivity of the reactor to temperature, catalyst loading and Acid:Ene ratio, is utilized to push the reactor to the practical limits in order to evaluate the maximum realizable performance. When increasing the temperature, the decomposition of formic acid must be taken into consideration [97, 108, 109]. The presence of ex-

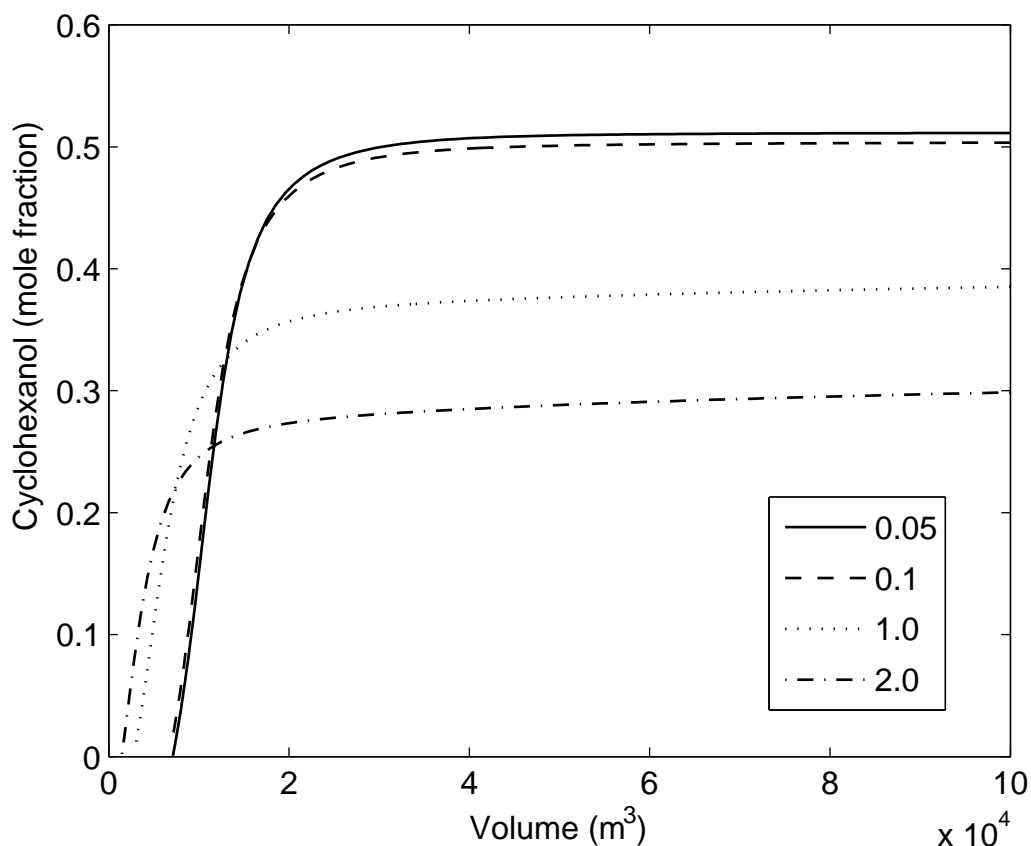


Figure 3.21: Effect of Acid:Ene ratio for real RS process concept. 343K, catalyst loading 30%, Ene:Water = 0.1

cess water (being a decomposition product) hinders the decomposition of formic acid [97]. As discussed above the typical design parameters are Ene:Water ratio = 0.1 and Acid:Ene ratio = 0.1, which means the Acid:Water ratio is typically 0.01. In other words, we have very large excess of water compared to the acid in the reactor. Under such conditions the decomposition of formic acid can be assumed to be negligible for a moderate increase in the reaction temperature. Figure 3.22 demonstrates the benefit of a higher reaction temperature (353 K).

3.8.3 RS countercurrent cascade process concept

As the system exhibits extensive phase splitting, the process can be visualized as reactive extraction. The idea behind countercurrent cascade process concept is to achieve some degree of process intensification. Two potential flow sheets are presented

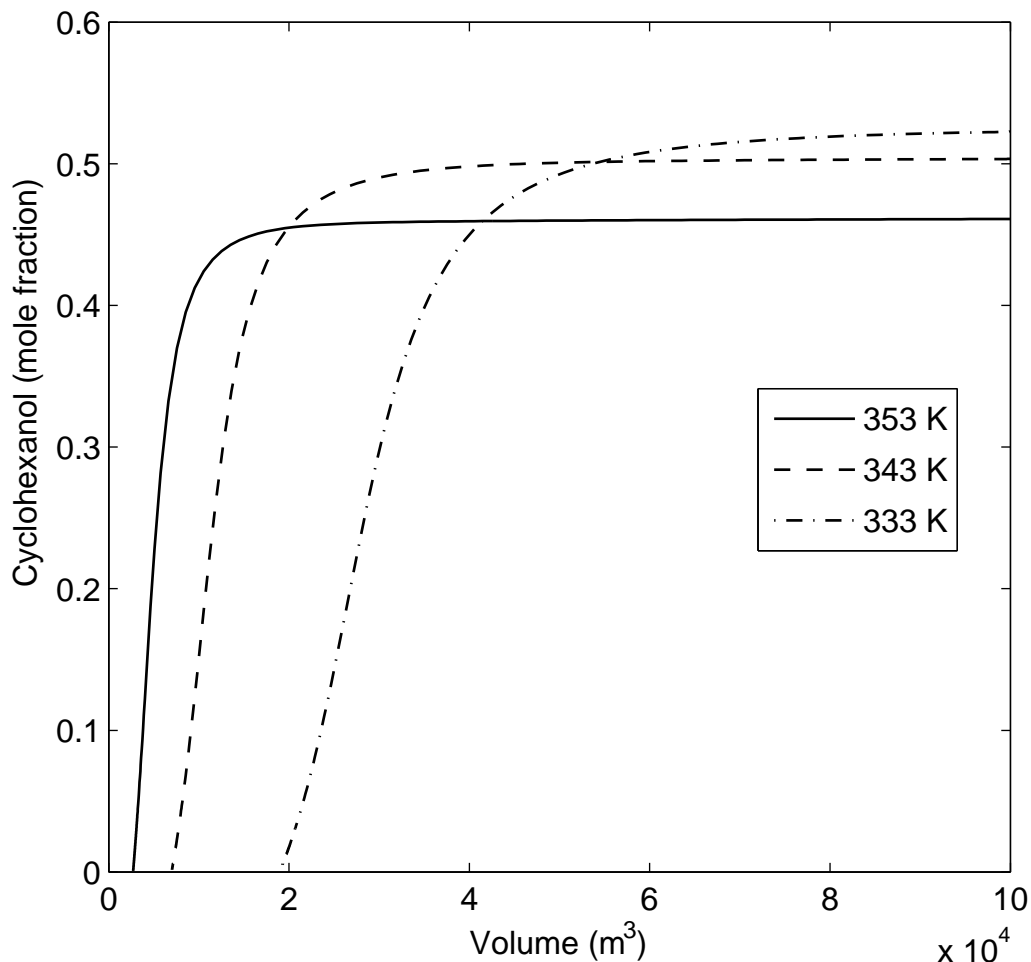


Figure 3.22: Effect of temperature for real RS process concept. Catalyst loading 30%, Ene:Water = 0.1, Acid:Ene = 0.1

in Figure 3.23. In both cases, a series of reactor-decanter cascades were employed with an aqueous stream flowing countercurrently to the organic stream. Similar to the RS case, water is used in excess to maintain phase splitting. The aqueous phase is readily recycled while the organic phase is distilled to recover the product. The two cases studied here differ in the pattern of overhead recycle. In case (a) the distillate is directly recycled to the first reactor, whereas in case (b) the distillate is decanted and the organic and aqueous streams are recycled at appropriate positions. The first case is partially counter-current. The second case is totally countercurrent. 10 stages were assumed so as to compare with the real RS case.

The simulation results of the cascade processes are compared with the real RS case in Figure 3.24. The improvement in the reactor performance with regard to cy-

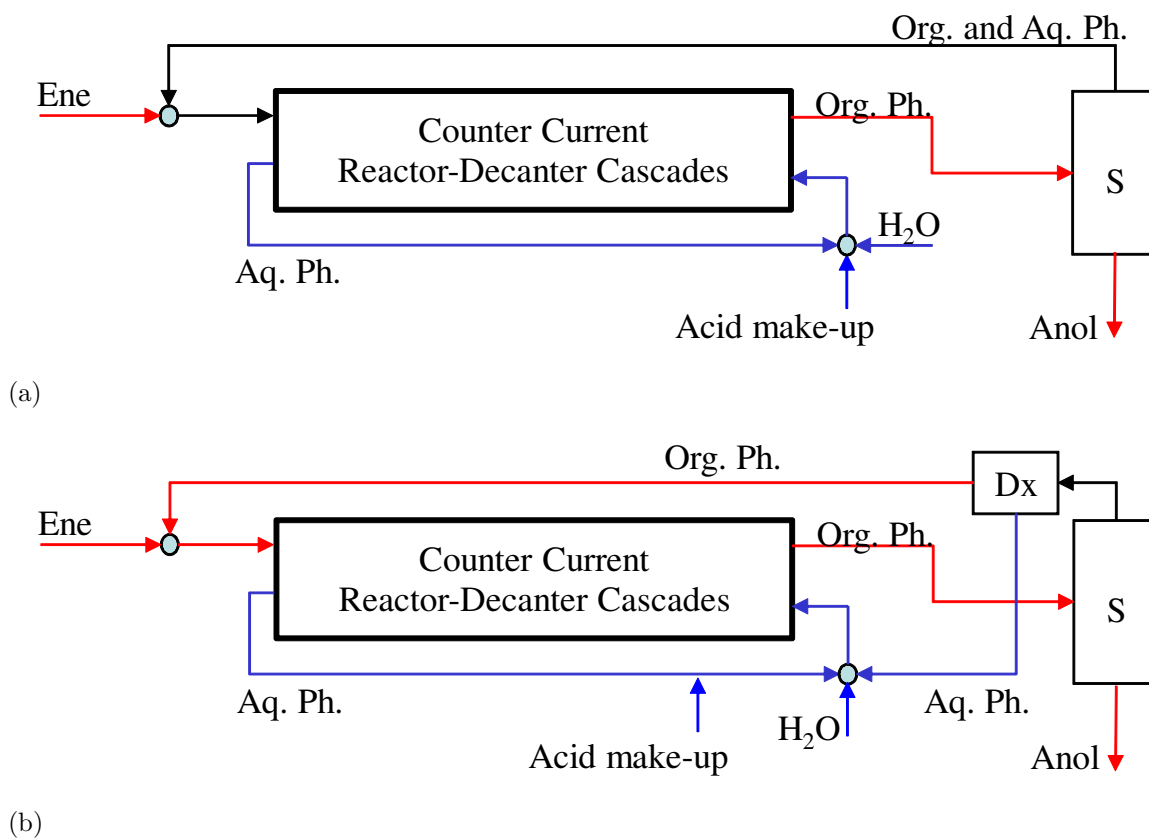


Figure 3.23: RS countercurrent cascade process concept; (a) mixed recycle-RSCa, (b) segregated recycle-RSCb; Anol = cyclohexanol, Ene = cyclohexene, Acid = formic acid, Dx = decanter, S = separator

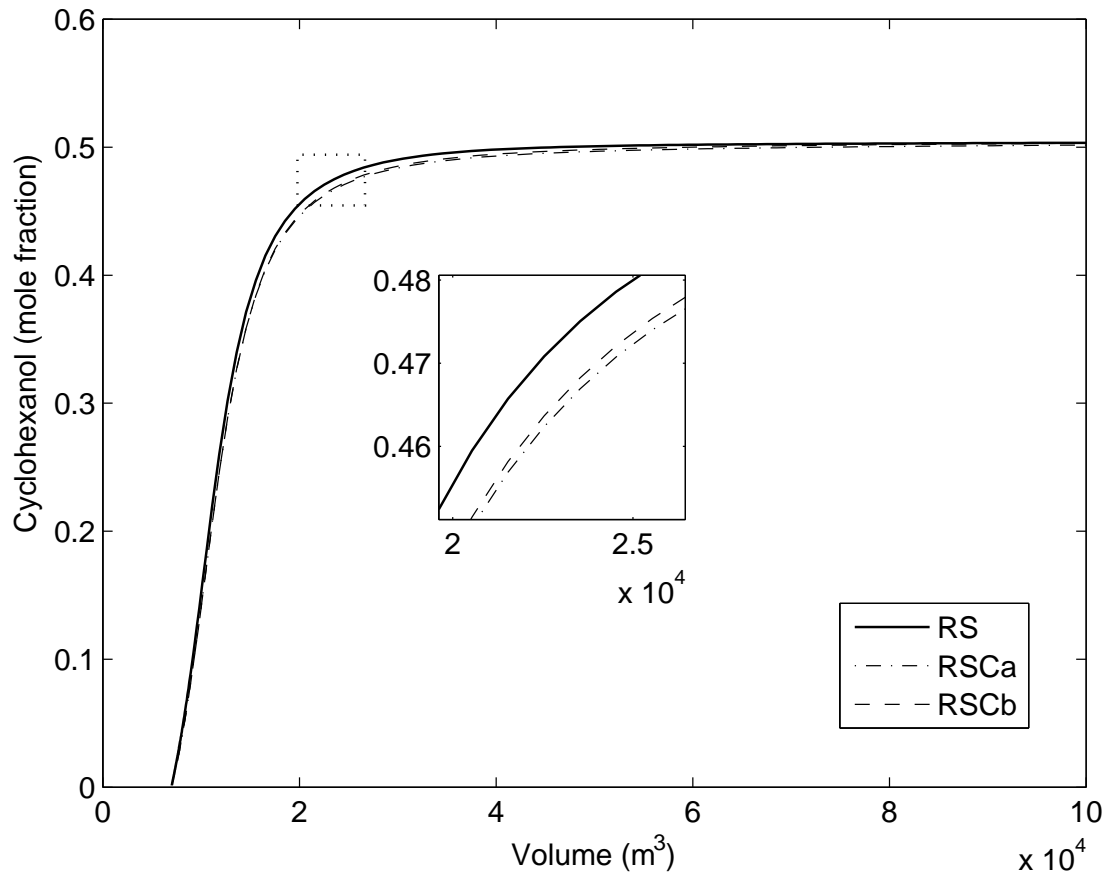


Figure 3.24: Comparison of RS and RS countercurrent cascade. 343K, Catalyst(Amberlyst) loading 30%, Ene:Water = 0.1, Acid:Ene = 0.1

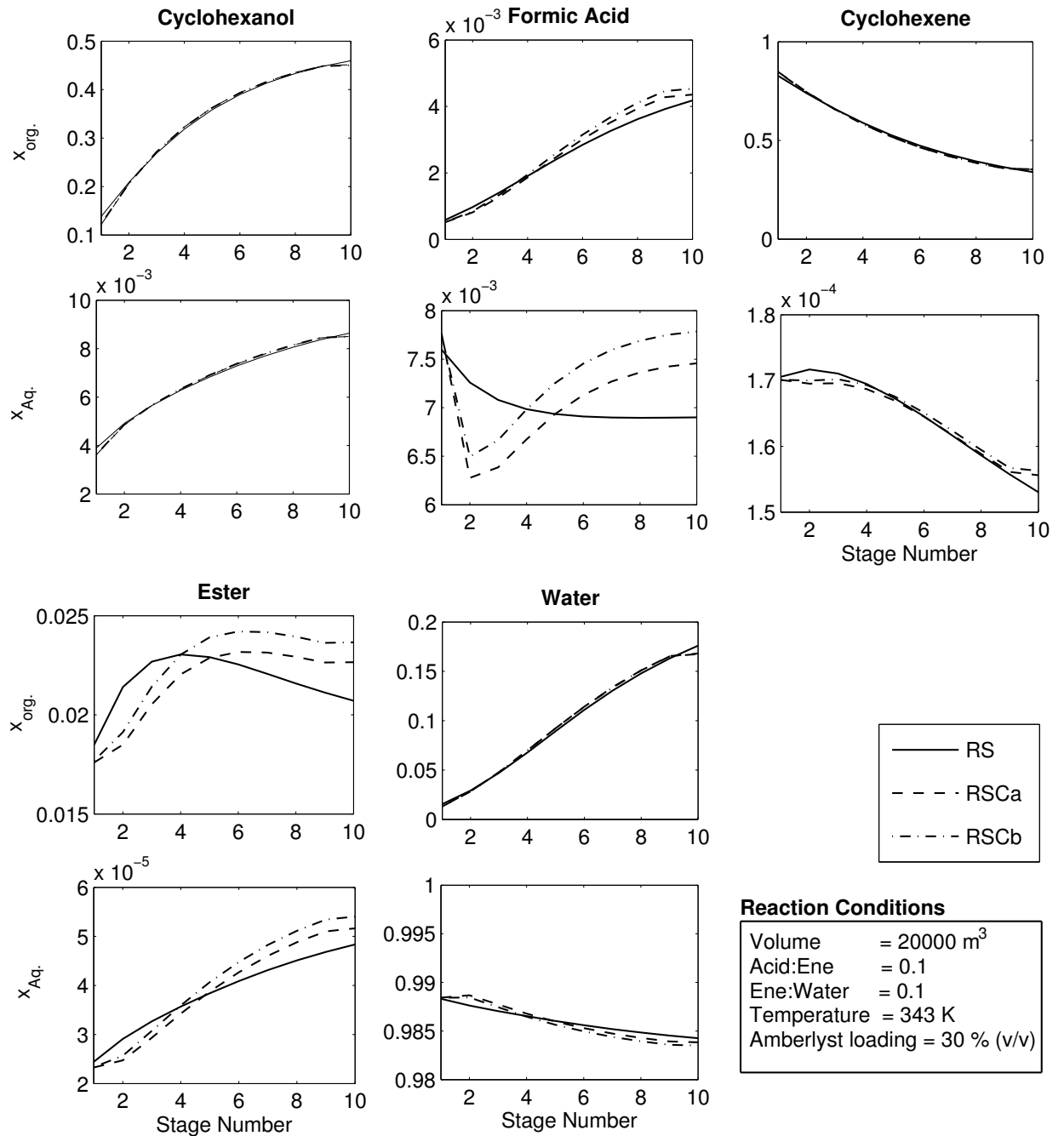


Figure 3.25: Profiles of RS, RSCa, RSCb

clohexanol output is not very significant. This behavior could be due to the excessive adsorption of water on the surface of the catalyst, which means that the flow direction of water did not affect the reaction rate significantly. Figure 3.25 provides a better understanding of the behavior. Even though the cyclohexanol profile is not very different, the other component profiles vary significantly with the different process options. Therefore, if the catalyst surface can be made more sensitive to concentration changes (in other words, if the adsorption coefficients can be tuned, e.g. by the Si:Al ratio of the zeolite), then the process intensification options can be effectively utilized.

3.8.4 R1S1 + R2S2 cascade process concept

In the RS set of process concepts, though high conversion and significant energy savings can be achieved, due to slower reaction rates the reactor size requirement was very high for practical implementation. Instead of carrying out all the reactions together, if the reaction zones are separated, the reactors can be operated at the best conditions for the respective reaction. This mode of operation realizes faster reaction rates but at the cost of a two step separation process. Cyclohexene and formic acid are fed to R1 which is the esterification reactor section. The product stream is sent to the separator section S1 which purifies the ester. The purified ester is then hydrolyzed in R2 which is followed by S2. S2 purifies the product cyclohexanol and also recovers the formic acid to be recycled back to R1.

3.8.4.1 R1S1

The first step, i.e. the esterification, is very effective. Figure 3.26 shows the performance of the esterification reactor. 80% conversion per pass of cyclohexene was possible within a reasonable reactor size (250 m³). Figure 3.26 also shows the effect of water on the performance of the esterification reactor section R1. The presence of water in the reactor drastically affects the reaction rates. Therefore, it is preferable to keep the water in the recycle streams as low as possible. The precise allowable limit can only be determined by whole plant optimization (i.e. including R2S2). The separation of ester is efficient because of the very high relative volatility. The energy requirement is given in Figure 3.27.

The undesirable effect of water on the performance of the esterification reaction is due to the excessive adsorption of water on the surface of Amberlyst 15. Unlike Amberlyst 15 that is hydrophilic, if the catalyst surface can be designed to be hydrophobic

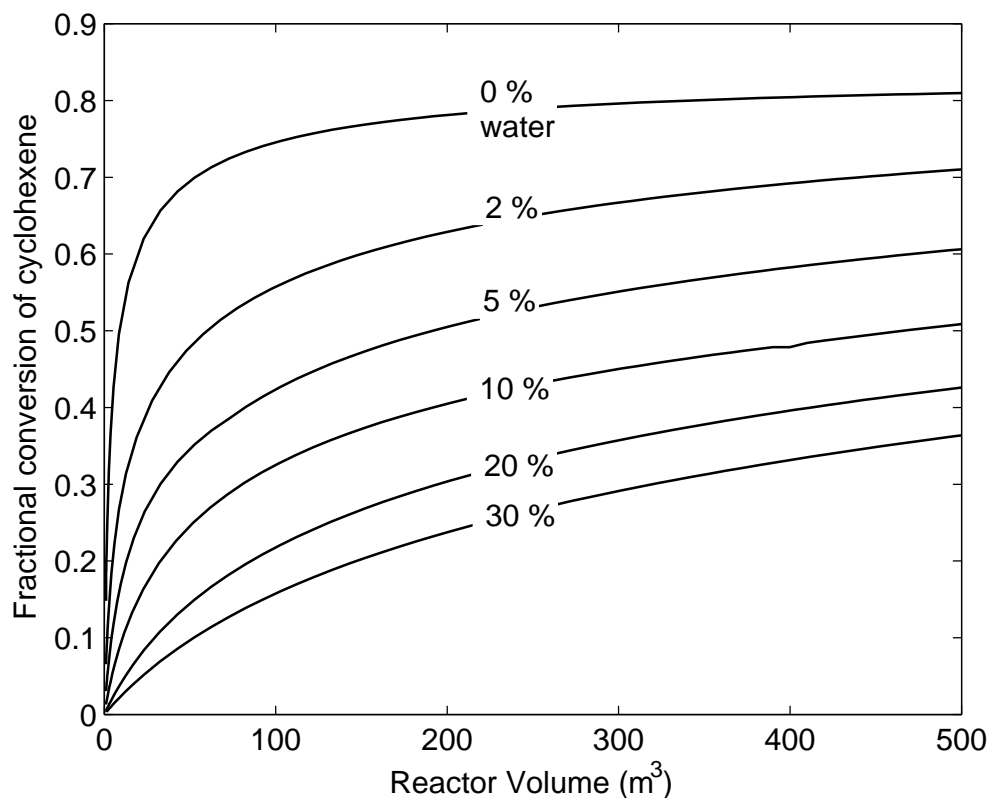


Figure 3.26: Effect of water on esterification. 343K, catalyst loading 10%, Ene:Acid = 1

(as is the case with some zeolite catalysts), the effect of water on the esterification reaction zone can be minimized. This could bring down significant separation cost for the recycle acid stream (water and formic acid exhibit azeotropy).

3.8.4.2 R2S2

While the R1S1 step can be effectively implemented, the second step R2S2 is complicated by phase splitting and multiple reactions occurring at considerable rates. The recovery of formic acid is challenging. Several flow sheet options for R2S2 were developed, analyzed and scrutinized. In the following two potential flow sheet solutions are presented.

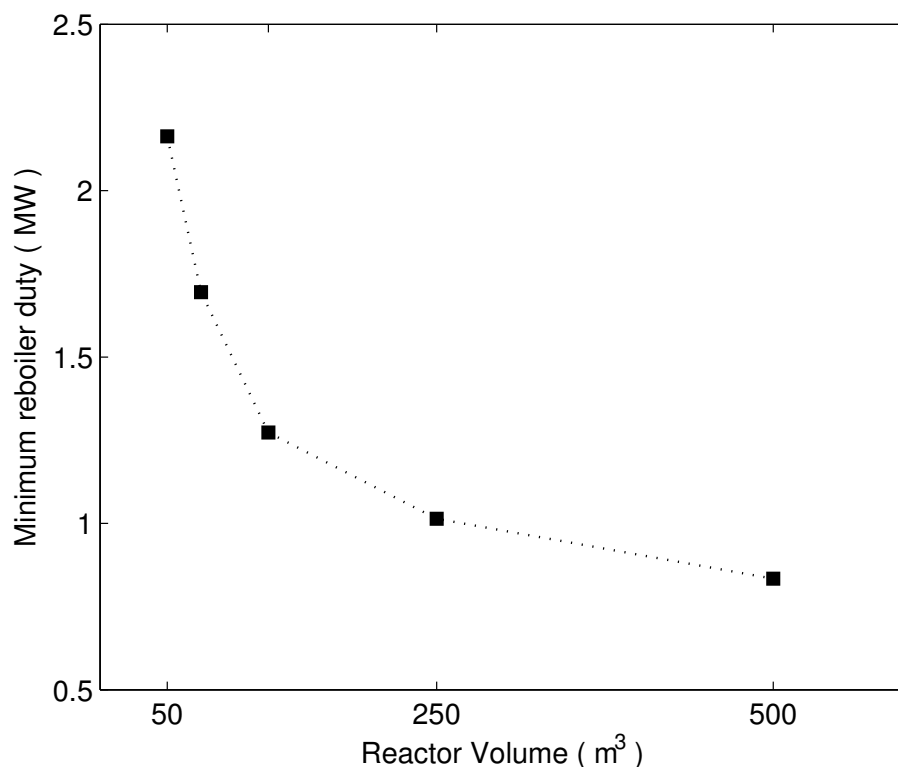


Figure 3.27: Energy requirement R1S1

3.8.4.3 R2S2 cascade case A

The first flow sheet option is schematically presented in Figure 3.28. Cyclohexene and formic acid are fed to R1, ester is separated in S1, the purified ester is then fed to a cascade of reactors and decanters where water is flowing countercurrently from the other end. The aqueous stream (lean in cyclohexanol) is recycled back. The organic stream (rich in cyclohexanol) is sent to the separation section. An optional intermediate extraction column is employed to wash the stream using cyclohexene which displaces some of the water and formic acid. The organic stream contains all the five components in considerable proportions. Therefore, the design of the separation train is very challenging. The selection of a multi component distillation sequence depends on the composition of the stream. But the reactor (R2) is highly sensitive to the feed, in other words to the recycle streams. The recycle streams cannot be determined unless the distillation sequence is fixed. A two step simulation approach was used to address this problem. In the first step ideal splits S2a and S2b (Figure 3.29) were assumed that provide pure streams. These pure streams are recycled back to the appropriate locations. This assumption, even though hypothetical, helps us to identify the best operating conditions of the hydrolysis zone R2. The performance

of R2 is studied and optimized for maximum conversion. In the second step, for this maximum conversion conditions, the distillation sequence is selected and simulated.

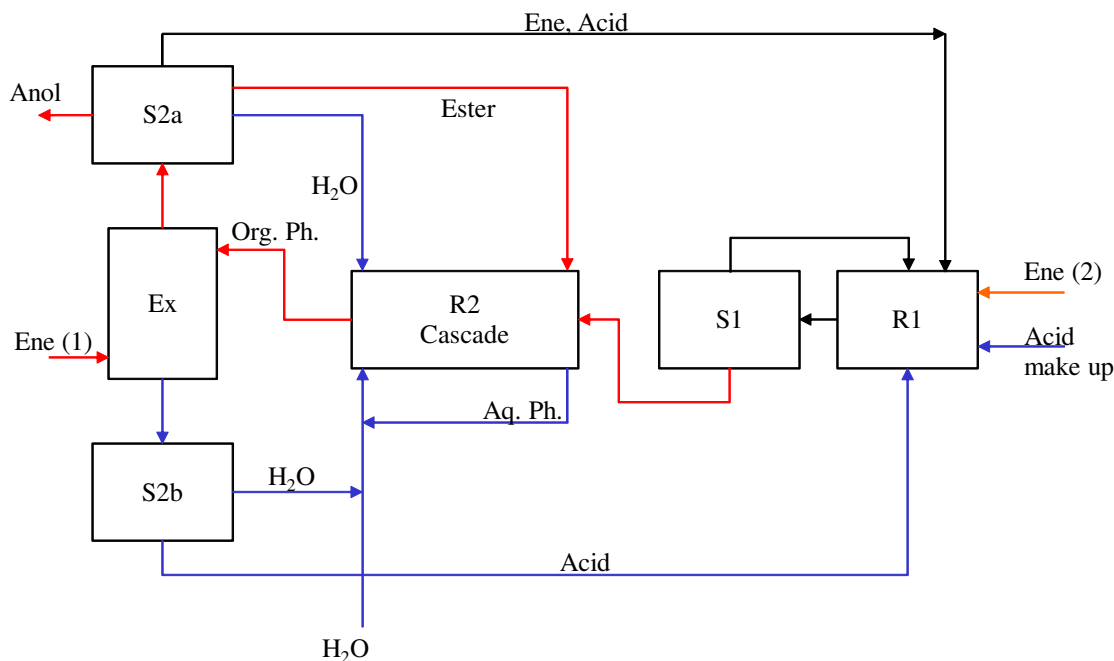


Figure 3.28: R1S1+R2S2C case A process concept; Anol = cyclohexanol, Ene = cyclohexene, Acid:formic acid, Ex-extraction column, S1, S2a and S2b are separator sections, R1 = reactor section 1 (esterification), R2 = reactor section 2 (hydrolysis)

The results of the first step, i.e., simulation with hypothetical separators are presented in Figure 3.29 and Figure 3.30. The reactor size requirement is less but the maximum cyclohexanol level is only about 16%. This occurs because of the presence of formic acid (a reaction product) which hinders the conversion of ester. It is uneconomical to recover the acid from the aqueous stream because the concentration of acid in the aqueous phase is less than 15%. Furthermore, water and formic acid form an azeotrope. Therefore, the formic acid has to be recovered from the organic phase and this in turn affects the overall conversion of the ester. Figure 3.30 gives the effect of Ester:Water ratio which could be an optimization parameter. Figure 3.30 also provides the effect of extraction on the enrichment of the product stream. In the present case, the extraction step is not beneficial. Addition of cyclohexene results in the dilution of the product stream prior to separation.

The second step of the simulation approach, i.e., to design a distillation column sequence for the best stream composition result obtained above is presented in Figure

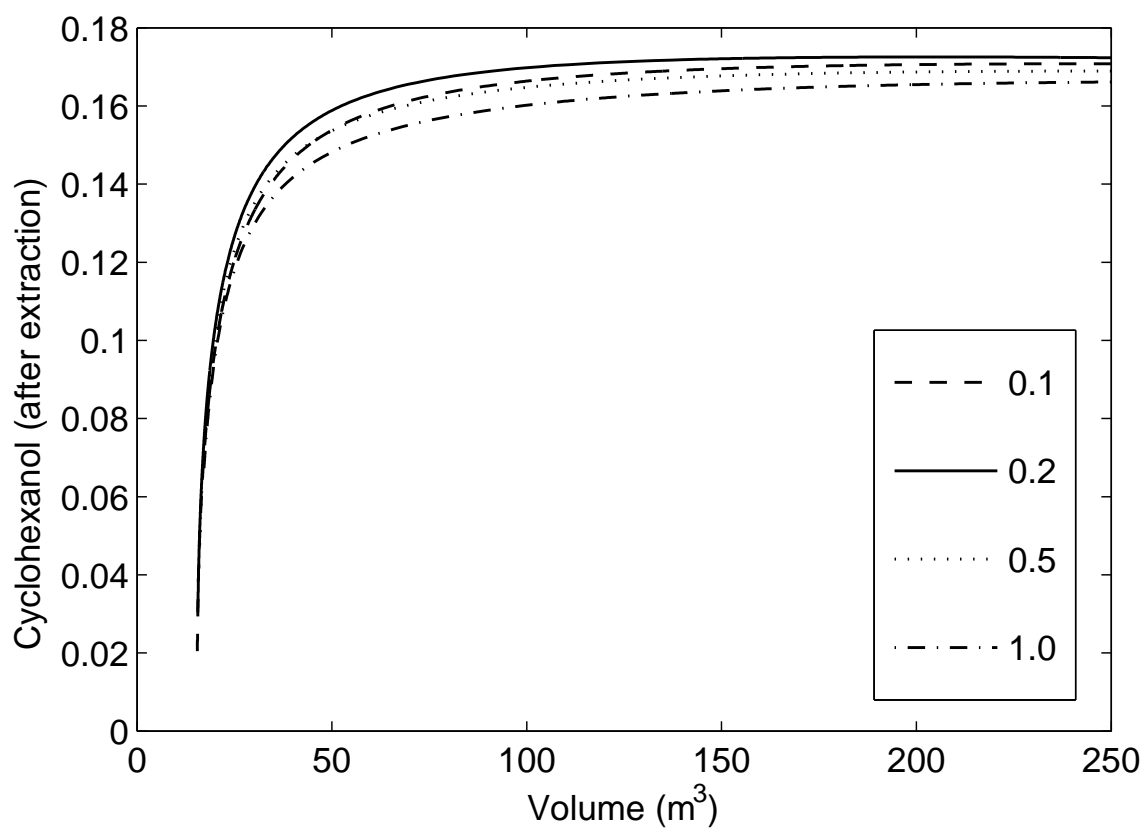


Figure 3.29: Effect of Ester:Water ratio on R2S2Ca. 343K, catalyst loading 30%, $E_{ne}(1) = 37 \text{ mols}^{-1}$ (refer to Figure 3.28)

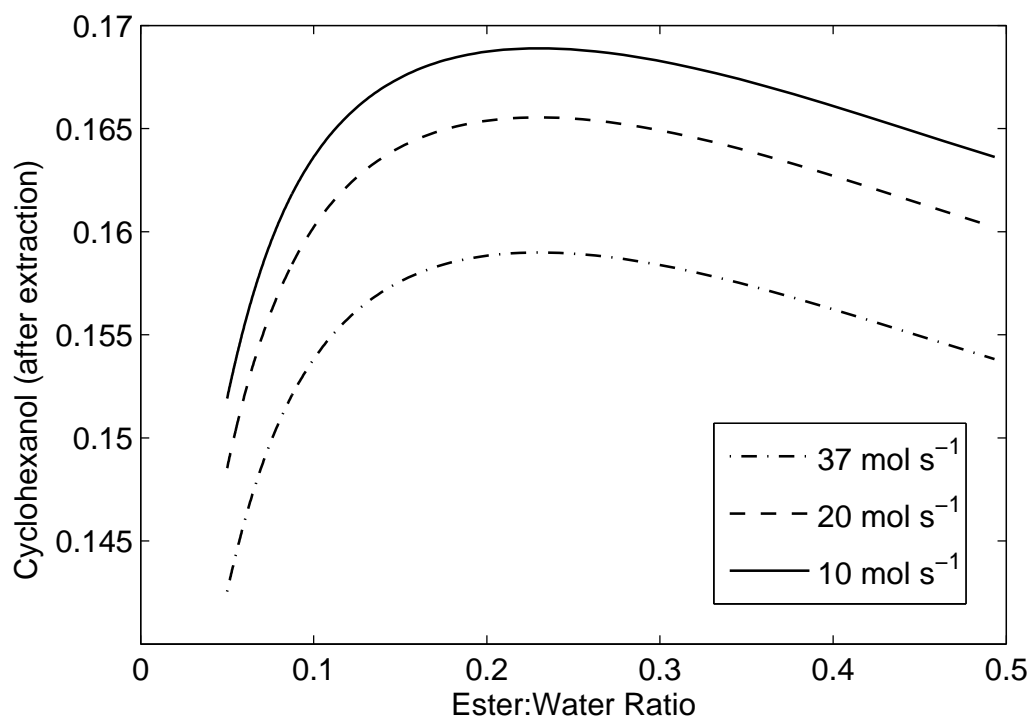


Figure 3.30: Effect of extractant flow rate - Ene(1) (refer to Figure 3.28) on R2S2Ca. 343K, volume 50 m^3 , catalyst loading 30%

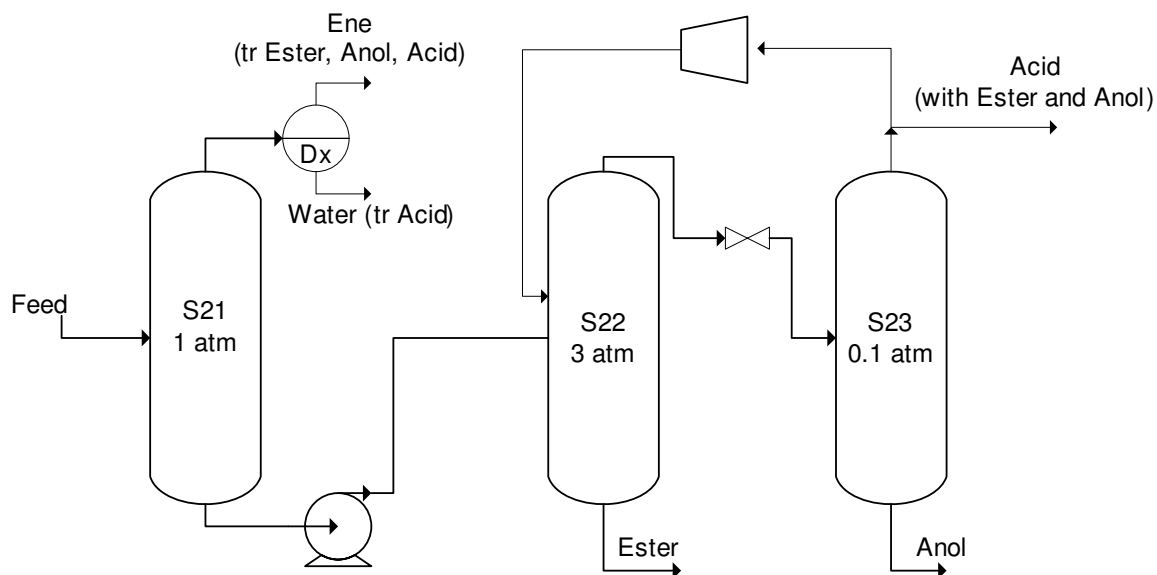


Figure 3.31: Separation design R2S2Ca. Anol = cyclohexanol, Ene = cyclohexene, Acid = formic acid, Dx = decanter, S21 S22 S23 are separators

separator section	S1	S21	S22	S23	Compressor
energy requirement (MW)	1.1	9.2	11.6	4.6	0.85

Table 3.7: Energy requirement R2S2Ca

3.31. The organic stream is first distilled in S21 which separates water and cyclohexene from the rest of the components. Some amount of ester and acid also flow with the distillate. The distillate splits readily and the organic and aqueous streams can be recycled to the appropriate locations. The bottoms from S21 are pumped to a pressure swing distillation column S22+S23. Interconnected streams are in vapor phase to save exergy losses. Acid rich distillate from S23 can be recycled to the esterification section.

A multi-stage isentropic compressor was considered in the simulations. A compression ratio of 3 per stage was considered. Even with multi-stage compression, it is not practical to have a compression ratio of 30 starting from vacuum. But it was considered so in the simulations in order to estimate the maximum energy potential of the process concept. The optimum amount of pressure swing (pressure difference between the columns) can only be determined by detailed simulation studies. But the present analysis gives the potential of the process concept and whether it is required to further study or optimize the process concept.

The typical energy requirement for such a process is given in Table 3.7. The process concept is highly energy intensive. To reduce the separation cost a good conversion of ester is necessary. The key would be to remove the formic acid out of the reaction zone. There are two alternatives to remove the acid from the reaction zones. The first option would be by reactive distillation (RD), but the RD option has its own shortcomings [8]. Despite good performance w.r.t conversion and product purity, the energy consumption was very high. There is a mismatch between distillation conditions and reaction conditions. Formic acid must be stripped, but at the same time water must be maintained in the reaction zone. Furthermore, ester must be maintained in the reaction zone at the same time cyclohexanol must be purified and removed as bottom product. If the RD concept can be slightly modified as distillation with side reactors, it could give a better control over the reaction zone. For example, the reaction temperature can be controlled, the aqueous phase need not be distilled and can be recycled by decantation back to the side reactors. The other alternative for formic acid recovery would be by reactive extraction from the aqueous phase, for

example using an amine [110, 111]. However, this option only shifts the problem one step further downstream to the amine recovery.

3.8.4.4 R2S2 cascade case B

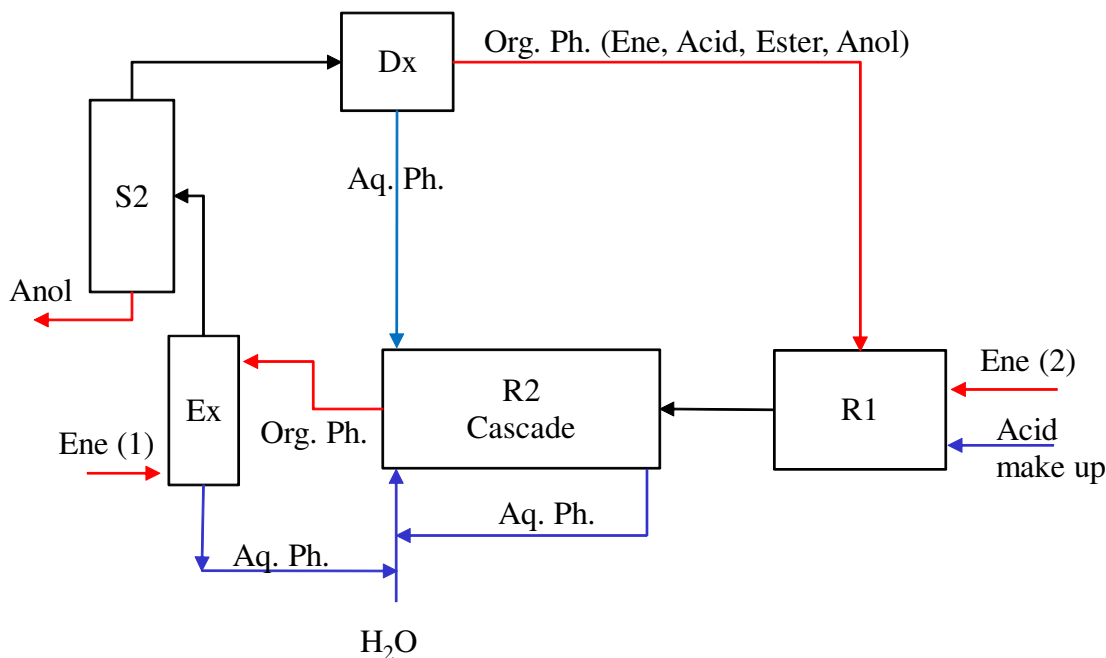


Figure 3.32: R1S1+R2S2C case B process concept. Anol = cyclohexanol, Ene = cyclohexene, Acid = formic acid, Dx:decanter, Ex-extraction column, S2-separator, R1-reactor section 1 (esterification), R2 reactor section 2 (hydrolysis)

This case is similar to the case A, but without the ester purification column S1 as represented in Figure 3.32. This process concept is in fact an intermediate between RS cascade and R2S2 cascade case A. The formic acid recycle between the two reaction zones (i.e. esterification and hydrolysis) is achieved from the organic phase overhead of S2. The amount of acid in the organic phase is a function of the amount of ester and cyclohexanol present in the overhead. Therefore, S2 is operated such that the unreacted ester and some amount of cyclohexanol are present in the overhead. Recycling the organic phase acts as a formic acid pump to the esterification reactor R1. Furthermore, in this case, R1 is most likely homogeneous.

The main idea behind this process concept is to manipulate the total amount of formic acid used in the whole process which is not possible in the former case. Two additional design parameters are present in this case. The first one is the size of

R1, which is kept at a constant value of 250 m^3 throughout the simulations. This value was chosen because 250 m^3 was more than sufficient to get the maximum conversion possible in R1 at 353 K. The second new design parameter is the split fraction of cyclohexanol in the distillation column S2. The higher the cyclohexanol in the distillate the higher is the amount of formic acid recycled to R1 resulting in a smaller reactor size requirement (refer to Figure 3.33). However, on the other hand it increases the amount of liquid to be distilled to meet the production rate. Figure 3.34 and 3.35 illustrate the effect of the Acid:Water ratio. The Acid:Water ratio represents the effective acidity of a system. It can be observed from Figure 3.34, that even though a higher Acid:Water ratio decreases the reactor size requirement, the level of ester is also increased considerably. This would result in a higher separation cost. In order to distinguish between the effects of Acid:Ene and Acid:Water ratios the following analysis was done. Figure 3.35(a) and 3.35(b) represent the effect of Acid:Ene at Acid:Water ratio of 0.05 and 0.25, respectively. At an Acid:Water ratio of 0.25, the increase in the Acid:Ene ratio caused a decrease in the ester level (Figure 3.35(b)). This behavior is the other way around at an Acid:Water ratio of 0.05 (Figure 3.35(a)), where the increase in Acid:Ene ratio cause an increase in the ester level. Therefore, it is not only the amount of acid that is important but the amount of acid in relation to water, i.e., the Acid:Water ratio could be the key parameter that could influence the behavior of the process qualitatively. Furthermore, it can be observed from Figure 3.35(b), that even though the Acid:Ene ratio is less, a higher Acid:Water ratio can substantially increase the level of ester in the product.

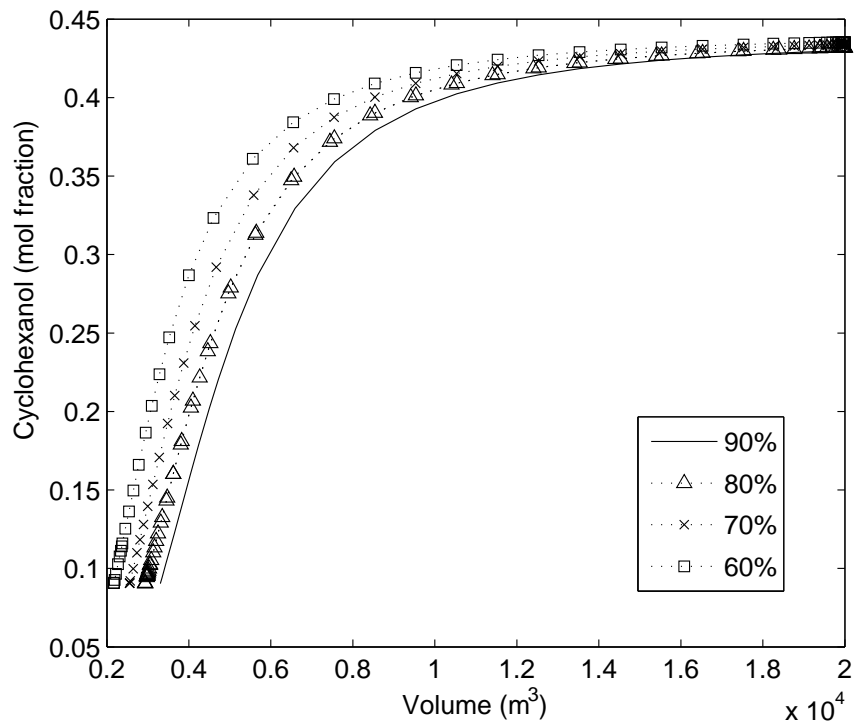


Figure 3.33: Effect of cyclohexanol split fraction on R2S2Cb

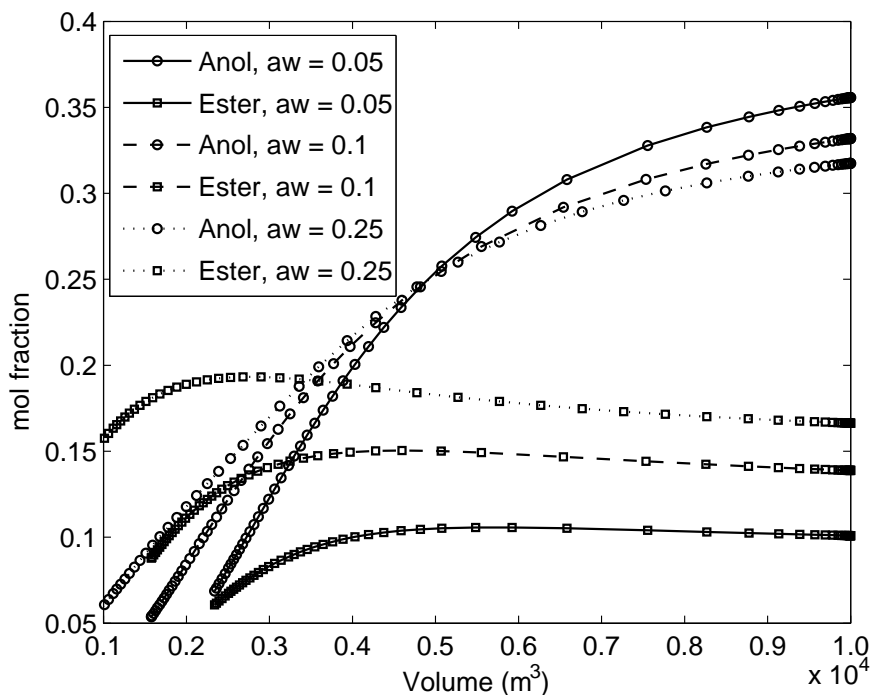
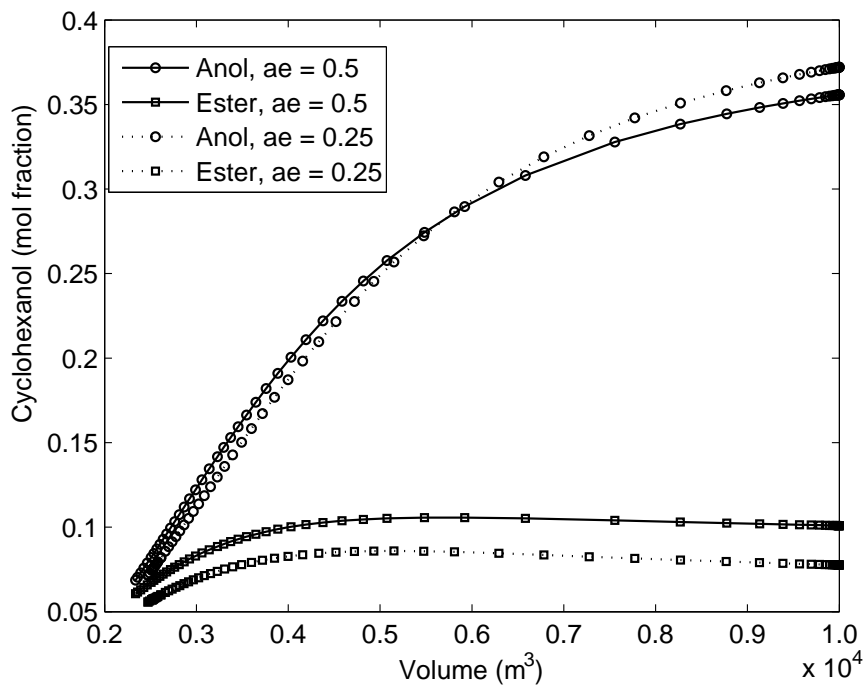


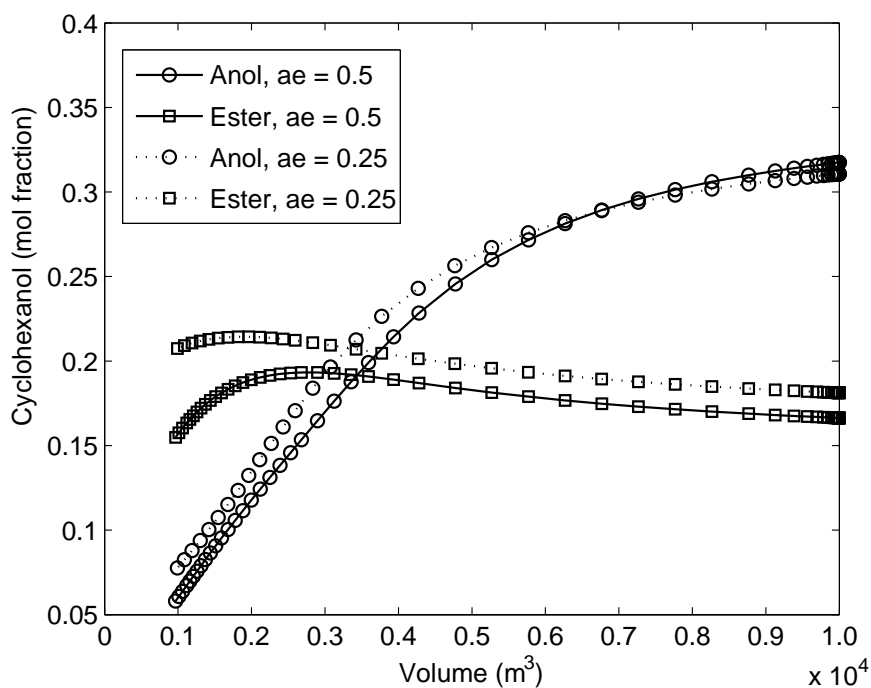
Figure 3.34: Effect of Acid:Water ratio on R2S2Cb. 353K, cyclohexanol split fraction = 80%, Acid:Ene = 0.5, Amberlyst loading 30%. Anol = cyclohexanol, Ene = cyclohexene, Acid = formic acid, Ester = cyclohexylformate

3.9 Summary of Chapter 3

The limitations of the direct hydration process route were discussed. Liquid-liquid phase splitting was limiting the attainable conversion to about 15%. A way to overcome this limitation is by using solvents so as to bring down the miscibility gap. Previous solvent based processes reported in the literature required excessive use of solvent and the downstream solvent recovery was very expensive. To bring down the separation costs as well as to overcome the thermodynamic limitations, a thermo-morphic solvent would be beneficial. Therefore, a search for thermo-morphic solvents was carried out using a systematic procedure. The most promising solvents that exhibit good thermo-morphic behavior are selected for experimental verification. LLE experiments were carried out to verify the thermo-morphic property. Dimethylsulfoxide showed a reasonably good thermo-morphic behavior, but the reaction kinetic experiments showed extremely slow reaction rate. This effect could be attributed to the stabilization of the protons by solvents [49]. It is extremely challenging to select a solvent which is good in solvency (dissolve both water and cyclohexene), which is



(a)



(b)

Figure 3.35: Effect of Acid:Ene ratio on R2S2Cb at 353K, catalyst loading 30%, cyclohexanol split fraction 80%. (a) Acid:Water=0.05, (b) Acid:Water=0.25. Anol = cyclohexanol, Ester = cyclohexylformate

inert in the reaction environment, which does not stabilize the protons affecting the reaction rate and which also exhibits a good thermo-morphic behavior.

Another promising way to improve the conversion of the hydration of cyclohexene is to change the chemical equilibrium by lowering the reaction temperature. Since at a low temperature the direct hydration reaction rate is not appreciable, an indirect hydration process route was proposed by Steyer et al. [1] which is significantly faster than the direct hydration reaction rate. As the previously proposed process concepts for indirect hydration were strongly limited by multiple steady states, a search for alternative process concepts was carried out.

Dedicated experiments were carried out to ensure the validity of the kinetic model in the widely varying compositional space and temperature range of process concepts. Esterification, hydrolysis and reverse hydrolysis experiments were carried out in batch reactor mode. Amberlyst 15 was used as the catalyst in most of the experiments. To study the effect of catalyst type, Zeolite ZSM-5 was employed in a few experiments so as to compare it with Amberlyst 15. Zeolite ZSM-5 performed better than Amberlyst 15 at higher temperature for the esterification reaction. It was the other way around for the hydrolysis reaction when it was considerably slower than Amberlyst 15. This suggests a scope of improvement towards an efficient design of the catalyst. Long time experiments were performed to accurately calculate the heat of formation of cyclohexylformate. The calculated value agrees well with the previous literature value predicted by group contribution methods [96]. The reaction equilibrium is found to be highly sensitive to the heat of formation of the ester. Parameter estimation was carried out and the updated kinetic parameters have been reported.

Various process concepts were developed [112]. They can be categorized under two broad sections as RS process concept and R1S1+R2S2 process concept. An ideal RS process gave the limiting case of maximum performance yielding substantial energy saving (2-4 times smaller) compared to the conventional Asahi process. But a real RS process concept required a very large reactor. Different methods to improve the performance of the concept were investigated. Higher temperature, higher catalyst loading, higher Acid:Ene ratio and countercurrent cascade process concepts were employed to bring down the reactor size requirement. Despite all the measures taken to improve the RS process concept, the reactor size requirement is still very large.

The second category of process concepts studied is R1S1+R2S2 with segregated reaction and separation steps. The first step, namely R1S1, was very effective. The reactor size requirement was less than $250 m^3$ and very high conversion was possible. But the hydrolysis step was complicated by extensive phase splitting and multiple

reactions proceeding at comparable rates. Various flow sheet options were considered and analyzed. The most promising flow sheet options were studied in detail. Two cases were considered. In case A, purified ester is hydrolyzed in counter-current cascades. The formic acid is recovered from the organic phase by distillation. Even though the reactor size requirement was very less, the energy requirement for such a process is very high. This was due to the presence of large amount of ester in the product stream that has to be separated and recycled.

Therefore, a second case (R2S2Cb) was studied where the product stream from the esterification is sent directly to the hydrolysis section. This case provided an additional degree of freedom for control, i.e., the acid level in the reactor, which in turn allowed us to maintain a lower level of ester in the product stream. This flexibility reduced the energy requirement as compared to the R2S2Ca case, but the reactor size requirement was higher.

Chapter 4

Conclusion and outlook

4.1 Conclusion

An overall view of the challenges in the process concepts development for the indirect hydration of cyclohexene using formic acid has been presented.

Thermo-morphic solvents can potentially provide an economical way to perform solvent based direct hydration of cyclohexene. A systematic procedure was demonstrated for the selection of thermo-morphic solvents for the direct hydration system. Dimethylsulfoxide showed a reasonably good thermo-morphic behavior, but the reaction kinetic experiments showed extremely slow reaction rate. This effect could be attributed to the stabilization of the protons by solvents.

Another way to improve the overall conversion of the direct hydration is by changing the chemical equilibrium by lowering the reaction temperature. At lower temperature the indirect hydration of cyclohexene using formic acid provides significantly higher reaction rates than the direct hydration rate.

The earlier proposed process concept for the indirect hydration of cyclohexene, i.e., coupled column reactive distillation exhibited multiple steady states with a very narrow operating window. Not only this system but many liquid-liquid processes exhibit such complex dynamic behavior. Multiple steady states are caused by nonlinearities in the system. An important nonlinearity in highly non-ideal liquid-liquid phase splitting systems is that of the activity models. From a theoretical point of view it is interesting to understand the effect of nonlinearity in the activity models on the multiple steady states in liquid-liquid systems. A generalized non-equilibrium model based on linear thermodynamics of irreversible processes was presented. It was found that the nonlinearity in even the simplest non-ideal activity model (Margules) can act as a source of multiple steady states. The parameters that affect the solubility of the

Parameter / Concepts	Qualitative Effect Sensitive (+) / Insensitive (-)
Heat of formation	+
Temperature	+
Catalyst loading	+
Acid:Ene ratio	+
Ene:Water ratio / Ester:Water ratio	-
Acid:Water ratio	+
Catalyst type	+
Counter-current operation	+/-
Benefit of extraction column	-
Anol split fraction (R2S2Cb)	+

Table 4.1: Overview of effects of parameters/intensification concepts

system such as for example the temperature can play a critical role in determining the multiple steady states behavior [113].

There are further challenges associated with the indirect hydration of cyclohexene. Particularly, the interplay of reactions, phase equilibrium, separation and feed back (recycle streams) should be understood. Therefore, a systematic study of process concepts was carried out.

Dedicated experiments were carried out to ensure the validity of the kinetic model in the widely varying compositional space and temperature range of process concepts. The updated kinetic parameters are reported. Long time batch kinetic experiments were performed to accurately calculate the heat of formation of cyclohexylformate. To study the effect of catalyst type, Zeolite ZSM-5 was employed in a few experiments so as to compare it with Amberlyst 15. Zeolite ZSM-5 performed better than Amberlyst 15 at higher temperature for the esterification reaction. It was the other way around for the hydrolysis reaction when it was considerably slower than Amberlyst 15. This suggests a scope of improvement towards an efficient design of the catalyst.

Various process concepts were developed [112]. They can be categorized under two broad sections as RS process concept and R1S1+R2S2 process concept. Table 4.1 and 4.2 present an overview of the key results of different process concepts studied. For the explanation of the abbreviations refer to section 3.6. The energy requirement in Table 4.2 is for 100 kt/a of cyclohexanol production.

Process concepts	PROS	CONS	Scope of improvement
RS, RSCa, RSCb	<ul style="list-style-type: none"> - High Conversion - Minimum energy (1.9 - 3.6 MW) 	<ul style="list-style-type: none"> - Very large reactor 	<ul style="list-style-type: none"> - Catalyst design
R1S1+ R2S2Ca	<ul style="list-style-type: none"> - Smaller reactor 	<ul style="list-style-type: none"> - Acid recovery - High energy (>15 MW) 	<ul style="list-style-type: none"> - Removal of acid from the reactor for e.g., reactive distillation, reactive extraction
R1S1 + R2S2Cb	<ul style="list-style-type: none"> - Moderate energy (5.3 MW) 	<ul style="list-style-type: none"> - Large reactor 	<ul style="list-style-type: none"> - Catalyst design

Table 4.2: Process concepts summary

In a nutshell, the energy consumption in a RS process concept is significantly lower (3.5 MW) as compared to 7.5 MW of the Asahi process, but the reactor size requirement is very large. The R1S1+R2S2Ca process concept has the smallest reactor size requirement but highest energy demand (more than 25 MW). The R1S1+R2S2Cb process concept has a moderate energy requirement (ca. 5.3 MW) and a relatively smaller reactor size requirement as compared to the RS process concept.

4.2 Outlook

The theoretical study presented in Chapter 2 can be further extended to study the interaction of nonlinearity in activity models with other sources of multiple steady states. For e.g. it would be interesting as well as challenging to study the effect of nonlinearity in the activity models on the multiple steady states of a reactive distillation column (where the reaction kinetic nonlinearity and feedback effects come into play).

The process concepts discussed in Chapter 3 can be further improved. The most promising option is the RS process concept with improved catalyst design. For example, the zeolite can be modified to control its surface characteristics; thereby avoiding flooding of water on the catalyst surface and therefore could improve the hydrolysis reaction. A recent work of Shan et al. [23] suggests that the mechanism of direct hydration catalyzed by the Zeolite and that by the ion-exchange resins are different. Referring to the work related to the Asahi process (see refs [4–6]), the design of the zeolite catalyst is based on several characteristics. The size of the catalyst, the size of the ring, the Si:Al ratio, etc. are finely tuned for the direct hydration reaction. The Si:Al ratio, e.g., affects the surface characteristics such as hydrophobicity or hydrophilicity, adsorption coefficients, etc. In the present work, the same catalyst was used for both reactions which may not be the ideal option. If the catalyst were to be designed specifically for esterification and hydrolysis, there is a better scope for improvement in the performance. In the case of RS process concept, the esterification reaction is the rate limiting step. Therefore, any development of catalyst must first address the improvement of the esterification reaction under excess aqueous conditions. The surface characteristics of the catalyst can be modified to adsorb the preferred components. For example, preferable adsorption of cyclohexene and formic acid will benefit esterification. Optimum catalyst design for this particular reaction type is the key to realize the RS process concept.

In the R1S1+R2S2Ca process concept, an interesting improvement could be the

removal of formic acid from the hydrolysis zone. This is because the conversion of ester in the hydrolysis step was hindered by formic acid. Selective removal of formic acid would benefit the conversion of ester. Alternative methods can be developed to remove formic acid from the reactor. In this regard, distillation with side reactors can be beneficial.

Cyclohexane is the most likely inert that could be present in the feed stream along with cyclohexene. The influence of cyclohexane adds another dimension of complexity to the design problem. It would require a separate study to address this case. However, the coupled column reactive distillation process concept proposed by Steyer et al. [2] could successfully handle cyclohexane inert in the feed stream [8]. The esterification RD column was efficient with nearly complete conversion of cyclohexene. Nearly pure cyclohexane was obtained from the top section of the column. This option could be highly advantageous as it has the potential to save the upstream extractive distillation cost that separates the benzene-cyclohexene-cyclohexane mixture. However, there were compromises with regard to the catalyst loading/hold up and reboiler duty for the case with inert when compared to the case without inert. In the present work of this thesis, the R1S1 step has been found to be very efficient, because up to 80% conversion of cyclohexene can be realized in R1 alone. Therefore, if the R1S1 step would be modified as R1RD1 (reactor 1 + reactive distillation 1), the cyclohexane problem can be tackled effectively. The load on the RD column will be less as compared to the pure RD case as it only has to convert the remaining 20% cyclohexene. A comparative study of RD, R1S1 and R1RD1 from energy and capital cost point of view would be interesting.

Furthermore, the solvent based process concepts for the direct hydration can also be an interesting option. Research in this direction is currently active [22, 48] and the success of the technology will depend on the effect of solvent on reaction kinetics and the downstream separation cost.

Appendix A

Physico-chemical parameters

A.1 NRTL parameters

The NRTL model [83] is used to calculate the activities and LLE. The NRTL parameters calculated from experiments by Steyer et al. [57, 58] are provided in the Table A.1.

A.2 Antoine parameters

Antoine parameters are used for calculating vapor pressure data for distillation column simulations. The Antoine parameters are provided in Table A.2.

The Antoine equation used was

$$\log P = A - \frac{B}{T + C} \quad (\text{A.1})$$

where P is in bars and T is in K.

binary pair	g_{12} $Jmol^{-1}$	g_{21} $Jmol^{-1}$	α_{12}
cyclohexene (1) + cyclohexanol (2)	3568.41	-0.96	0.80
cyclohexanol (1) + formic acid (2)	-1778.81	3290.04	0.69
cyclohexene (1) + water (2)	14 175.42	695.00	0.27
water (1) + cyclohexane (2)	25 048.50	17 650.00	0.26
cyclohexene (1) + cyclohexane (2)	42.48	60 957.20	0.83
water (1) + FCE (2)	15 899.10	5877.86	0.29
cyclohexene (1) + FCE (2)	-2390.29	3308.21	0.22
water (1) + formic acid (2)	3507.57	-4043.93	0.14
cyclohexene (1) + formic acid (2)	7828.68	7619.60	0.34
cyclohexane (1) + FCE (2)	3627.17	-2134.86	0.32
cyclohexanol (1) + water (2)	1336.76	10 959.40	0.36
cyclohexane (1) + formic acid (2)	10 153.60	9943.91	0.29
cyclohexanol (1) + cyclohexane (2)	19.93	4071.64	0.99
FCE (1) + formic acid (2)	-415.71	3158.48	0.77
cyclohexanol (1) + FCE (2)	1540.33	337.62	0.31

Table A.1: NRTL parameters

substance	A	B	C	T range (K)
cyclohexene	3.98	1206.02	-52.78	310-360
cyclohexanol	4.07	1258.75	-123.67	320-435
water	5.01	1605.78	-52.20	300-375
cyclohexane	3.97	1191.56	-53.27	305-355
FCE	4.10	1489.03	-71.48	305-435
formic acid	4.58	1608.22	-21.90	265-385

Table A.2: Antoine parameters

Appendix B

Experimental data

The experimental batch reaction kinetic data and LLE data are provided here. Every sample has been analyzed three times in GC to ensure the accuracy of the measurements.

B.1 Esterification experiments

Table B.1: Esterification: mol ratio 1:1

T	mol ratio	Amberlyst 15	Ene	Acid		
333 K	Ene:Acid 1:1	7 g	41 g	23 g		
Ene	Acid	Ester	Anol	Water	Time (h)	
0.928	0.072	0.000	0	0	0.25	
0.926	0.072	0.002	0	0	0.25	
0.926	0.072	0.001	0	0	0.25	
0.877	0.094	0.028	0	0	0.67	
0.876	0.094	0.029	0	0	0.67	
0.875	0.094	0.029	0	0	0.67	
0.816	0.118	0.060	0	0.004	1.5	
0.814	0.119	0.061	0	0.004	1.5	
0.814	0.119	0.061	0	0.004	1.5	
0.577	0.254	0.147	0.002	0.019	5.5	
0.576	0.255	0.147	0.002	0.019	5.5	
0.575	0.255	0.148	0.002	0.019	5.5	

Cont inued...

Ene	Acid	Ester	Anol	Water	Time (h)
0.376	0.339	0.234	0.007	0.044	21
0.374	0.341	0.234	0.007	0.045	21
0.374	0.341	0.234	0.007	0.044	21
0.341	0.295	0.303	0.010	0.050	29
0.339	0.305	0.299	0.010	0.047	29
0.339	0.305	0.300	0.010	0.047	29
0.295	0.266	0.382	0.013	0.045	46
0.294	0.269	0.380	0.013	0.044	46
0.293	0.272	0.379	0.013	0.044	46
0.280	0.249	0.413	0.014	0.044	54
0.279	0.259	0.407	0.014	0.041	54
0.278	0.260	0.405	0.014	0.042	54
0.250	0.226	0.460	0.018	0.045	71
0.249	0.236	0.454	0.018	0.043	71
0.248	0.237	0.453	0.018	0.044	71
0.205	0.202	0.533	0.021	0.039	97
0.204	0.210	0.528	0.021	0.038	97
0.203	0.211	0.527	0.021	0.038	97
0.182	0.191	0.564	0.024	0.039	120
0.181	0.200	0.558	0.024	0.038	120
0.180	0.202	0.556	0.024	0.038	120
0.150	0.169	0.621	0.025	0.036	148
0.148	0.178	0.615	0.024	0.035	148
0.148	0.179	0.613	0.025	0.035	148
0.155	0.181	0.594	0.029	0.041	169
0.153	0.190	0.588	0.029	0.039	169
0.153	0.192	0.586	0.029	0.039	169
0.138	0.174	0.620	0.030	0.039	193
0.137	0.181	0.615	0.030	0.038	193
0.136	0.183	0.613	0.030	0.038	193
0.126	0.174	0.632	0.031	0.037	217
0.126	0.176	0.631	0.031	0.036	217
0.115	0.206	0.599	0.031	0.049	245
0.114	0.215	0.592	0.031	0.048	245
0.114	0.217	0.590	0.031	0.047	245
0.098	0.238	0.580	0.031	0.053	310
0.098	0.245	0.574	0.031	0.052	310

Table B.2: Esterification: mol ratio 1:2

T 333 K	mol ratio Ene:Acid 1:2	Amberlyst 15 5.6 g	Ene 20.4 g	Acid 23 g	
Ene	Acid	Ester	Anol	Water	Time (h)
0.330	0.646	0	0	0.015	0
0.332	0.356	0.254	0.006	0.052	16.5
0.304	0.406	0.237	0.005	0.049	16.5
0.307	0.402	0.237	0.005	0.050	16.5
0.234	0.280	0.424	0.012	0.049	41
0.213	0.340	0.389	0.011	0.047	41
0.214	0.339	0.390	0.011	0.046	41
0.163	0.280	0.494	0.016	0.047	64.5
0.154	0.311	0.473	0.016	0.046	64.5
0.156	0.305	0.477	0.016	0.047	64.5
0.118	0.282	0.537	0.018	0.045	89
0.117	0.288	0.532	0.018	0.044	89
0.094	0.244	0.596	0.021	0.044	116.75
0.096	0.219	0.606	0.022	0.057	116.75
0.091	0.265	0.579	0.021	0.044	116.75
0.079	0.232	0.627	0.022	0.040	142.5
0.077	0.248	0.613	0.021	0.040	142.5
0.076	0.254	0.610	0.021	0.039	142.5
0.068	0.238	0.635	0.022	0.038	167.17
0.067	0.249	0.626	0.022	0.037	167.17
0.067	0.248	0.627	0.022	0.037	167.17
0.062	0.229	0.649	0.023	0.038	190.17
0.061	0.240	0.640	0.022	0.037	190.17
0.060	0.244	0.637	0.022	0.037	190.17
0.054	0.219	0.664	0.024	0.039	232.67
0.054	0.224	0.662	0.024	0.037	232.67
0.058	0.155	0.714	0.025	0.047	232.67
0.049	0.223	0.666	0.024	0.038	289.67
0.048	0.230	0.661	0.024	0.038	289.67
0.049	0.228	0.662	0.024	0.037	289.67
0.049	0.196	0.687	0.024	0.044	352.17
0.047	0.220	0.671	0.024	0.038	352.17
0.047	0.221	0.671	0.024	0.036	352.17
0.053	0.140	0.780	0.027	0	407.25
0.046	0.220	0.673	0.024	0.037	407.25
0.045	0.223	0.672	0.024	0.036	407.25

Table B.3: Esterification: mol ratio 1:3

T	mol ratio	Amberlyst 15	Ene	Acid		
333 K	Ene:Acid 1:3	9.42 g	20.4 g	34.8 g		
Ene	Acid	Ester	Anol	Water	Time (h)	
0.244	0.739	0	0	0.017	0	
0.104	0.620	0.186	0.005	0.085	7.17	
0.105	0.618	0.187	0.005	0.085	7.17	
0.105	0.619	0.186	0.005	0.085	7.17	
0.018	0.558	0.318	0.010	0.096	29.55	
0.017	0.590	0.292	0.009	0.092	29.55	
0.017	0.587	0.294	0.009	0.092	29.55	
0.009	0.565	0.321	0.010	0.095	50	
0.009	0.581	0.307	0.009	0.094	50	
0.008	0.583	0.303	0.009	0.097	50	
0.008	0.538	0.344	0.011	0.100	69.75	
0.007	0.582	0.307	0.010	0.094	69.75	
0.007	0.579	0.308	0.009	0.097	69.75	
0.007	0.581	0.308	0.010	0.095	78.25	
0.007	0.580	0.308	0.009	0.096	78.25	
0.007	0.580	0.306	0.009	0.098	78.25	

Table B.4: Esterification: mol ratio 1:1, without catalyst

T	mol ratio	catalyst	Ene	Acid		
333 K	Ene:Acid 1:1	0 g	41 g	23 g		
Ene	Acid	Ester	Anol	Water	Time (h)	
0.500	0.475	0	0	0.025	0	
0.924	0.063	0.013	0	0	2	
0.912	0.075	0.013	0	0	2	
0.911	0.076	0.013	0	0	2	
0.876	0.097	0.028	0	0	4.5	
0.873	0.100	0.028	0	0	4.5	
0.872	0.101	0.028	0	0	4.5	
0.725	0.185	0.090	0	0	19.5	
0.720	0.190	0.089	0	0	19.5	
0.720	0.191	0.089	0	0	19.5	

B.2 Comparison of Amberlyst 15 and Zeolite ZSM-5

B.2.1 Esterification

Table B.5: Zeolite, 333 K, Esterification

T	mol ratio	Zeolite ZSM-5	Ene	Acid		
333 K	Ene:Acid 1:1	7 g	41 g	23 g		
Ene	Acid	Ester	Anol	Water	Time (h)	
0.500	0.475	0	0	0.025	0	
0.896	0.066	0.038	0.000	0.000	0.5	
0.892	0.070	0.038	0.000	0.000	0.5	
0.891	0.071	0.038	0.000	0.000	0.5	
0.809	0.112	0.073	0.001	0.006	1.2	
0.808	0.113	0.073	0.001	0.006	1.2	
0.808	0.112	0.073	0.001	0.006	1.2	
0.765	0.131	0.096	0.001	0.007	2.05	
0.765	0.131	0.096	0.001	0.007	2.05	
0.764	0.131	0.096	0.001	0.007	2.05	
0.617	0.219	0.142	0.002	0.019	4.47	
0.614	0.223	0.142	0.002	0.019	4.47	
0.614	0.224	0.142	0.002	0.019	4.47	
0.544	0.272	0.159	0.003	0.023	6	
0.541	0.276	0.159	0.003	0.022	6	
0.542	0.276	0.158	0.003	0.022	6	

Table B.6: Zeolite, 343 K, Esterification

T	mol ratio	Zeolite ZSM-5	Ene	Acid		
343 K	Ene:Acid 1:1	7 g	41 g	23 g		
Ene	Acid	Ester	Anol	Water	Time (h)	
0.500	0.475	0	0	0.025	0	
0.807	0.110	0.073	0.001	0.009	0.5	
0.803	0.115	0.073	0.001	0.009	0.5	
0.802	0.116	0.073	0.001	0.008	0.5	

Cont inued...

Ene	Acid	Ester	Anol	Water	Time (h)
0.802	0.116	0.073	0.001	0.008	0.5
0.741	0.140	0.109	0.001	0.009	1
0.741	0.140	0.109	0.001	0.009	1
0.741	0.140	0.109	0.001	0.009	1
0.560	0.264	0.151	0.003	0.023	2
0.559	0.264	0.151	0.003	0.023	2
0.559	0.265	0.151	0.003	0.023	2
0.453	0.306	0.201	0.006	0.035	4
0.453	0.307	0.201	0.006	0.035	4
0.453	0.307	0.201	0.005	0.035	4
0.364	0.345	0.229	0.008	0.055	6
0.364	0.344	0.229	0.008	0.055	6
0.364	0.345	0.229	0.008	0.055	6

Table B.7: Amberlyst, 343 K, Esterification

T	mol ratio	Amberlyst 15	Ene	Acid	
343 K	Ene:Acid 1:1	7 g	41 g	23 g	
Ene	Acid	Ester	Anol	Water	Time (h)
0.500	0.475	0	0	0.025	0
0.854	0.094	0.046	0.000	0.007	0.5
0.850	0.098	0.046	0.000	0.006	0.5
0.848	0.100	0.046	0.000	0.006	0.5
0.796	0.124	0.072	0.001	0.008	1
0.796	0.124	0.072	0.001	0.008	1
0.795	0.124	0.072	0.001	0.009	1
0.680	0.185	0.118	0.002	0.015	2
0.678	0.189	0.118	0.002	0.015	2
0.677	0.189	0.118	0.002	0.015	2
0.508	0.290	0.166	0.004	0.033	4
0.507	0.291	0.166	0.004	0.033	4
0.507	0.290	0.166	0.004	0.033	4
0.443	0.317	0.192	0.005	0.044	6
0.440	0.320	0.191	0.005	0.044	6
0.440	0.321	0.191	0.005	0.044	6

Table B.8: Amberlyst, 333 K, Esterification

T	mol ratio	Amberlyst 15	Ene	Acid		
333 K	Ene:Acid 1:1	7 g	41 g	23 g		
Ene	Acid	Ester	Anol	Water	Time (h)	
0.914	0.071	0.015	0.000	0.000	0.25	
0.914	0.071	0.015	0.000	0.000	0.25	
0.914	0.071	0.015	0.000	0.000	0.25	
0.871	0.093	0.036	0.000	0.000	0.67	
0.870	0.094	0.036	0.000	0.000	0.67	
0.871	0.094	0.036	0.000	0.000	0.67	
0.812	0.118	0.066	0.001	0.005	1.5	
0.811	0.119	0.066	0.001	0.004	1.5	
0.811	0.119	0.065	0.001	0.005	1.5	
0.576	0.253	0.150	0.002	0.019	5.5	
0.575	0.255	0.149	0.002	0.019	5.5	
0.574	0.255	0.150	0.002	0.019	5.5	

B.2.2 Hydrolysis

Table B.9: Zeolite, 343 K, Hydrolysis

T	mol ratio	Zeolite ZSM-5	Ester	Water		
343 K	Ester-Water 1:2	7 g	32 g	9 g		
Ene	Acid	Ester	Anol	Water	Time (h)	
0	0.005	0.986	0.010	0	0	
0	0.004	0.986	0.010	0	0	
0	0.005	0.985	0.010	0	0	
0.000	0.004	0.817	0.042	0.136	0.5	
0.000	0.005	0.816	0.042	0.136	0.5	
0.000	0.005	0.815	0.042	0.137	0.5	

Cont inued...

Ene	Acid	Ester	Anol	Water	Time (h)
0.001	0.008	0.644	0.072	0.275	1.5
0.001	0.008	0.652	0.073	0.266	1.5
0.001	0.009	0.653	0.073	0.264	1.5
0.003	0.032	0.499	0.190	0.276	2.5
0.001	0.021	0.655	0.141	0.182	2.5
0.001	0.022	0.657	0.141	0.179	2.5
0.002	0.043	0.520	0.209	0.226	4.5
0.002	0.045	0.519	0.209	0.225	4.5
0.002	0.045	0.518	0.209	0.226	4.5
0.005	0.105	0.153	0.327	0.410	23
0.005	0.108	0.152	0.325	0.409	23
0.005	0.109	0.152	0.324	0.410	23

Table B.10: Amberlyst, 343 K, Hydrolysis

T 343 K	mol ratio Ester-Water 1:2	Amberlyst 15 7 g	Ester 32 g	Water 9 g		
Ene	Acid	Ester	Anol	Water	Time (h)	
0	0.086	0.486	0.170	0.257	0.5	
0	0.087	0.485	0.170	0.257	0.5	
0	0.087	0.485	0.171	0.257	0.5	
0	0.166	0.199	0.215	0.421	2.17	
0	0.160	0.200	0.216	0.424	2.17	
0	0.167	0.198	0.214	0.421	2.17	
0.000	0.171	0.182	0.213	0.433	4.5	
0.000	0.175	0.182	0.214	0.429	4.5	
0.000	0.175	0.182	0.213	0.430	4.5	
0.001	0.175	0.206	0.238	0.380	23	
0.001	0.179	0.205	0.237	0.378	23	
0.001	0.179	0.204	0.237	0.379	23	

Table B.11: Zeolite, 333 K, Hydrolysis

T	mol ratio	Zeolite ZSM-5	Ester	Water	
333 K	Ester-Water 1:2	7 g	32 g	9 g	
Ene	Acid	Ester	Anol	Water	Time (h)
0.000	0.011	0.841	0.048	0.099	0.5
0.000	0.011	0.841	0.048	0.099	0.5
0.000	0.011	0.842	0.048	0.100	0.5
0.001	0.033	0.718	0.103	0.146	1.5
0.001	0.033	0.718	0.102	0.146	1.5
0.001	0.033	0.717	0.102	0.146	1.5
0.002	0.084	0.495	0.181	0.238	4.25
0.002	0.085	0.495	0.181	0.236	4.25
0.002	0.086	0.496	0.181	0.236	4.25
0.002	0.122	0.353	0.215	0.309	6
0.002	0.124	0.352	0.215	0.307	6
0.002	0.124	0.353	0.214	0.306	6

Table B.12: Amberlyst, 333 K, Hydrolysis

T	mol ratio	Amberlyst 15	Ester	Water	
333 K	Ester-Water 1:2	7 g	32 g	9 g	
Ene	Acid	Ester	Anol	Water	Time (h)
0	0.056	0.588	0.153	0.203	0.5
0	0.060	0.586	0.152	0.201	0.5
0	0.060	0.586	0.152	0.202	0.5
0	0.154	0.226	0.227	0.393	1.5
0	0.156	0.225	0.227	0.391	1.5
0	0.157	0.225	0.227	0.391	1.5
0	0.169	0.184	0.231	0.416	4
0	0.171	0.184	0.231	0.414	4
0	0.171	0.184	0.232	0.413	4
0.000	0.165	0.170	0.217	0.448	6
0.000	0.169	0.170	0.217	0.444	6
0.000	0.169	0.170	0.216	0.445	6

B.3 Reverse hydrolysis experiments

Table B.13: Reverse hydrolysis, without catalyst

T	mol ratio	catalyst	Anol	Acid		
333 K	Anol-Acid 1:1	0 g	50 g	23 g		
Ene	Acid	Ester	Anol	Water	Time (h)	
0	0.500	0	0.500	0	0	
0.003	0.233	0.258	0.251	0.255	1.68	
0.003	0.237	0.257	0.250	0.253	1.68	
0.003	0.238	0.257	0.249	0.253	1.68	
0.002	0.201	0.299	0.219	0.279	4.5	
0.002	0.202	0.297	0.218	0.281	4.5	
0.002	0.205	0.296	0.217	0.279	4.5	
0.002	0.192	0.308	0.211	0.286	7.5	
0.002	0.197	0.306	0.210	0.285	7.5	
0.002	0.198	0.306	0.210	0.284	7.5	
0.003	0.192	0.312	0.206	0.287	23.5	
0.003	0.197	0.310	0.205	0.285	23.5	
0.003	0.199	0.310	0.204	0.284	23.5	

Table B.14: Reverse hydrolysis, 333 K, 1:1

T	mol ratio	Amberlyst 15	Anol	Acid		
333 K	Anol-Acid 1:1	3.14 g	50 g	23 g		
Ene	Acid	Ester	Anol	Water	Time (h)	
0	0.500	0	0.500	0	0	
0.000	0.260	0.225	0.297	0.218	0.17	
0.000	0.264	0.224	0.295	0.217	0.17	
0.000	0.261	0.224	0.294	0.220	0.17	
0.001	0.207	0.289	0.243	0.260	0.5	
0.000	0.208	0.289	0.244	0.258	0.5	
0.000	0.209	0.290	0.244	0.257	0.5	

Cont inued...

Ene	Acid	Ester	Anol	Water	Time (h)
0.001	0.171	0.326	0.224	0.279	1.33
0.001	0.187	0.320	0.220	0.272	1.33
0.001	0.186	0.321	0.220	0.272	1.33
0.001	0.179	0.331	0.218	0.271	4.23
0.001	0.179	0.331	0.218	0.271	4.23
0.001	0.182	0.330	0.218	0.270	4.23
0.002	0.172	0.338	0.219	0.270	21
0.002	0.182	0.333	0.216	0.268	21
0.002	0.184	0.334	0.216	0.265	21

Table B.15: Reverse hydrolysis, 333 K, 2:1

T 333 K	mol ratio Anol-Acid 2:1	Amberlyst 15 3.15 g	Anol 50 g	Acid 11.5 g		
Ene	Acid	Ester	Anol	Water	Time (h)	
0	0.230	0.053	0.592	0.125	0	
0	0.236	0.053	0.587	0.125	0	
0	0.237	0.053	0.586	0.124	0	
0	0.157	0.141	0.508	0.194	0.17	
0	0.159	0.141	0.507	0.193	0.17	
0	0.164	0.140	0.504	0.193	0.17	
0	0.119	0.194	0.468	0.219	0.5	
0	0.120	0.194	0.467	0.219	0.5	
0	0.121	0.194	0.467	0.219	0.5	
0	0.098	0.222	0.450	0.230	1	
0	0.100	0.221	0.449	0.230	1	
0	0.100	0.221	0.448	0.230	1	
0.001	0.070	0.247	0.455	0.227	15	
0.000	0.086	0.242	0.445	0.227	15	
0.000	0.079	0.244	0.449	0.228	15	

Table B.16: Reverse hydrolysis, 333 K, 1:2

T	mol ratio	Amberlyst 15	Anol	Acid	
333 K	Anol-Acid 1:2	3.11 g	25 g	23 g	
Ene	Acid	Ester	Anol	Water	Time (h)
0	0.491	0.108	0.232	0.169	0
0	0.495	0.107	0.229	0.168	0
0	0.495	0.108	0.229	0.168	0
0	0.404	0.221	0.123	0.251	0.08
0	0.405	0.221	0.123	0.252	0.08
0	0.405	0.221	0.123	0.252	0.08
0	0.365	0.265	0.080	0.290	0.32
0	0.368	0.264	0.079	0.288	0.32
0	0.367	0.265	0.080	0.289	0.32
0	0.359	0.274	0.070	0.296	0.67
0	0.355	0.276	0.071	0.298	0.67
0	0.359	0.275	0.071	0.296	0.67
0	0.355	0.273	0.070	0.302	4
0	0.353	0.273	0.070	0.303	4
0	0.355	0.273	0.070	0.302	4

Table B.17: Reverse hydrolysis, 313 K, 1:2

T	mol ratio	Amberlyst 15	Anol	Acid	
313 K	Anol-Acid 1:2	3.16 g	27 g	24.18 g	
Ene	Acid	Ester	Anol	Water	Time (h)
0	0.519	0.061	0.293	0.126	0
0	0.520	0.061	0.292	0.127	0
0	0.520	0.062	0.292	0.127	0
0	0.431	0.173	0.180	0.215	0.13
0	0.431	0.174	0.181	0.214	0.13
0	0.431	0.174	0.180	0.216	0.13
0	0.374	0.241	0.122	0.264	0.5
0	0.374	0.241	0.121	0.264	0.5
0	0.374	0.241	0.121	0.264	0.5
0	0.343	0.275	0.094	0.288	1.05
0	0.343	0.275	0.094	0.288	1.05

Cont inued...

Ene	Acid	Ester	Anol	Water	Time (h)
0	0.330	0.291	0.080	0.299	2.83
0	0.329	0.291	0.080	0.300	2.83
0	0.333	0.290	0.080	0.298	2.83
0	0.300	0.305	0.083	0.312	20.5
0	0.326	0.293	0.080	0.300	20.5
0	0.326	0.293	0.080	0.300	20.5

Table B.18: Reverse hydrolysis, 313 K, 1:1

T	mol ratio	Amberlyst 15	Anol	Acid	
313 K	Anol-Acid 1:1	3.16 g	50 g	23 g	
Ene	Acid	Ester	Anol	Water	Time (h)
0	0.520	0.022	0.135	0.323	0
0	0.520	0.022	0.134	0.324	0.028
0	0.520	0.022	0.134	0.324	0.028
0	0.383	0.055	0.074	0.488	0.028
0	0.383	0.056	0.074	0.487	0.075
0	0.382	0.055	0.074	0.489	0.075
0	0.314	0.073	0.047	0.566	0.075
0	0.314	0.073	0.047	0.566	0.125
0	0.315	0.073	0.047	0.566	0.125
0	0.280	0.081	0.035	0.603	0.125
0	0.281	0.081	0.035	0.603	0.392
0	0.267	0.085	0.030	0.619	0.392
0	0.266	0.085	0.030	0.620	0.392
0	0.269	0.084	0.030	0.617	0
0	0.241	0.088	0.031	0.640	0

B.4 Thermo-morphic LLE data

B.4.1 DMSO-cyclohexene

Table B.19: Binary LLE: DMSO-cyclohexene

T (K)	Ene	DMSO	Ene	DMSO
296	0.973	0.027	0.105	0.895
296	0.976	0.024	0.106	0.894
320	0.940	0.060	0.169	0.831
320	0.938	0.062	0.168	0.832
338	0.898	0.102	0.237	0.763
338	0.898	0.102	0.238	0.763
346	0.869	0.131	0.294	0.706
346	0.844	0.156	0.285	0.715
352	0.822	0.178	0.339	0.661
352	0.818	0.182	0.340	0.660

B.4.2 NMF-cyclohexene

Table B.20: Binary LLE:NMF-cyclohexene

T (K)	Ene	NMF	Ene	NMF
295	0.988	0.012	0.092	0.908
343	0.988	0.012	0.172	0.829
343	0.983	0.017	0.183	0.817
352	0.971	0.029	0.194	0.806
352	0.976	0.024	0.199	0.801
354	0.976	0.024	0.195	0.805
354	0.971	0.029	0.194	0.806
361	0.971	0.029	0.201	0.799
361	0.972	0.028	0.208	0.793
363	0.941	0.060	0.214	0.786
363	0.943	0.057	0.217	0.783
399	0.894	0.106	0.258	0.742
401	0.914	0.086	0.255	0.745
401	0.936	0.064	0.257	0.743
408			0.298	0.702

B.4.3 Ternary DMSO - Ene - Water

Table B.21: Ternary LLE: DMSO - Ene - Water

T = 296 K		phase1			phase 2		
	Ene	DMSO	Water	Ene	DMSO	Water	
	1.000	0.000	0	0.001	0.237	0.762	
	0.988	0.000	0.012	0.001	0.237	0.762	
	0.973	0.000	0.027	0.004	0.464	0.532	
	0.976	0.000	0.025	0.004	0.465	0.531	
	0.957	0.011	0.032	0.024	0.679	0.298	
	0.969	0.011	0.020	0.023	0.679	0.298	
	0.953	0.020	0.026	0.074	0.851	0.076	
	0.935	0.019	0.046	0.066	0.862	0.072	
binary	0.973	0.027	0.000	0.105	0.895	0.000	
	0.976	0.024	0.000	0.106	0.894	0.000	
T = 360 K		phase1			phase 2		
	Ene	DMSO	Water	Ene	DMSO	Water	
	0.967	0.022	0.012	0.020	0.476	0.505	
	0.962	0.024	0.014	0.018	0.477	0.505	
	0.917	0.056	0.027	0.055	0.609	0.335	
	0.913	0.046	0.041	0.052	0.608	0.339	
	0.915	0.067	0.019	0.085	0.673	0.242	
	0.875	0.098	0.027	0.087	0.672	0.241	
	0.900	0.064	0.036	0.095	0.662	0.243	
	0.905	0.053	0.042	0.092	0.670	0.237	
T = 372 K		phase1			phase 2		
	Ene	DMSO	Water	Ene	DMSO	Water	
	0.940	0.030	0.030	0.024	0.480	0.496	
	0.923	0.044	0.033	0.026	0.478	0.497	
	0.920	0.062	0.019	0.069	0.608	0.323	
	0.886	0.086	0.029	0.070	0.608	0.323	
	0.835	0.123	0.042	0.120	0.643	0.236	
				0.117	0.654	0.229	
				0.116	0.653	0.231	
				0.113	0.655	0.232	

B.4.4 Batch kinetic experiment: direct hydration in DMSO

Table B.22: Solvent DMSO: Direct hydration

T	Zeolite ZSM-5	DMSO	Ene	Water
393 K	7 g	50.34 g	12.29 g	3.64 g
Anol	Ene	Water	DMSO	t (min)
0	0.150	0.119	0.730	0
0.0004	0.147	0.127	0.726	30
0.0004	0.146	0.126	0.728	30
0.0004	0.146	0.126	0.728	60
0.0004	0.145	0.123	0.732	60
0.0004	0.142	0.126	0.731	120
0.0004	0.142	0.126	0.731	180
0.0004	0.141	0.126	0.732	240

Bibliography

- [1] F. Steyer and K. Sundmacher. Cyclohexanol production via esterification of cyclohexene with formic acid and subsequent hydration of the ester - reaction kinetics. *Industrial and Engineering Chemistry Research*, 46(4):1099–1104, 2007.
- [2] F. Steyer, H. Freund, and K. Sundmacher. A novel reactive distillation process for the indirect hydration of cyclohexene to cyclohexanol using a reactive entrainer. *Industrial and Engineering Chemistry Research*, 47(23):9581–9587, 2008.
- [3] F. Steyer and K. Sundmacher. Use of a reactive entrainer for the synthesis of cyclohexanol in a process coupled reactive distillation column. *Chemie-Ingenieur-Technik*, 78(9):1200, 2006.
- [4] O. Mitsui and Y. Fukuoka. Process for producing cyclic alcohol. United States Patent 4588846, 05 1986.
- [5] H. Ishida. Liquid-phase hydration process of cyclohexene with zeolites. *Catalysis Surveys from Japan*, 1(2):241–246, 1997.
- [6] H. Ishida, Y. Fukuoka, O. Mitsui, and M. Köono. *Studies in Surface Science and Catalysis*, volume 83, chapter Liquid-Phase Hydration of Cyclohexane with Highly Silicious Zeolites, pages 473–480. 1994.
- [7] H. Freund, A. Katariya, R. Kumar, F. Steyer, and K. Sundmacher. Application of catalytic distillation in a novel process concept for the production of cyclohexanol. In *DGMK Tagungsbericht*, pages 237–239, 2007.
- [8] A. Katariya, H. Freund, and K. Sundmacher. Two-step reactive distillation process for cyclohexanol production from cyclohexene. *Industrial and Engineering Chemistry Research*, 48(21):9534–9545, 2009.

-
- [9] R. Kumar, A. Katariya, H. Freund, and K. Sundmacher. Development of a novel catalytic distillation process for cyclohexanol production: Mini plant experiments and complementary process simulations. *Organic Process Research and Development*, 15(3):527–529, 2011.
- [10] H. Freund, R. Kumar, A. Katariya, and K. Sundmacher. Intensification options for different hierarchical process levels illustrated in the conceptual design of a novel cyclohexanol production process. In *AIChE Annual Meeting, Conference Proceedings*, 2010.
- [11] R. Kumar, A. Katariya, H. Freund, and K. Sundmacher. A continuous reactive distillation process for the production of cyclohexanol from cyclohexene. In *AIChE 100 - 2008 AIChE Annual Meeting, Conference Proceedings*, 2008.
- [12] W. B. Fisher and J. F. VanPeppen. Cyclohexanol and cyclohexanone. In *Kirk-Othmer Encyclopedia of Chemical Technology*. John Wiley & Sons, Inc., 2000.
- [13] M. T. Musser. Cyclohexanol and cyclohexanone. In *Ullmann's Encyclopedia of Industrial Chemistry*. Wiley-VCH Verlag GmbH & Co. KGaA, 2000.
- [14] S. Randlow, H. C. Kaufman, J. H. Colvert, and E. F. Janes. Oxidation of cyclohexane. *Canadian Patent*, (CA 1020960), 1977.
- [15] G. R. Gildert. Oxidation of cyclohexane. *U.S. Patent*, (6,187,9806), 2001.
- [16] J. F. V. Peppen. Hydrogenation of phenol. *U.S. Patent*, (5,015,787), 1991.
- [17] G. C. Arnold. Hydrogenation of phenol. *U.S. Patent*, (3,998,884), 1976.
- [18] H. Ishida and K. Akagishi. Deterioration behavior of H-ZSM-5 and H-mordenite under hydrothermal condition. *Nippon Kagaku Kaishi / Chemical Society of Japan - Chemistry and Industrial Chemistry Journal*, (7):615–616, 1996.
- [19] H. Ogawa, H. Xiuhua, and T. Chihara. Hydration of cyclohexene by alkyl-immobilized H-ZSM-5 catalyst in decalin-water system. *Catalysis Letters*, 55(2):121–123, 1998.
- [20] M. Misono and T. Inui. New catalytic technologies in japan. *Catalysis Today*, 51(3-4):369–375, 1999.

-
- [21] D. Wang, X. Shu, and M. He. Studies on production of cyclohexanol by hydration of cyclohexene I. effects of zeolite structure and crystal size. *Chinese Journal of Catalysis*, 23(6):505–506, 2002.
- [22] P. Yuan, Y. Liu, F. Bai, L. Xu, Z. Cheng, and W. Yuan. Hydration of cyclohexene in sub-critical water over WO_x-ZrO₂ catalysts. *Catalysis Communications*, 12(8):753–756, 2011.
- [23] X. Shan, Z. Cheng, and P. Yuan. Reaction kinetics and mechanism for hydration of cyclohexene over ion-exchange resin and H-ZSM-5. *Chemical Engineering Journal*, 175(1):423–432, 2011.
- [24] G Rinck. Comparative consumer testing - German - Ulmer, B. and Kluy, G. *Betriebswirtschaftliche Forschung und Praxis*, 18(10):608, 1966.
- [25] G. D. Lyubarskii and G. K. Kervalishvili. Hydrogenation of phenol. *Khim. Promst. (Moscow)*, 7:491–492, 1972.
- [26] R. S. Suppino, R. Landers, and A. J. G. Cobo. Partial hydrogenation of benzene on Ru catalysts: Effects of additives in the reaction medium. *Applied Catalysis A: General*, 452:9–16, 2013.
- [27] P. Zhang, T. Wu, T. Jiang, W. Wang, H. Liu, H. Fan, Z. Zhang, and B. Han. Ru-Zn supported on hydroxyapatite as an effective catalyst for partial hydrogenation of benzene. *Green Chemistry*, 15(1):152–159, 2013.
- [28] W. Wang, H. Liu, T. Wu, P. Zhang, G. Ding, S. Liang, T. Jiang, and B. Han. Ru catalyst supported on bentonite for partial hydrogenation of benzene to cyclohexene. *Journal of Molecular Catalysis A: Chemical*, 355:174–179, 2012.
- [29] H. Liu, S. Liang, W. Wang, T. Jiang, and B. Han. The partial hydrogenation of benzene to cyclohexene over Ru-Cu catalyst supported on ZnO. *Journal of Molecular Catalysis A: Chemical*, 341(1-2):35–41, 2011.
- [30] P. Yuan, B. Wang, Y. Ma, H. He, Z. Cheng, and W. Yuan. Partial hydrogenation of benzene over the metallic Zn modified Ru-based catalyst. *Journal of Molecular Catalysis A: Chemical*, 309(1-2):124–130, 2009.
- [31] J. Wang, Y. Wang, S. Xie, M. Qiao, H. Li, and K. Fan. Partial hydrogenation of benzene to cyclohexene on a Ru-Zn/m-ZrO₂ nanocomposite catalyst. *Applied Catalysis A: General*, 272(1-2):29–36, 2004.

- [32] E. T. Silveira, A. P. Umpierre, L. M. Rossi, G. Machado, J. Morais, G. V. Soares, I. J. R. Baumvol, S. R. Teixeira, P. F. P. Fichtner, and J. Dupont. The partial hydrogenation of benzene to cyclohexene by nanoscale ruthenium catalysts in imidazolium ionic liquids. *Chemistry - A European Journal*, 10(15):3734–3740, 2004.
- [33] J. W. Da-Silva and A. J. G. Cobo. The role of the titania and silica supports in Ru-Fe catalysts to partial hydrogenation of benzene. *Applied Catalysis A: General*, 252(1):9–16, 2003.
- [34] K. Suzuki, H. Ishida, and H. Nagahara. Partial hydrogenation of benzene to cyclohexene over supported ruthenium carbonyl cluster-derived catalysts. In *Studies in Surface Science and Catalysis*, volume 145, pages 545–546. 2002.
- [35] S. Hu and Y. Chen. Partial hydrogenation of benzene on Ru-Zn/SiO₂ catalysts. *Industrial and Engineering Chemistry Research*, 40(26):6099–6104, 2001.
- [36] H. Nagahara, M. Konishi, O. Mitsui, Y. Fukuoka, and M. Kono. Partial hydrogenation of benzene with ruthenium catalyst-H₂O system effects of alcohols as co-catalyst. *Nippon Kagaku Kaishi / Chemical Society of Japan - Chemistry and Industrial Chemistry Journal*, (10):655–656, 1998.
- [37] H. Nagahara, M. Ono, M. Konishi, and Y. Fukuoka. Partial hydrogenation of benzene to cyclohexene. *Applied Surface Science*, 121-122:448–451, 1997.
- [38] S. Hu and Y. Chen. Partial hydrogenation of benzene to cyclohexene on ruthenium catalyst supported on La₂O₃-ZnO binary oxides. *Industrial and Engineering Chemistry Research*, 36:51535159, 1997.
- [39] P. T. Suryawanshi and V. V. Mahajani. Liquid phase hydrogenation of benzene to cyclohexene using ruthenium-based heterogeneous catalyst. *Journal of Chemical Technology and Biotechnology*, 69:154–160, 1997.
- [40] J. Ning, J. Xu, J. Liu, and F. Lu. Selective hydrogenation of benzene to cyclohexene over colloidal ruthenium catalyst stabilized by silica. *Catalysis Letters*, 109:175–180, 2006.
- [41] H. Zhang, S. M. Mahajani, M. M. Sharma, and T. Sridhar. Hydration of cyclohexene with solid acid catalysts. *Chemical Engineering Science*, 57(3):315–322, 2002.

-
- [42] J. E. S. Venart. Flixborough: A final footnote. *Journal of Loss Prevention in the Process Industries*, 20(4-6):621–643, 2007.
- [43] K. Sundmacher, F. Steyer, and Z. Qi. Synthesis of cyclohexanol by three-phase reactive distillation: Kinetics and phase equilibria. *Chemie-Ingenieur-Technik*, 73(6):766, 2001.
- [44] F. Steyer, Z. Qi, and K. Sundmacher. Synthesis of cyclohexanol by three-phase reactive distillation: Influence of kinetics on phase equilibria. *Chemical Engineering Science*, 57(9):1511–1520, 2002.
- [45] W. Peschel, T. Adrian, H. Rust, A. Bottcher, T. Hill, U. Muller, and Papp R. Simultaneous hydrogenation of benzene and hydration of cyclohexene in a catalytic distillation column. *U.S. Patent*, (6,943,274B2), 2005.
- [46] X. Shan, Z. Cheng, and Y. Li. Solvent effects on hydration of cyclohexene over H-ZSM-5 catalyst. *Journal of Chemical and Engineering Data*, 56(12):4310–4316, 2011.
- [47] J. Li, J. Wei, Y. Wang, and Z. Xinqiang. Effect of isophorone on hydration of cyclohexene. *Speciality Petrochemicals*, 28(4):55–59, 2011.
- [48] T. Qiu, X. . Wang, H. Tian, and Z. . Huang. Liquid-liquid equilibrium for the system water+1,4-dioxane+cyclohexanol over the temperature range of 313.2-343.2K. *Fluid Phase Equilibria*, 324:28–32, 2012.
- [49] H. J. Panneman and A. A. C. M. Beenackers. Solvent effects in the liquid phase hydration of cyclohexene catalyzed by a macroporous strong acid ion exchange resin. *Chemical Engineering Science*, 47(9-11):2635–2640, 1992.
- [50] H. Panneman and A. A. C. M. Beenackers. Solvent effects on the hydration of cyclohexene catalyzed by a strong acid ion exchange resin. 1. solubility of cyclohexene in aqueous sulfolane mixtures. *Industrial and Engineering Chemistry Research*, 31(4):1227–1231, 1992.
- [51] H. Panneman and A. A. C. M. Beenackers. Solvent effects on the hydration of cyclohexene catalyzed by a strong acid ion-exchange resin. 3. effect of sulfolane on the equilibrium conversion. *Industrial & Engineering Chemistry Research*, 31(6):1433–1440, 1992.

- [52] H. Panneman and A. A. C. M. Beenackers. Solvent effects on the hydration of cyclohexene catalyzed by a strong acid ion-exchange resin. 2. effect of sulfolane on the reaction kinetics. *Industrial & Engineering Chemistry Research*, 31(6):1425–1433, 1992.
- [53] A. A. Patwardhan and M. M. Sharma. Esterification of carboxylic acids with olefins using cation exchange resins as catalysts. *Reactive Polymers*, 13(1-2):161–176, 1990.
- [54] D.R. Cova and C.W. Roos. Esterification of olefins by carboxylic acid. *Industrial and Engineering Chemistry Process Design and Development*, 7(2):301–302, 1968.
- [55] J. A. Ballantine, M. Davies, I. Patel, J. H. Purnell, M. Rayanakorn, K. J. Williams, and J. M. Thomas. Organic reactions catalysed by sheet silicates: ether formation by the intermolecular dehydration of alcohols and by addition of alcohols to alkenes. *Journal of Molecular Catalysis*, 26(1):37–56, 1984.
- [56] B. Saha and M. M. Sharma. Esterification of formic acid, acrylic acid and methacrylic acid with cyclohexene in batch and distillation column reactors: Ion-exchange resins as catalysts. *Reactive and Functional Polymers*, 28(3):263–278, 1996.
- [57] F. Steyer and K. Sundmacher. VLE and LLE data set for the system cyclohexane + cyclohexene + water + cyclohexanol + formic acid + formic acid cyclohexyl ester. *Journal of Chemical and Engineering Data*, 50(4):1277–1282, 2005.
- [58] F. Steyer and K. Sundmacher. VLE and LLE data for the system cyclohexane + cyclohexene + water + cyclohexanol. *Journal of Chemical and Engineering Data*, 49(6):1675–1681, 2004.
- [59] S. S. E. H. Elnashaie and J. R. Grace. Complexity, bifurcation and chaos in natural and man-made lumped and distributed systems. *Chemical Engineering Science*, 62(13):3295–3325, 2007.
- [60] G. Peter and S. K. Stephen. *Chemical Oscillations and Instabilities: Non-Linear Chemical Kinetics*. Oxford University Press, USA, 1994.
- [61] D. Kondepudi and I. Prigogine. *Modern Thermodynamics: From Heat Engines to Dissipative Structures*. John Wiley & Sons, 1st edition, 1998.

-
- [62] R. A. Schmitz and N. R. Amundson. An analysis of chemical reactor stability and control-Va two-phase systems in physical equilibrium-1. *Chemical Engineering Science*, 18(5):265–289, 1963.
- [63] P. A. M. Springer, R. Baur, and R. Krishna. Composition trajectories for heterogeneous azeotropic distillation in a bubble-cap tray column: Influence of mass transfer. *Chemical Engineering Research and Design*, 81(4):413–426, 2003.
- [64] Z. Svandova, J. Markos, and L. Jelemensky. Impact of mass transfer coefficient correlations on prediction of reactive distillation column behaviour. *Chemical Engineering Journal*, 140(1-3):381–390, 2008.
- [65] Z. Qi and K. Sundmacher. The impact of interfacial mass transfer on the feasible products of countercurrent reactive separation processes. *Separation and Purification Technology*, 34(1-3):201–211, 2004.
- [66] A. M. Katariya, R. S. Kamath, K. M. Moudgalya, and S. M. Mahajani. Non-equilibrium stage modeling and non-linear dynamic effects in the synthesis of TAME by reactive distillation. *Computers and Chemical Engineering*, 32(10):2243–2255, 2008.
- [67] N. Bekiaris, G. A. Meski, and M. Morari. Multiple steady states in heterogeneous azeotropic distillation. *Industrial and Engineering Chemistry Research*, 35(1):207–227, 1996.
- [68] Z. Qi and K. Sundmacher. Bifurcation analysis of reactive distillation systems with liquid-phase splitting. *Computers and Chemical Engineering*, 26(10):1459–1471, 2002.
- [69] K. P. Zeyer, S. Pushpavanam, and A. Kienle. Nonlinear behavior of reactor-separator networks: Influence of separator control structure. *Industrial and Engineering Chemistry Research*, 42(14):3294–3303, 2003.
- [70] J. Morud and S. Skogestad. Dynamic behaviour of integrated plants. *Journal of Process Control*, 6(2-3 SPEC. ISS.):145–156, 1996.
- [71] R. Gani and S. B. Jorgensen. Multiplicity in numerical solution of nonlinear models: Separation processes. *Computers and Chemical Engineering*, 18(SUPPL):S55–S61, 1994.

- [72] R. A. Schmitz and N. R. Amundson. An analysis of chemical reactor stability and control-Vb. two-phase gas-liquid and concentrated liquid-liquid reacting systems in physical equilibrium-2. *Chemical Engineering Science*, 18(7):391–414, 1963.
- [73] R. A. Schmitz and N. R. Amundson. An analysis of chemical reactor stability and control-VI. two-phase chemical reacting systems with heat and mass transfer resistances. *Chemical Engineering Science*, 18(7):415–445, 1963.
- [74] R. A. Schmitz and N. R. Amundson. An analysis of chemical reactor stability and control-VII. two-phase chemical reacting systems with fast reactions. *Chemical Engineering Science*, 18(7):447–456, 1963.
- [75] M. E. E. Abashar. Dynamic behavior of two-phase systems in physical equilibrium. *Chemical Engineering Journal*, 97(2-3):183–194, 2004.
- [76] D. Barnea, M. S. Hoffer, and W. Resnick. Dynamic behaviour of an agitated two-phase reactor with dynamic variations in drop diameter-I. numerical simulations. *Chemical Engineering Science*, 33(2):205–217, 1978.
- [77] M. P. Harold, J. J. Ostermaier, D. W. Drew, J. J. Lerou, and D. Luss. The continuously-stirred decanting reactor: Steady state and dynamic features. *Chemical Engineering Science*, 51(10):1777–1786, 1996.
- [78] F. Steyer, D. Flockerzi, and K. Sundmacher. Equilibrium and rate-based approaches to liquid-liquid phase splitting calculations. *Computers and Chemical Engineering*, 30(2):277–284, 2005.
- [79] M. Mangold, A. Kienle, E. D. Gilles, and K. D. Mohl. Nonlinear computation in DIVA - methods and applications. *Chemical Engineering Science*, 55(2):441–454, 2000.
- [80] E. J. Doedel, A. R. Champneys, T. F. Fairgrieve, Y. A. Kuznetsov, B. Sandstede, and X. Wang. AUTO97: Continuation and bifurcation software for ordinary differential equations. *AUTO: Software for Continuation and Bifurcation Problems in Ordinary Differential Equations*, 1997.
- [81] A. Chakrabarti and M. M. Sharma. Cyclohexanol from cyclohexene via cyclohexyl acetate: catalysis by ion-exchange resin and acid-treated clay. *Reactive Polymers*, 18(2):107–115, 1992.

- [82] A. K. Kolah, L. Peereboom, C. T. Lira, J. Huang, C. B. Panchal, R. W. Lyczkowski, E. A. Dada, R. D. Doctor, and D. J. Miller. Advanced reactive distillation concepts for the indirect hydration of cyclohexene to cyclohexanol. In *AIChE Spring Meeting and 7th Global Congress on Process Safety, Conference Proceedings*, 2011.
- [83] H. Renon and J. M. Prausnitz. Local compositions in thermodynamic excess functions for liquid mixtures. *AIChE J.*, 14:135–144, 1968.
- [84] Z. Qi, A. Kolah, and K. Sundmacher. Residue curve maps for reactive distillation systems with liquid-phase splitting. *Chemical Engineering Science*, 57(1):163–178, 2002.
- [85] Y. Takamatzu and T. Kaneshima. Process for the preparation of cyclohexanol. *European Patent EP 1 243 572 A1*, 2002.
- [86] A. Behr. Cyclohexanol und cyclohexanon. *Winnacker K uchler Chemische Technik*, 5:70–74, 2005.
- [87] A. Behr, M. Urschey, and V. A. Brehme. Aqueous biphasic catalysis as a powerful tool for catalyst recycling in telomerization and hydrogenation chemistry. *Green Chemistry*, 5(2):198–204, 2003.
- [88] J. H. Hildebrand, J. M. Prausnitz, and R. L. Scott. Regular and related solutions. *AIChE Journal*, 17(3):iv, 1971.
- [89] J. H. Hildebrand and R. L. Scott. *The Solubility of Non-Electrolytes*. New York: Reinhold, 3rd edition, 1950.
- [90] C. M. Hansen. *Hansen Solubility Parameters: A User’s Handbook*. CRC Press, 2nd edition, 2007.
- [91] A. Fredenslund, R. L. Jones, and J. M. Prausnitz. Group-contribution estimation of activity coefficients in nonideal liquid mixtures. *AIChE Journal*, 21(6):1086–1099, 1975.
- [92] A. Fredenslund, J. Gmehling, M. L. Michelsen, P. Rasmussen, and J. M. Prausnitz. Computerized design of multicomponent distillation columns using the UNIFAC group contribution method for calculation of activity coefficients. *Industrial and Engineering Chemistry Process Design and Development*, 16(4):450–462, 1977.

-
- [93] A. Behr, G. Henze, L. Johnen, and C. Awungacha. Advances in thermomorphic liquid/liquid recycling of homogeneous transition metal catalysts. *Journal of Molecular Catalysis A: Chemical*, 285:20–28, 2007.
- [94] A. Rehfinger. *Reaction-technical investigation of the liquid-phase synthesis of MTBE with a strongly acidic macroporous ion exchange resin catalyst*. PhD thesis, Clausthal Technical University, Clausthal-Zellerfeld, Germany, 1988.
- [95] F. Steyer. *A Novel Reactive Distillation Process for the Production of Cyclohexanol from Cyclohexene*. PhD thesis, Fakultät für Verfahrens- und Systemtechnik der Otto-von-Guericke-Universität Magdeburg, 2010.
- [96] A. Vatani, M. Mehrpooya, and F. Gharagheizi. Prediction of standard enthalpy of formation by a QSPR model. *International Journal of Molecular Sciences*, 8(5):407–432, 2007.
- [97] H. N. Barham and L. W. Clark. The decomposition of formic acid at low temperatures. *Journal of the American Chemical Society*, 73(10):4638–4640, 1951.
- [98] J. H. Ernest, J. D. Seader, and R. D. Keith. *Separation Process Principles*. Wiley, 3rd edition, 2010.
- [99] M. F. Doherty and M. F. Malone. *Conceptual design of distillation systems*. Mc. Graw-Hill, Newyork, 2001.
- [100] A. M. Katariya, K. M. Moudgalya, and S. M. Mahajani. Nonlinear dynamic effects in reactive distillation for synthesis of TAME. *Industrial and Engineering Chemistry Research*, 45(12):4233–4242, 2006.
- [101] K. Sundmacher and A. Kienle. *Reactive Distillation: Status and Future Directions*. Wiley-VCH, 1st edition, 2003.
- [102] S. Ung and M. F. Doherty. Synthesis of reactive distillation systems with multiple equilibrium chemical reactions. *Industrial and Engineering Chemistry Research*, 34(8):2555–2565, 1995.
- [103] J. Gangadwala, G. Radulescu, A. Kienle, F. Steyer, and K. Sundmacher. New processes for recovery of acetic acid from waste water. *Clean Technologies and Environmental Policy*, 10(3):245–254, 2008.

-
- [104] J. Gangadwala. *Optimal Design of Combined Reaction Distillation Processes*. PhD thesis, Fakultät für Elektrotechnik und Informationstechnik der Otto-von-Guericke-Universität Magdeburg, 2007.
- [105] J. Bausa and W. Marquardt. Quick and reliable phase stability test in VLLE flash calculations by homotopy continuation. *Computers and Chemical Engineering*, 24(11):2447–2456, 2000.
- [106] K. Ye, H. Freund, and K. Sundmacher. Modelling (vapour + liquid) and (vapour + liquid + liquid) equilibria of water (H₂O) + methanol (MeOH) + dimethyl ether (DME) + carbon dioxide (CO₂) quaternary system using the Peng-Robinson EoS with Wong-Sandler mixing rule. *Journal of Chemical Thermodynamics*, 43(12):2002–2014, 2011.
- [107] K. Ye, H. Freund, Z. Xie, B. Subramaniam, and K. Sundmacher. Prediction of multicomponent phase behavior of CO₂-expanded liquids using CEoS/GE models and comparison with experimental data. *Journal of Supercritical Fluids*, 67:41–52, 2012.
- [108] G. Ciuhandu, A. Dumitreanu, and Z. Simon. Decarbonylation kinetics of formic acid in aqueous sulphuric acid solutions. *J.Prakt.Chemie*, 318:202–206, 1976.
- [109] M. M. T. Khan, S. B. Halligudi, and S. Shukla. Reduction of co₂ by molecular hydrogen to formic acid and formaldehyde and their decomposition to CO and H₂O. *Journal of Molecular Catalysis*, 57(1):47–60, 1989.
- [110] H. Uslu. Reactive extraction of formic acid by using tri octyl amine (TOA). *Separation Science and Technology*, 44(8):1784–1798, 2009.
- [111] A. Keshav and K. L. Wasewar. Back extraction of propionic acid from loaded organic phase. *Chemical Engineering Science*, 65(9):2751–2757, 2010.
- [112] R. A. Imam, H. Freund, R. P. M. Guit, C. Fellay, R. J. Meier, and K. Sundmacher. Evaluation of different process concepts for the indirect hydration of cyclohexene to cyclohexanol. *Organic Process Research & Development*, 17:343–358, 2013.
- [113] R. A. Imam, H. Freund, and K. Sundmacher. Dynamics of liquid-liquid systems based on linear thermodynamics of irreversible processes. *Computers and Chemical Engineering*, 35(4):630–637, 2011.

Curriculum Vitae

Personal details

Name : Rayees Ahamed Imam
Date of birth : 14 October 1981
Place of birth : Guduvancheri-Tamil Nadu, India
Address : 1 Ellai Gandhi Street, Guduvancheri, India 603202
Nationality : Indian
Marital status : Married

Schooling

06/1995-04/1997 : Government Higher Secondary School, Guduvancheri

Education

06/1997-04/2000 : Diploma in Chemical Technology, Institute of Chemical Technology, Chennai, India
06/2001-05/2004 : Bachelor of Technology in Chemical Engineering, University of Madras, India
07/2004-04/2006 : Master of Technology in Chemical Engineering, Indian Institute of Technology (IIT), Chennai, India

Work Experience

12/1999-03/2000 : Trainee at Tamilnadu Petroproducts Limited, India
04/2007-07/2012 : Research Fellow at Max Planck Institute for Dynamics of Complex Technical Systems, Magdeburg, Germany
11/2013 onwards : Scientist at SABIC Technical Research Center, India